Chapter 3
Second Generation Visible-Light-Active Photocatalysts: Preparation, Optical Properties, and Consequences of Dopants on the Band Gap Energy of TiO_2

Nick Serpone, Alexei V. Emeline, Vyacheslav N. Kuznetsov, and Vladimir K. Ryabchuk

Abstract First generation metal-oxide photocatalysts based mostly on nominally pure, pristine titanium dioxide have been the object of great debate in the past 30 years with regard (i) to the nature of the oxidative agent (•OH radicals vs. holes h^+); (ii) to the site at which the reaction takes place (surface vs. bulk solution); (iii) to whether TiO_2 is indeed a photocatalyst since turnover numbers are difficult to determine owing to the nature of the particle surface; and (iv) to how the process efficiency can be ascertained, among many other issues yet to be resolved satisfactorily. One issue that has taken some time to be resolved is the notion of how we can make better use of sunlight's visible radiation seeing that the absorption edge of TiO_2 is at 387 nm (ca. 3.2 eV – the band gap energy) for the anatase polymorph. A successful strategy that is gaining some momentum is to dope this metal oxide with suitable dopants (e.g., metal ions and/or non-metals) to shift the absorption edge to longer wavelengths. Doping has been achieved using various physical and chemical strategies, which have led to materials whose absorption edges have been red-shifted to wavelengths ~550 nm (and beyond in some cases). The debate that now occupies discussions of doped-TiO_2 materials regards the causes for this red shift. Several reports, based on density functional theory (DFT), have asserted that the band gap of doped-TiO_2 is narrowed because of interactions between the dopant states and the O 2*p* states of the valence band, thereby pushing the valence band edge upward. Others have proposed isolated dopant states located within the band gap to explain the red shift of the absorption edges of doped-TiO_2 systems through excitation of the electrons in these states to the conduction band of TiO_2. Absorption spectra, calculated from several diffuse reflectance spectra (DRS) reported in the literature for both metal ion-doped TiO_2s and systems doped with non-metals (e.g., carbon, sulfur, nitrogen, and fluorine), are remarkably similar if not identical in the visible spectral region. The broad spectral envelope observed at wavelengths

N. Serpone (✉)
Dipartimento di Chimica Organica, Universita di Pavia, Pavia, Italy
e-mail: nick.serpone@unipv.it

M. Anpo and P.V. Kamat (eds.), *Environmentally Benign Photocatalysts*, Nanostructure Science and Technology, DOI 10.1007/978-0-387-48444-0_3,

greater than 400 nm can be deconvoluted into 2–3 single bands, which indicate different species give rise to these bands. This chapter is therefore concerned, albeit in a very restrictive way, with the various strategies used to dope TiO_2, with their modeling by DFT methods, and finally with their optical properties with which we shall argue that the absorption edge red-shift originates from a singular source involving mostly the formation of (additional to existing) oxygen vacancies in the metal-oxide lattice (both surface and bulk) that can act as electron traps to yield *F*-type color centers and/or Ti^{3+} color centers.

1 Introduction

Metal-oxide heterogeneous photocatalysis developed with the several studies of the late 1970s and the 1980s that explored means to photogenerate clean alternative fuels (e.g., H_2 from water splitting). Semiconductor particulate systems provided stability and the possibility of modifying the particle surface, itself having good catalytic properties, by addition of functional or bifunctional co-catalysts (e.g.Pt, RuO_2, and others) to improve catalytic functions and to accentuate process dynamics. The search for solar energy conversion methodologies provided the impetus that ultimately led to significant advances in the last two decades of the twentieth century. Active exploration of irradiated semiconductors was aimed at the production of hydrogen and at the photooxidation of organic substrates, as the latter had been recognized as *sacrificial electron donors* in energy conversion processes.

Of a more practical nature were the problems encountered in rendering and implementing metal-oxide photocatalysis as a viable technology in energy conversion and environmental remediation, which ultimately rested with the use of TiO_2 as the major focus of hundreds of studies. This exhaustive literature describes heterogeneous photocatalysis and TiO_2 as an excellent photocatalyst in a variety of details as applied to the photochemical remediation of air and water. An extensive review by Diebold (2003) has summarized the properties of TiO_2 from the physics and surface science perspectives.

One issue quickly recognized with TiO_2 was that it absorbs but a small fraction (ca. 3–5%) of the sunlight reaching the Earth's surface. The absorption onset of UV light by the anatase polymorph begins around 387 nm (band gap energy, E_{bg} ~3.2 eV; for rutile E_{bg} ~3.0 eV or ca. 413 nm) and increases to shorter wavelengths. This led to the use of sensitizers to harness much of the solar energy to convert it into useful work. As a viable technology in environmental remediation, an issue that hampered heterogeneous photocatalysis in practical applications with aqueous slurries was the need for an additional filtration step to devices/reactors. TiO_2 needed to be immobilized on some appropriate inert support (glass, metals and plastics, among others). Of a more fundamental nature, however, was the issue that, once photogenerated, electrons and holes tend to recombine rather efficiently and rapidly against an otherwise slow redox chemistry occurring on the photoactivated TiO_2 surface.

The science underlying heterogeneous photocatalysis shows that the energy level of the bottom of the conduction band (CB) in a semiconductor like TiO_2 is a measure of the reduction potential of photogenerated electrons, whereas the upper level of the valence band is a measure of the oxidation potential of photogenerated holes. The flatband potentials, V_{fb}, of the conduction and valence bands, fixed by the nature of the material and in the case of metal oxides by proton exchange equilibriums at the interface (i.e., pH dependent), determine the energy of electrons and holes at the interface. Hence, reductive and oxidative processes of couples with redox potentials more positive and more negative than the V_{fb} of the conduction and valence bands, respectively, can be driven by surface trapped electrons and holes. That is, the charge carriers (e^- and h^+) are ultimately poised at the particle surface to engage in various processes, the most important of which are photoreductions and photooxidations. Most research efforts in understanding the fundamental nature of heterogeneous photocatalysis with metal oxides (TiO_2, ZrO_2, and others) have focused on assessing the factors that underlie the temporal evolution of surface redox reactions on such metal-oxide materials.

Clearly, photoactivated semiconductor particles function as pools of electrons and holes that can be exploited in a variety of multi-electron transfer processes. The presence of a redox catalyst (e.g. Pt, RuO_2) loaded onto the particle surface greatly improves the catalytic efficacy of the semiconductor material. Such deposits usually lead to more efficient charge separation since the particle becomes polarized subsequent to irradiation, with the deposits tending to be good electron sinks. However, such deposits (i.e., dopants) can also act as recombination centers of photoelectrons and photoholes so that the redox efficacy can become largely compromised.

As a first-generation material, pristine TiO_2 has served well in photoassisted degradation and mineralization reactions of a large number of organic substrates in the quest to dispose of environmental contaminants in aqueous and atmospheric ecosystems. Unfortunately, its absorption edge at $\lambda < 400$ nm and thus its overall efficiency and usefulness, based on the total solar radiation reaching the Earth's surface, are limited. Accordingly, efforts were expended in the late 1980s to develop second-generation titanium dioxides (Lawless 1993) that could bridge both the UV (290–400 nm) and the visible (400–700 nm) radiation, and thereby enhance overall efficiency. The requirement was to red-shift the absorption edge of TiO_2 to wavelengths longer than 400 nm. Attempts toward achieving this goal rested, in part, on photosensitizing this metal oxide with suitable dyes that act as visible-light-harvesters, but which eventually lead to their own destruction, and with suitable metal-ion dopants, which unfortunately act either as recombination centers of photogenerated charge carriers (in some cases) or are simply ineffective in aiding the surface redox reactions, especially when metal doping is achieved by wet impregnation methods (Lawless 1993). However, studies by Anpo and Takeuchi (2003) have shown that metal-ion implantation produces metal-doped TiO_2 that enhances photo-induced surface redox reactions even in the visible-light region, where the wet chemical methods failed.

First reports of anion-doped TiO_2 began to appear in the early 1990s, although an earlier article by Sato (1986) also reported hints of an N-doped TiO_2. It was not until the 2001 study in *Science* by Asahi and coworkers (2001) on the doping of TiO_2 by various anions to produce visible-light-active (VLA) N-doped TiO_2, that researchers took anion-doping seriously as a prelude to produce second-generation TiO_2 materials that would increase photoactivity over the UV and much of the visible-light region. Subsequent studies reported several other VLA N-doped TiO_2 materials, together with C-doped TiO_2 and S-doped TiO_2. Since these reports appeared, a lively debate in the recent literature has centered on the causes that lead the absorption onset of TiO_2 to be shifted to the visible region. Asahi and coworkers (Asahi et al. 2001; Morikawa et al. 2001) proposed that N-doping of TiO_2 shifts the absorption edge of $TiO_{2-x}N_x$ to lower energies and increases the photoactivity in the visible light region through narrowing of the TiO_2 band gap. Carbon- and sulfur-doped TiO_2 displayed similar red-shifts of the absorption edges and increased photoactivity. Others, however, have proposed that electronic transitions in these doped TiO_2 systems subsequent to visible-light irradiation involve transitions from N 2*p* localized states to the CB of titanium oxide.

Just as first-generation TiO_2 specimens led to several lively debates on the fundamental science that underlies TiO_2-assisted photoredox surface processes (oxidations and reductions) following photoactivation, so are the second-generation TiO_2 specimens generating enthusiastic discussions on the root cause that shifts the absorption onset to longer wavelengths, and thereby increase photoactivity into the visible spectral range. This chapter focuses, albeit not exhaustively, on (i) various preparative methods of VLA TiO_2 materials, (ii) their XRD and XPS spectroscopic features, followed by (iii) their optical properties in the visible spectral region, (iv) the causes that lead to the red shift of the absorption edges of doped TiO_2s, and finally (v) a brief visit into the lively debate concerning band gap narrowing.

2 Visible-Light Photoactivity of Undoped TiO_2 Specimens

To the best of our knowledge, the first study that dealt with VLA nominally pristine (undoped) TiO_2 was reported in the early 1970s by Teichner and coworkers (Formenti et al. 1971) who prepared anatase TiO_2 by a flame reactor method, and when irradiated in an O_2 atmosphere (120 Torr, 1 h, 27°C) found it to be photoactive in a broad range of wavelengths from 290 to 575 nm (4.30–2.15 eV). This induced the formation of $O_2^{-\bullet}$ species as evidenced by its EPR spectral signature. Spectral dependencies of the quantum yields (Φ) of simple photostimulated reactions have been measured for various undoped specimens (Cherkashin et al. 1980; Emeline et al. 2000, 2002). The reported data are in reasonably good agreement (see Figs. 1 and 2); however, the interpretations of the spectral dependencies of Φ in the visible region have not been coherently uniform (Cherkashin et al. 1980; Emeline et al. 2000, 2002).

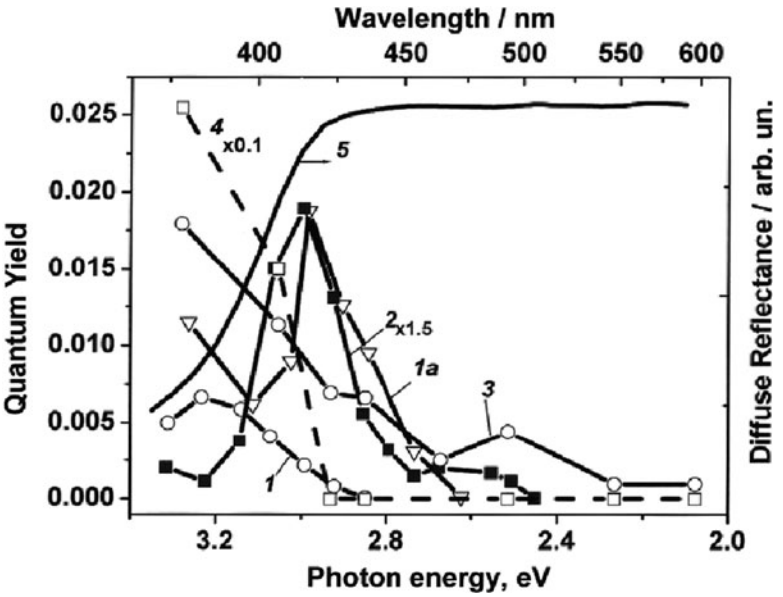

Fig. 1 Spectral dependencies of the quantum yields of photostimulated adsorption of O_2 on the surface of TiO_2 specimens: Degussa P25 pre-treated at 327°C (curve *1*) and at 577°C (curve *1a*), rutile (Aldrich) pretreated at 327°C (curve *2*), homemade rutile pretreated at 547°C (curve *3*). Spectral dependence of the quantum yield of photostimulated adsorption of CO on the surface of homemade rutile pre-treated at 547°C (see text) (curve *4*). Curve *5* represents the diffuse reflectance spectrum of Degussa P25 TiO_2

A large number of absorption spectra of various TiO_2 specimens that absorb in the visible region have been examined (Kuznetsov and Serpone 2006); they are discussed in greater detail later in the chapter (see Sect. Optical Features of Doped TiO_2). For the moment, suffices to note that in all cases the spectra could be interpreted as the sum of overlapping absorption bands (ABs) that originate from the reduction of TiO_2 under some pretreatment conditions, or otherwise when the specimen was prepared. It seems reasonable, therefore, to revisit the earlier data on nominally clean TiO_2.

The spectral dependencies of Φ in the visible and near-band-gap regions, reported earlier by Cherkashin et al. (1980) and by Emeline and coworkers (2000, 2002), were digitized and are collected in Figs. 1 and 2. Three types of action spectra are clearly evident: (1) spectra *1* and *4* of Fig. 1 demonstrate excitation of the photoreaction in the region of *intrinsic* (i.e., band-to-band) absorption; (2) spectra *1a*, *2* and *3* of Fig. 1 and spectra *1*, *1a*, *2*, *3*, and *4* of Fig. 2 display maximal absorption at 2.9–3.0 eV, i.e., in the region of *extrinsic* absorption; and (3) spectra *2* and *3* of Fig. 1 and spectra *3* and *4* of Fig. 2 clearly show additional bands with maxima in the region 2.5–2.6 eV. Comparison of the positions of band maxima constituting the spectral dependencies (Figs. 1 and 2) and the main absorption bands in the spectra of various reduced TiO_2 samples (AB1 at 2.9 eV and AB2 at 2.55 eV) (Kuznetsov and Serpone

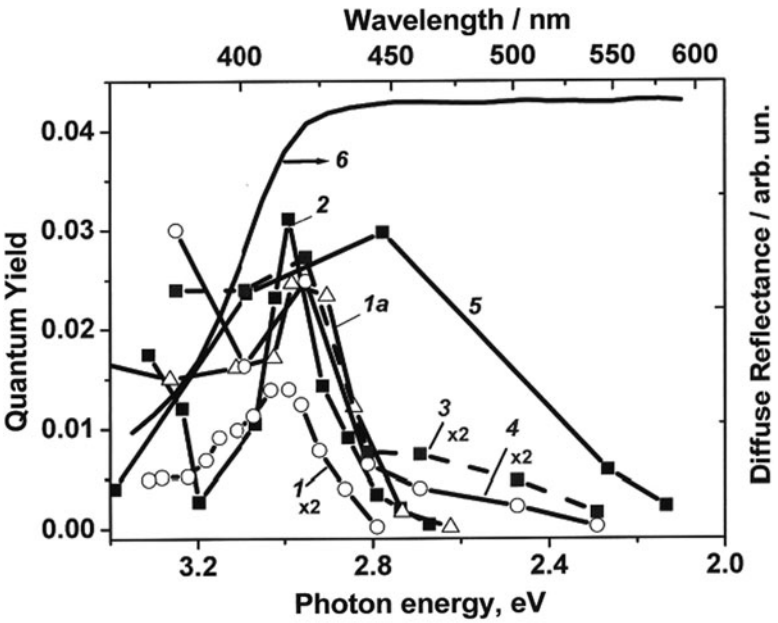

Fig. 2 Spectral dependencies of the quantum yields of photostimulated adsorption of H_2 (curves *1, 1a, 2, 3*) and CH_4 (curve *4*) on the surface of TiO_2 specimens: Degussa P25 pre-treated at 327°C (curve *1*) and at 577°C (curve *1a*), rutile (Aldrich) pre-treated at 327°C (curve *2*), rutile (curves *3* and *4*). Spectral dependence of the efficiency of photoformation of a hole species [O^- O_2] at –186°C on the surface of anatase pre-treated at 527°C (curve *5*). Curve *6* represents the diffuse reflectance spectrum of P25 TiO_2

2006) infers that photoactivity in the visible region of nominally pristine TiO_2 originates from TiO_2 reduction, which gives rise to defects/color centers. Note that Figs. 1 and 2 illustrate the action spectra of TiO_2 specimens of *different origins*: in particular, Degussa P25 and Aldrich rutile (Emeline et al. 2002), rutile (Emeline et al. 2000), superfine anatase (Russia) and rutile obtained from homemade superfine anatase by calcination in air at ca. 1000°C for 2 h (Cherkashin et al. 1980).

The spectral dependencies of Φ of photostimulated adsorption of H_2 and O_2 in the studies of Cherkashin et al. (1980) and of Emeline and coworkers (2000, 2002) were determined using a "black-body"-like cell with the rate of photoadsorption measured manometrically. Curve *5* in Fig. 2 depicts the spectral dependence of the efficiency of photoinduced formation of [O^-O_2, i.e., O_3^-] species. In this case, the rate of evolution of the EPR signal ($g = 2.001$and $g_{||} = 2.008$), attributed to the O_2 molecule adsorbed on the photoinduced hole center, was normalized by the intensity of the incident light. Thus, spectrum *5* of Fig. 2 can be considered as being independent of the other spectra, but does demonstrate at least the same spectral region of photo-activity.

Samples of TiO_2 used in earlier studies (Cherkashin et al. 1980; Emeline et al. 2000, 2002) were heat-treated in air and then under oxygen/vacuum conditions at

temperatures around 327–577°C for several hours to purify the TiO_2 specimens of adventitious organic impurities. Prior to every photoadsorption measurement, the samples were typically preheated in an O_2 atmosphere ($p_{O2} = 100$ Pa) at 427°C for 1 h (Cherkashin et al. 1980), or at 327°C for 15–20 min (Emeline et al. 2002) and subsequently cooled down in an O_2 atmosphere (Cherkashin et al. 1980) or under a dynamic vacuum (Emeline et al. 2002). The surface of the samples was thus fully oxidized under these conditions. It is appropriate then to query whether a contradiction exists with the above assignment of the spectral bands in the spectral dependencies of photoreactions. Note that these purified samples exhibited no remarkable absorption features in the diffuse reflectance spectra at energies below 3.0 eV (i.e., at $\lambda >$ ca. 400 nm).

Color centers (defects) responsible for the 2.9-eV (AB1) and 2.55-eV (AB2) bands are only slightly active and weakly interact with O_2 so that formation of defects from the reduction of TiO_2 can also take place in air (Kuznetsov and Serpone 2006). Processes involving preparation of VLA TiO_2 specimens normally occur when the samples are heat-treated in air, or otherwise involve heating TiO_2 samples in air as a separate treatment stage.

Related to the above seeming contradiction, it is of import to consider some results that show the coexistence of a partly reduced bulk and an oxidized surface of titania specimens. If organometallic precursors or addition of any organic substrate are used in preparing TiO_2 systems, the organic residues can provide heat-activated reduction of TiO_2. Only a few studies demonstrated the existence of carbon-type species in VLA TiO_2 systems obtained when using organic precursors. Lettmann and coworkers (2001) report that pyrolysis (247°C, 3 h) of various alcohols used in the sol-gel process to obtain undoped TiO_2 leads to carbonaceous species embedded in the TiO_2 matrix. Commercial Hombikat UV-100 TiO_2 can also be made VLA-active when impregnated with various alcohols and then heat-treated at 247°C (Lettmann et al. 2001).

Three types of carbonaceous species have been detected in TiO_2 samples prepared by sol-gel methods using as the precursor titanium tetraisopropoxide, Ti(i-PrO)$_4$, dissolved in i-PrOH (Colon et al. 2006). The principal species were: (i) organic residues from the alkoxide precursor, (ii) slightly oxidized organics, and (iii) species further oxidized such as e.g., carboxylates. The organic-like carbon could be removed after calcination at 697°C for 2 h in air, although some graphitic carbon and some CO_3^{2-}-like species *still remained* in TiO_2 at C levels $\geq$4.5 at.%.

Nominally clean, commercial TiO_2 powders can also include some adventitious metallic impurities. Diebold (2003) described the basic concepts of metal deposition on TiO_2 and details about different metals embedded in this metal oxide. Evidently, several metals can reduce TiO_2 with the metal becoming oxidized in the process. Thus, redox reactions and metal-doping TiO_2 specimens are some of the possible pathways that can lead to formation of defects/color centers in titania.

Formation of defects and color centers, connected with the reduction of TiO_2 in the case of nominally clean specimens, is an uncontrollable process. It can occur during the stage of industrial production and/or during the treatment preceding experimental studies. Removal of adventitiously adsorbed organic impurities from

the metal-oxide surface is typically achieved by heat-treatment at temperatures about 327–627°C in air, followed by treatment under oxygen/vacuum conditions at the same temperatures for several hours. This is necessary when photostimulated reactions of oxygen-containing molecules are to be examined. Accordingly, calcination of a metal-oxide *surface* can potentially stimulate the formation of defects/color centers in the *lattice bulk* through organic/inorganic impurity-assisted reduction of the sample. To date, however, there exists only indirect evidence for these inferences.

The influence of temperature of the pretreatment stage on the photoactivity of Degussa P25 TiO_2 has been examined by Emeline and coworkers (2002). The dramatic increase of the 3.0-eV band in the wavelength-dependent quantum yield spectrum of the photoadsorption of O_2 (Fig. 1, curves *1* and *1a*) and the significant increase of nearly the same band in the quantum yield spectra of photoadsorption of H_2 (Fig. 2, curves *1* and *1a*) can be taken as an increase in the number of defects responsible for the absorption band at 2.9–3.0 eV. This increase in the number of defects originates from an increase in the pretreatment temperature of 327–577°C. The photoactivity at 2.86 eV (433 nm) of N-doped TiO_2 systems, prepared by hydrolysis of either $Ti(i\text{-}PrO)_4$ or $TiCl_4$ with aqueous NH_3, shows a remarkable growth (from 0 to maximum value) in a very narrow temperature range 297–397°C and 347–447°C, respectively (Sato et al. 2005). The visible-light absorption and visible-light activity of metal-ion implanted TiO_2 systems reported by Anpo and Takeuchi (2003) was observed only after the samples had been calcined at temperatures ranging from 450 to 550°C.

It is important to emphasize that nominally clean TiO_2 display long-term (months) photoactivity in the visible-light region owing to the stability of color centers under certain experimental conditions. Prior to every photoadsorption measurement, TiO_2 samples were preheated in an oxygen environment at 327–427°C and then cooled in an O_2 atmosphere or under vacuum conditions (Cherkashin et al. 1980; Emeline et al. 2000, 2002). We can thus conclude that defects/color centers in the lattice bulk that absorb visible light remain stable under such treatments.

Related to the above inference, we now consider some results that show the co-existence of partially reduced bulk and oxidized surface of titania. VLA TiO_2 thin films that absorb in the range 3.10–1.55 eV have been fabricated by a radio-frequency-magnetron sputtering (RF-MS) deposition method under an Ar atmosphere ($p_{Ar} = 1$–3 Pa) and a substrate temperature of 600°C (Kitano et al. 2006a). SIMS measurements revealed that the O/Ti ratio of VLA TiO_2 decreased from the top surface (2.00 ± 0.01) to the inside bulk (1.93 ± 0.01). Moreover, VLA TiO_2 was stable even under calcination treatment at 450°C in air or in photocatalytic reactions, indicating that the films' surface was covered with a stoichiometric and stable TiO_2 phase that prevented the complete oxidation of bulk TiO_2. Note also that the absorption band at 3.0 eV, originating from an impurity-assisted reduction of the anatase crystal, was suppressed fully *only* after calcination at 800°C for 60 h under an oxygen pressure of 1 MPa (Sekiya et al. 2000).

Temperature-programmed desorption (TPD) spectra of CO_2 after adsorption of O_2, both in the dark (chemisorption on a vacuum-reduced surface) or under

irradiation, confirmed the presence of adventitious carbonaceous species in Degussa P25 TiO_2. The sample of TiO_2 was deposited on the wall of a quartz cell and then heated in air to 327°C and kept at this temperature for ca. 4 h. The sample cell was connected to a high-vacuum system and pretreated in alternating O_2 flow (130 Pa) and vacuum (10^{-6} Pa) at 577°C for 30 h. During all stages of the experiments, the gas composition above the sample was controlled by an MI-1201 mass spectrometer. TPD spectra were obtained under heating at a constant rate $\beta = 0.25$°C s^{-1} in the range 17–577°C. Oxygen was purified by diffusion through the walls of a silver capillary tube. Further details regarding the TPD spectra analysis are available elsewhere (Kuznetsov 2002).

Figure 3 illustrates typical TPD spectra of oxygen chemisorbed (curve *1*) and photoadsorbed (curve *2*) on the surface of a TiO_2 sample cleaned using the above procedure. Oxygen coverage corresponding to spectrum *1* in Fig. 3 is ~1×10^9 molecules cm^{-2}; the corresponding coverage for spectrum *2* is ca. 6×10^{10} molecules cm^{-2}. Absence of the dependence of the 410-K peak on oxygen coverage is direct evidence for first-order kinetics of desorption (i.e., monomolecular desorption) with respect to coverage (Redhead 1962), and consequently infers adsorption of molecular O_2 rather than atomic oxygen. The principal peak at 410 K of the oxygen TPD spectra is characteristic of the vacuum-annealed (reduced at 527–577°C) rutile surface of single crystals (Henderson et al. 1999) and powdered samples (Beck et al. 1986).

Figure 3 also reports the TPD spectra of CO_2 measured simultaneously with the TPD spectra of O_2. The coverage of CO_2 in the range ~5×10^8 molecules cm^{-2}

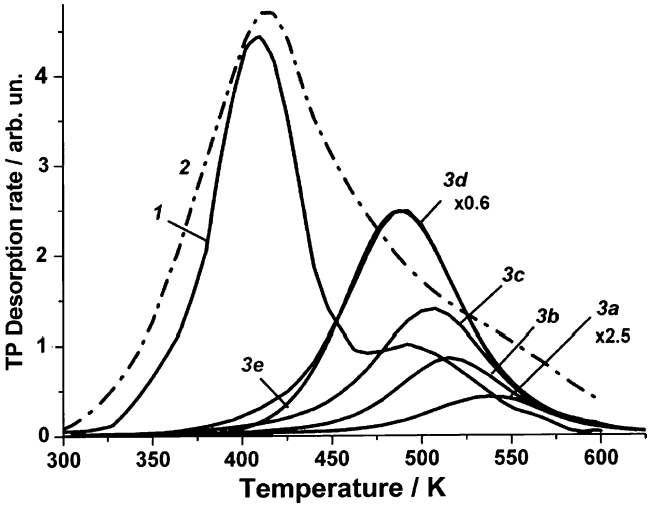

Fig. 3 Temperature-programmed desorption spectra of oxygen chemisorbed (curve *1*) and photoadsorbed (curve *2*) on the surface of Degussa P25 TiO_2 pre-treated in air and under O_2/vacuum conditions at 577°C for 30 h. Spectra *3a–3d* represent the TPD spectra of CO_2 resulting from oxygen adsorption and thermal desorption. Curve *3e* is a numerically calculated peak of recombinative desorption (see text)

(spectrum *3a*) to ca. 10^{10} molecules cm^{-2} (spectrum *3d*) always correlated with O_2 coverage and did not exceed 30% of O_2 coverage. Three main features of CO_2 desorption are worth noting: (i) desorption occurred only after O_2 was chemisorbed or photoadsorbed and was absent when the sample was kept in a vacuum, (ii) the TPD spectra of CO_2 consisted of a singe peak of somewhat symmetrical shape, and (iii) the position of the peak's maximum (T_{max}) depended on coverage. A shift (decrease) of T_{max} of ~50 K when coverage increased by a factor of ~25 (Fig. 3) is direct evidence of second-order kinetics of desorption (i.e., recombinative desorption) with respect to coverage (Redhead 1962). Moreover, the near symmetrical TPD peak, characteristic only of recombinative desorption, could be calculated numerically using experimental values of the initial CO_2 coverage: ca. 10^{10} molecules cm^{-2} and $\beta = 0.25°C\ s^{-1}$ along with the fitting values of the activation energy of desorption 0.88 eV and the pre-exponential factor 10^{-3} cm^2 $molecules^{-1}$ s^{-1}. The calculated (curve *3e*) and experimental (curve *3d*) peaks coincide quite well. However, near 410 K an additional CO_2 peak seems to appear. It is worth noting that TPD spectra of CO_2, molecularly adsorbed on the surface of powdered rutile TiO_2 pre-heated at 727°C in vacuum, revealed a single peak at the lower temperature of ~415 K (Yanagisawa and Sumimoto 1994).

Because desorption of CO_2 and O_2 occurs simultaneously (Fig. 3), it is reasonable to suppose that once oxygen is liberated from adsorption sites (at $T > 400$ K atomic species can dominate) it can interact with any C-containing species leading to CO_2 formation. Thus, desorption of CO_2 having non-adsorptive origins is a very clear indicator of the presence of carbonaceous inclusions in TiO_2 specimens. After nearly 3 months of almost daily experiments, the effectiveness of O_2-assisted CO_2 formation remained virtually unchanged. Hence, C-containing species are located in the volume/subsurface region of TiO_2 and rise to the surface by diffusion when TiO_2 is subjected to a heat treatment, including programmed heating. The overall quantity of CO_2 formed during the TPD experiments (after ca. 50 spectra) is ~10^{16} molecules. Since the sample's weight $w = 0.1$ g, the sample contains $(N_A/M)w \approx 10^{21}$ entities (molecules) of TiO_2; N_A is Avogadro's number (6×10^{23} mol^{-1}) and M denotes the molecular weight of TiO_2 (80 g mol^{-1}). The invariant efficiency of formation of CO_2 indicated that a negligible fraction (a few %) of C-species took part in the reaction. Hence, the content C of the above species in the sample equaled to or exceeded 0.1% (i.e., $C \geq (10^{16}/1\%)/10^{21}$).

Experimental data (Kuznetsov and Serpone, 2006) showed that nominally clean TiO_2 P25 included sufficient quantity of C-containing species, even after the long-term heat pretreatment in an O_2 atmosphere and after photo- and heat-treatment in O_2 and in vacuum during numerous experiments. With such evidence, we concluded that defects/color centers resulted from reactions of carbonaceous species with lattice bulk oxygen, thus leading to the display of photoactivity in the visible spectral region. Indeed, a specimen we investigated demonstrated permanent photoactivity under both UV- and visible-light ($\lambda \leq 546$ nm, $h\nu \geq 2.27$ eV) irradiation in the photodesorption of chemisorbed and photoadsorbed oxygen, as well as photoadsorption and photodisproportionation of nitric oxide (NO). Based on presently available published data, only the 2.9-eV AB1 and 2.55-eV AB2 bands

provide light absorption and consequently activation of TiO_2 in this spectral region (Kuznetsov and Serpone 2006).

Photostimulated adsorption of O_2 acceptor molecules occurs on electron surface centers formed by trapping of photogenerated free electrons by surface defects, whereas photoadsorption of H_2 donor molecules takes place at hole surface centers (trapped photogenerated holes). Thus, irradiation into the AB1 and AB2 bands (Figs. 1 and 2) should also generate free electrons and free holes. A similar manifestation of color centers responsible for the AB1 and AB2 absorption bands in compositions of TiO_2 with various polymers (Kuznetsov and Serpone 2007) suggests that formation of color centers is initiated by photoholes and assisted by organic molecules, whereas the destruction of the same centers is initiated by photoelectrons and assisted by oxygen (see Sect. Optical Features of Doped TiO_2).

The above analysis leads to the conclusion that preparative methods of nominally pristine TiO_2 and/or pretreatment of TiO_2 samples are reductive and ultimately provide an uncontrollable formation of intrinsic defect/color centers and thus long-term visible-light photoactivity. The number of these centers is unfortunately insufficient to be measured precisely by diffuse reflectance spectroscopy, but do become apparent in photoadsorption/photodesorption processes and in photoreactions of molecules. In practice, commercially available undoped TiO_2 photocatalyst specimens, including Degussa P25 TiO_2 (Lettmann et al. 2001; Li et al. 2004a; Ren et al. 2007) and Hombikat UV-100 TiO_2 (Lettmann et al. 2001) show appreciable activity in the photodegradation of various molecules even under visible-light irradiation. However, the origin of the visible-light activity of these specimens is not the subject of the present discussion.

3 Preparation and Characteristics of VLA TiO_2 samples

3.1 Undoped Titanium Dioxide Specimens

Hydrolysis of Ti(i-PrO)$_4$ in aqueous isopropanol by dispersion in dilute H_2SO_4 followed by calcination at ca. 700°C yields a sulfated anatase TiO_2, which displays weak absorption in the 400–600 nm region (Colon et al. 2006). XPS analysis shows that loss of surface acidic hydroxyl groups below 500°C, followed by decomposition of sulfate species, leads to formation of oxygen vacancies (V_Os) within the anatase lattice. Calcination above 600°C decomposes the surface sulfates, eliminates surface V_Os but leaves intact a significant number of stable subsurface oxygen vacancies, as indicated by XPS findings of low O/Ti ratios. Formation of stable V_Os during calcination at high temperatures leads to creation of intermediate states located within the band gap of TiO_2, responsible for the small absorption band in the visible spectral range (Fig. 4) subsequent to electron trapping by the V_Os. Although the existence of Ti^{3+} in the bulk also leads to a red shift in absorption, the XPS results precluded these species, and no shift in absorption edge of the anatase TiO_2 occurred (see inset in Fig. 4).

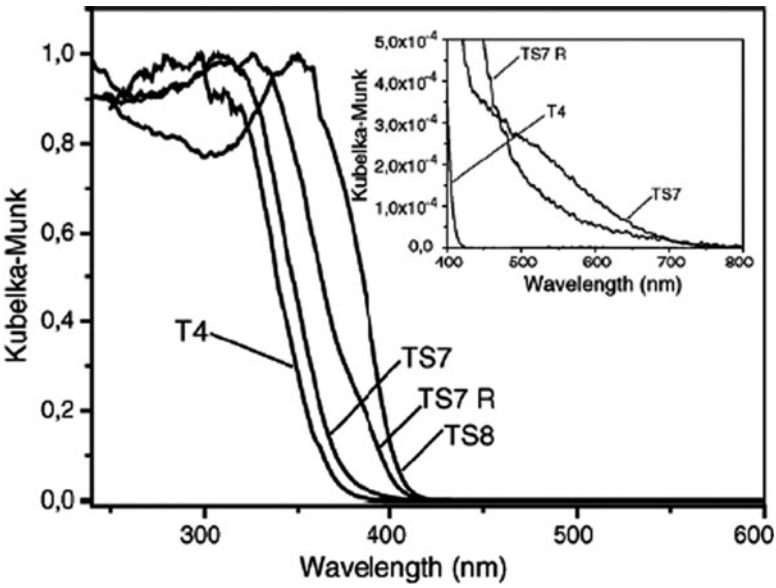

Fig. 4 UV–visible diffuse reflectance spectra for a series of sulfated TiO_2 specimens calcined at different temperatures (TS7 calcined at 700°C). Reproduced with permission from Colon et al. (2006). Copyright 2006 by Elsevier B.V.

Common methods used to create defect sites (e.g., V_O and/or Ti^{3+}) on the TiO_2 surface are typically UV-light irradiation, annealing the sample in vacuum, ion sputtering, and plasma treatment. These methods follow a previous step, which typically involves preparing crystalline TiO_2 powders/films. Suriye and coworkers (2006) have reported a new method of creating surface defects on TiO_2, which occurs concomitantly with the preparation of TiO_2 by the sol-gel method through varying the quantities of oxygen during the calcination process. Hydrolysis of titanium ethoxide in water/ethanol yields white precipitates of hydrous oxides, following which separation of the amorphous oxides by centrifugation and redispersion in ethanol minimizes particle agglomeration. Drying the resulting materials and calcining at 450°C in a N_2 mixture containing various quantities of O_2 (0–100 %) produces specimens with the anatase architecture (XRD analysis). Low-temperature (−196°C) EPR analysis confirmed the presence of Ti^{3+} species ($g = 1.996$) on the TiO_2 surface formed not by reduction of Ti^{4+} (low calcination temperature and absence of H_2) but during calcinations. That is, during oxidation of inorganic and organic residues that releases enough energy (increases with increase in O_2) to facilitate loss of surface OH groups by a process depicted in Fig. 5 and best summarized by reaction (3.1), according to which removal of an OH group that occupies positively charged oxygen lattice sites ($O^{\bullet}$) releasing H_2O_{gas} in addition to forming an oxygen atom at a neutral lattice site (O_{Ox}) and a double positively charged oxygen

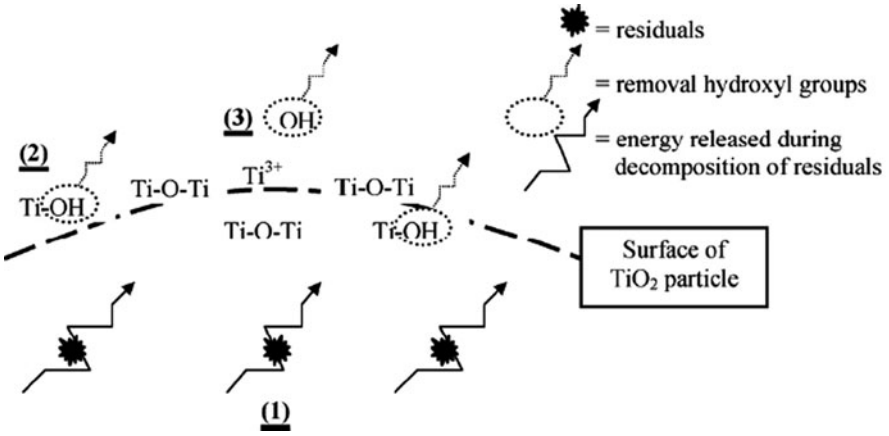

Fig. 5 Simplified scheme illustrating (*1*) the energy release during the degradation of residuals at high concentrations of O_2, (*2*) the loss of OH groups and (*3*) the formation of the surface defects (Ti^{3+}). Reproduced with permission from Suriye et al. (2006). Copyright 2006 by Elsevier B.V.

$$2(OH_{O^{\bullet}}) \rightarrow H_2O_{gas} + O_O x + V_O^{\bullet\bullet}(F^{++}) \tag{3.1}$$

notation; i.e., an F^{++} center, an anion vacancy V_A). Dehydroxylation of the metal-oxide surface can also lead to formation of F and F^{+} centers other than F^{++} centers (Mori-Sanchez et al. 2002). Germane to this discussion, Nakamura et al. (2000) showed that plasma-treated TiO_2 exhibits visible-light activity up to ca. 600 nm compared to untreated TiO_2 in the removal of NO. This was later confirmed by Ihara and coworkers (Ihara et al. 2001) by irradiation at $\lambda > 406$ nm. The process requires trapped electrons to convert NO to NO_3^- ions. Combined optical and EPR studies placed the wavelength above which no trapped electrons are observed at 639 nm. These authors located the V_O energy levels at 0.75–1.18 eV below the CB of TiO_2 (Fig. 6). The V_Os trap the electrons on excitation of the TiO_2 valence band with 506–614 nm visible-light radiation. The trapped electrons in the oxygen vacancies (F centers) determine the VLA activity of TiO_2, because the nanoparticles with F centers provide unique energy levels that correspond to visible-light excitation (see Fig.6). Sun and coworkers (2004a, b) examined F centers quantitatively by EPR in high-surface-area TiO_2 anatase nanoparticles prepared by metal-organic chemical vapor deposition (MOCVD) techniques. Surface rather than bulk processes dominate the temperature- and time-dependent concentration of F centers. Oxygen evolution occurs by the thermodynamic mechanism illustrated by reactions (3.2, 3.3), the sum of which yields the overall reaction (3.4).

$$O_{O^x} \rightleftarrows V_O^{\bullet\bullet}(F^{++}) + 2e^- + {}^1\!/_2 O_2(g) \tag{3.2}$$

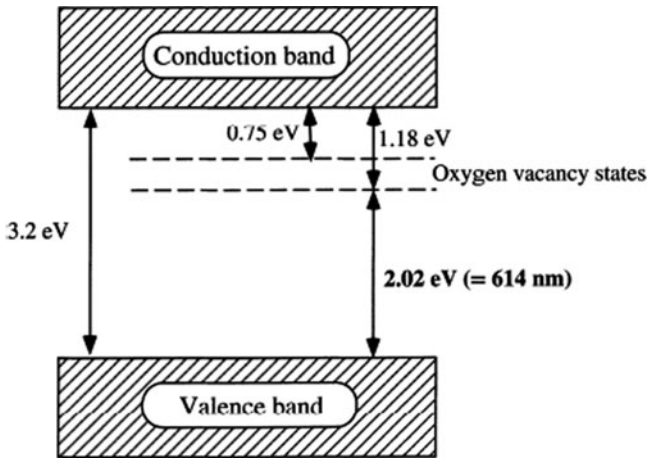

Fig. 6 A proposed band structure model for the anatase TiO_2 with oxygen vacancies. Reproduced with permission from Nakamura et al. (2000). Copyright 2000 by Elsevier Science B.V.

$$V_O^{\bullet\bullet}(F^{++}) + e^- \rightleftarrows V_O^{\bullet}(F^{+}) \tag{3.3}$$

$$O_{O^x} \rightleftarrows V_O^{\bullet}(F^{+}) + e^- + \tfrac{1}{2}O_2(g) \tag{3.4}$$

Germane to this, room-temperature photoluminescence (PL) spectra of TiO_2 nanowire arrays showed a broadband envelope in the visible spectral range that was resolved into three bands at ca. 425, 465, and 525 nm (Lei et al. 2001). In line with the work of Saraf et al. (1998), they were attributed to self-trapped excitons, F, and F^+ centers, respectively.

Hydrolysis of Ti(n-BuO)$_4$ in ethanol/water acidified with HNO_3 to catalyze the hydrolyic process and the condensation reactions yields TiO_2, which after drying at 120°C and calcining at 150–600°C gives TiO_2 specimens that absorb visible light (Fig. 7) (Lin et al. 2006). Specimens calcined at 150–300°C were particularly VLA in the degradation of NO_x pollutants. Anatase predominated at calcination temperatures below 500°C, while rutile was the dominant phase at 600°C. Some brookite also formed between 200 and 500°C (X-ray dispersion analysis, XRD).

Using a slightly modified but similar procedure from that of Lin et al. (2006), Dong and coworkers (Dong et al. 2006) placed Ti(n-BuO)$_4$ in absolute alcohol acidified with HNO_3, followed by dropwise addition of ethanol-water to hydrolyze completely the butoxide. Calcination at 300°C in air for 1 h gave a yellowish anatase (XRD) TiO_2 specimen whose absorption spectrum is reported in Fig. 8. Most intriguing, this procedure produced TiO_2 codoped with both C and N. X-ray photoelectron spectra (XPS) displayed two strong peaks in the C 1s spectrum at 284.6 and 281 eV due, respectively, either to graphitic or hydrogenated C–C bonds, or to Ti–C bonds with C in the latter case positioned either at interstitial or substitutional positions. The XPS N 1s spectrum showed peaks at 400 and

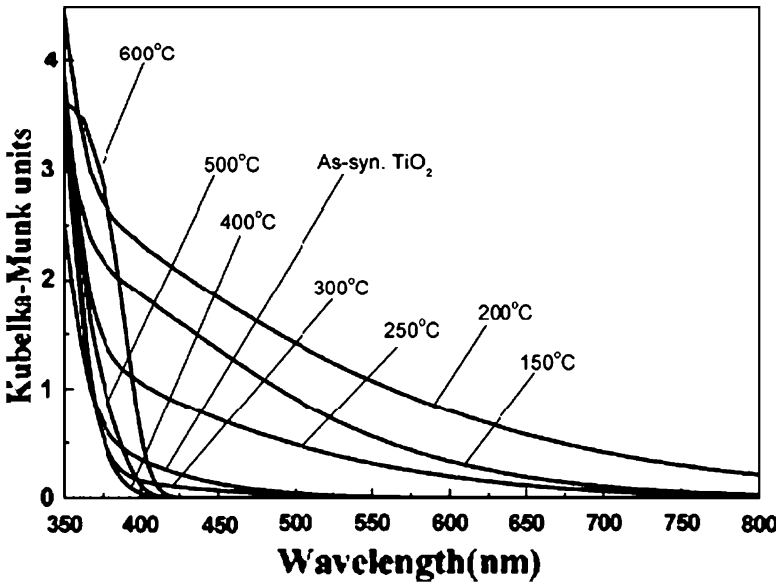

Fig. 7 UV–visible absorption spectra of sol-gel synthesized TiO_2 calcined at various temperatures. Reproduced with permission from Lin et al. (2006). Copyright 2006 by the American Chemical Society

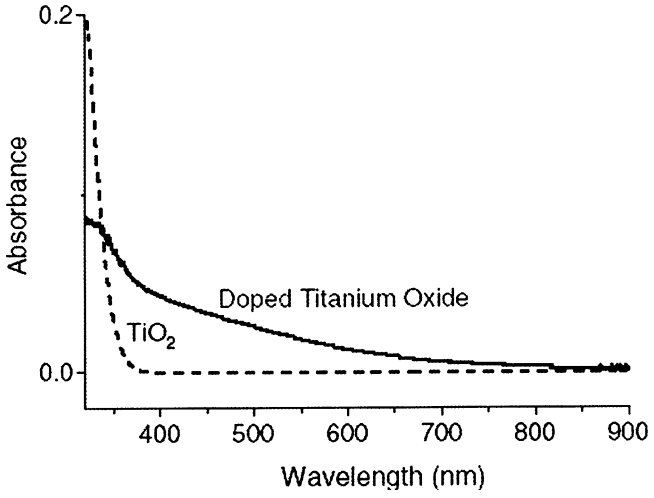

Fig. 8 UV–visible absorption spectra of $TiO_{2-x-y}C_xN_y$ (1.1% C and 0.4% N) and a commercial sample of TiO_2. Reproduced from Dong et al. (2006). Copyright 2006 by Springer

396 eV resulting, respectively from N–O and Ti–N bonding with N atoms in the latter case (band at 396 eV) substituting the O atoms in the lattice.

An interesting innovative method of using visible-light radiation to photoactivate pristine TiO_2 (Wang et al. 2006) to photogenerate electrons and holes involves doping TiO_2 with the upconversion luminescence agent $40CdF_2•60BaF_2•1.0Er_2O_3$ which converts visible light at 488 nm into five UV wavelengths between 200 and 450 nm. The preparation involves adding a mixture of the upconversion agent and nano-rutile TiO_2 powder to distilled water and then adequately dispersing it by ultrasound for ca. 30 min; after filtration and separation of the resulting powder, calcination at 500°C for 3 h gives the doped nano TiO_2 material.

3.2 Transition Metal-Ion Doped Titanium Dioxides

Anpo and Takeuchi (2003) were one of the first groups (if not the first) to make extensive use of metal-ion-implantation and RF-MS deposition methods to develop second-generation VLA TiO_2 photocatalysts, together with VLA small TiO_2 species incorporated within cavities and frameworks of zeolites and mesoporous rous molecular sieves. These methods have opened up several innovative venues to utilize sunlight or artificial UV–visible light.

Metal-ion implantation of TiO_2 with various 3*d* transition metal ions (e.g., V, Cr, Mn, Fe, and Ni) has led to a non-insignificant shift of light absorption by TiO_2 materials into the visible spectral region. Figure 9 illustrates this spectral shift in the absorption onset in the case of Cr ion-implanted TiO_2 with the extent of the red-shift being a function of the quantity and nature of the metal-ion dopant. The order of the red-shift followed the trend: V > Cr > Mn > Fe > Ni. However, the red-shifts in the absorption features were observed *only* after calcination of the metal-ion implanted TiO_2 samples in an O_2 atmosphere at temperatures around 450–550°C. By contrast, absorption spectra of Cr ion-doped TiO_2 prepared by impregnation or by chemical methods showed no shift of the TiO_2 absorption edge (Fig. 10).

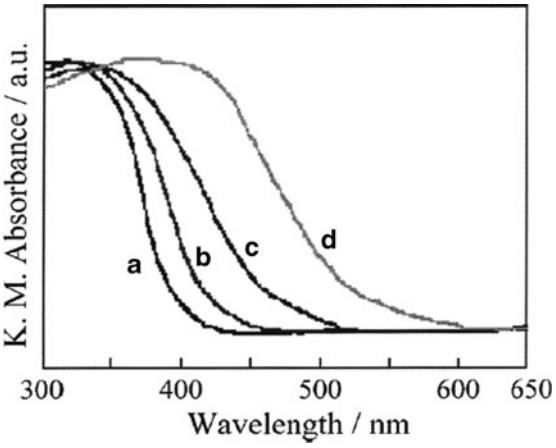

Fig. 9 UV–vis absorption spectra of (a) TiO_2 and (*b–d*) Cr ion-implanted TiO_2. The quantity of implanted Cr ions (μmol/g) is, respectively: (*a*) 0, (*b*) 0.22, (*c*) 0.66, and (*d*) 1.3. Reproduced with permission from Anpo and Takeuchi (2003). Copyright 2003 by Elsevier Science (USA)

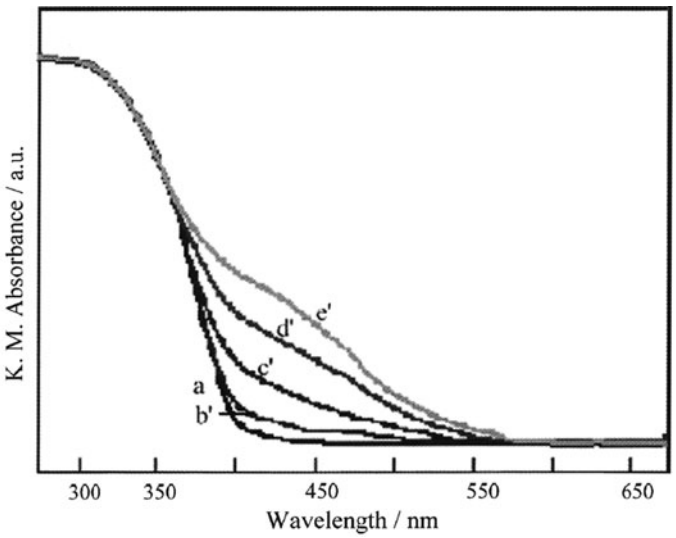

Fig. 10 UV–vis absorption spectra of (a) TiO_2 (a) and (b'–d') Cr ion-doped TiO_2 specimens prepared by an impregnation method. Amount (as μmol/g-TiO_2) of doped Cr ions was (*a*) 0, (b') 0.49, (c') 4.9, (d') 24.5, and (e') 49. Reproduced with permission from Anpo and Takeuchi (2003). Copyright 2003 by Elsevier Science (USA)

Clearly, the two completely different preparative methodologies altered the optical properties of TiO_2. UV-light (λ <400 nm) photoactivity of the metal-ion-implanted TiO_2s remained unchanged relative to undoped TiO_2s. The major difference between the two sets of TiO_2s is that in metal-ion implanted TiO_2 the metal-ion dopants do not act as electron-hole recombination centers, contrary to impregnated systems. However, the quantity of metal ions that can be implanted into the TiO_2 lattice has an upper limit, below which the photoefficiency increases with metal-ion concentration but above which the photoefficiency decreases.

XAFS spectra showed that in TiO_2 systems, doped either by impregnation or by a sol-gel method, the Cr ions are present as aggregated chromium oxides reminiscent of Cr_2O_3 and CrO_3. In contrast, in metal-ion implanted TiO_2 systems the Cr ions are present in highly dispersed and isolated states, i.e., states in which the Cr ions substitute Ti ions in the metal-oxide lattice.

Electrochemical anodization of Ti yields layers of TiO_2 nanotubes which, subsequent to Cr doping by metal-ion implantation, produces a TiO_2 with the anatase structure (XRD) but with a certain degree of amorphization of the TiO_2 (Ghicov et al. 2007). The effect is, however, reversible by subsequent thermal treatment. Visible-light photoresponsive Cr- and V-doped TiO_2 thin films supported on Vycor glass can also be fabricated by metal-ion implantation (Takeuchi et al. 2000). The films are quite photoactive in degrading NO_x to N_2 and O_2 at λ >450 nm.

Some unique VLA-active TiO_2 materials responsive to visible light at λ >450 nm have also been developed by implantation of V ions into TiO_2 thin films supported on a quartz substrate (Zhou et al. 2006). The films are photoactive in degrading

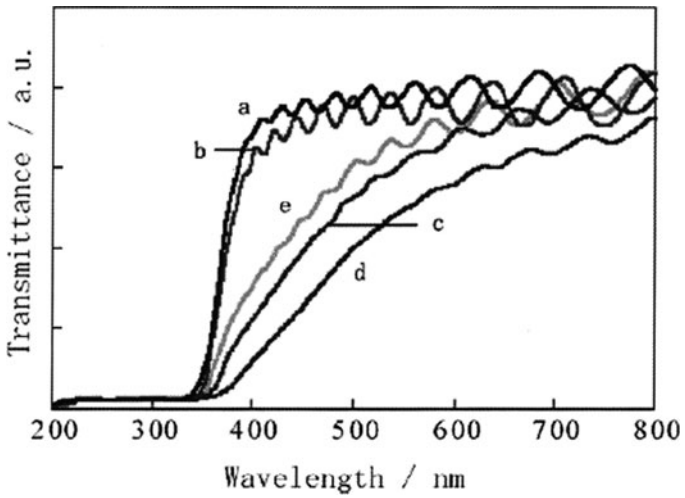

Fig. 11 UV–vis transmittance spectra of TiO_2 thin films prepared by the RF-MS deposition method at temperatures of (*a*) 100°C, (*b*) 200°C, (*c*) 400°C, (*d*) 600°C, and (*e*) 700°C. Reproduced with permission from Anpo and Takeuchi (2003). Copyright 2003 by Elsevier Science (USA)

HCOOH to CO_2 and H_2O under visible-light irradiation ($\lambda > 450$ nm). XPS spectra showed no peaks attributable to VO_x species, indicating that the implanted V ions were dispersed deep inside the TiO_2 bulk lattice.

Anpo and Takeuchi (2003) also developed an alternative method to prepare VLA TiO_2 thin films by the RF-MS deposition method. Figure 11 displays the UV–visible diffuse reflectance spectra (DRS) of TiO_2 thin films prepared by RF-MS at different substrate temperatures. Films prepared at temperatures above 500°C exhibited efficient absorption in the visible region; the film prepared at 600°C showed the highest absorption.

VLA Cr-doped TiO_2s have also been obtained (Zhu et al. 2006a) by a combined sol-gel/hydrothermal treatment method in which the quantity of Cr decreased from the surface into the lattice (XPS, AAS). Preparation involves hydrolysis of Ti(i-PrO)$_4$ in acidified HNO_3 isopropanol/water. Aging the resulting mixture, followed by filtration and drying at70°C yields a dried TiO_2 gel, which is then Cr-doped by mixing it with a hydrated $Cr(NO_3)_3$ salt in water/isopropanol solvent and autoclaving it at 200°C for 8 h. EPR analysis showed that Cr^{3+} occupy Ti^{4+} positions in the anatase lattice (XRD) along with Cr^{4+} ions to maintain electroneutrality. The photoactivity of Cr-doped TiO_2 greatly improved under UV- and visible-light irradiation for optimal concentrations of Cr of 0.15 and 0.2%, respectively. Doping Cr^{3+} greatly increases light absorption of the TiO_2 in the visible spectral region. The band at 450 nm originated from either a charge transfer band $Cr^{3+} \rightarrow Ti^{4+}$ or from a d–d transition $^4A_{2g} \rightarrow {}^4T_{1g}$ of Cr^{3+} in an octahedral environment of the anatase TiO_2 network. The broad band at 620–800 nm apparently originated from $^4A_{2g} \rightarrow {}^4T_{2g}$ transitions of Cr^{3+}.

Except for metal-ion implantation, substitutional doping of TiO_2 with metal ions (e.g., Fe) by other preparative methods may also extend the photoresponse of TiO_2 to longer wavelengths. Regrettably, this does not guarantee photoactivity under visible-light irradiation.

VLA Fe-doped TiO_2 can be prepared (Teoh et al. 2007) by a one-step flame spray pyrolysis (FSP) technique. A mixture of Ti(i-PrO)$_4$, xylene and CH_3CN, together with a predetermined quantity of iron naphthenate (the Fe source), was atomized through a nozzle and combusted in a methane/oxygen flame. Increasing the Fe/Ti ratio from 0.005 to 0.30 gradually shifted the absorption threshold of the Fe-doped TiO_2 from 396 to 564 nm, corresponding to band gap energies of 3.13 and 2.20 eV, respectively. Donor levels of the Fe dopants were located within the TiO_2 band gap close to the valence band, allowing for *extrinsic* excitation of the doped TiO_2 under visible-light illumination. This implicates a transition of the higher energy level 3*d*-electrons from the Fe dopant to the TiO_2 CB. The absorption band at ~490 nm of Fe-doped TiO_2 at Fe/Ti ratios greater than 0.10, however, finds no accepted assignment as to whether it is due to a d–d transition or to a charge transfer transition. Both Navio et al. (1996) and Li et al. (2003) observed an absorption band centrally shifted to 530 nm in Fe-doped TiO_2 specimens synthesized by wet impregnation and sol-gel methods, respectively, followed by calcination at high temperatures. The 530-nm band was attributed to a segregated hematite phase subsequently confirmed by XRD methods.

Doping Fe^{3+} into TiO_2 during hydrothermal crystallization to optimize the distribution of iron in the TiO_2 anatase lattice (XRD) was achieved (Zhu et al. 2006b) by doping TiO_2 with different amounts of Fe^{3+} through a combined sol-gel/hydrothermal treatment methods in a manner otherwise similar to that used for Cr-doped TiO_2 (see above). EPR spectra confirmed incorporation of Fe^{3+} into the anatase lattice. UV–visible absorption spectra reported in Fig. 12 show both *intrinsic* band gap absorption at 380 nm for pure anatase TiO_2 (E_{bg} ~ 3.2 eV) and enhanced absorptions in the *extrinsic* region 400–650 nm with increasing Fe content. The band at ~415 nm is probably due to excitation of 3*d* electrons from Fe^{3+} levels to the TiO_2 CB (a charge transfer transition), whereas the broad band at ca. 500 nm likely originates from $^2T_{2g} \rightarrow {}^2A_{2g}$, $^2T_{1g}$ d–d transitions of Fe^{3+} or from charge transfer between two Fe^{3+} (reaction 3.5). However, the latter inference is highly unlikely, unless the two Fe^{3+} ions are in totally different environments in the TiO_2 lattice.

$$Fe^{3+} + Fe^{3+} \rightarrow Fe^{4+} + Fe^{2+} \tag{3.5}$$

Doping with Fe^{3+} can introduce additional V_Os on the surface and in the bulk of TiO_2, thus favoring adsorption of H_2O, formation of surface OH^- group, and promoting photoactivity. Efficient separation of photogenerated charge carriers (reaction 3.6) can also lead to increased activity as the Fe^{3+} can trap photogenerated holes (reaction 3.7) through Fe^{3+}/Fe^{4+} energy levels apparently located above the valence band edge of anatase TiO_2. Trapped holes in Fe^{4+} migrate to the surface and oxidize the OH^- groups to $^{\bullet}OH$ radicals (reaction 3.8). Countering reactions

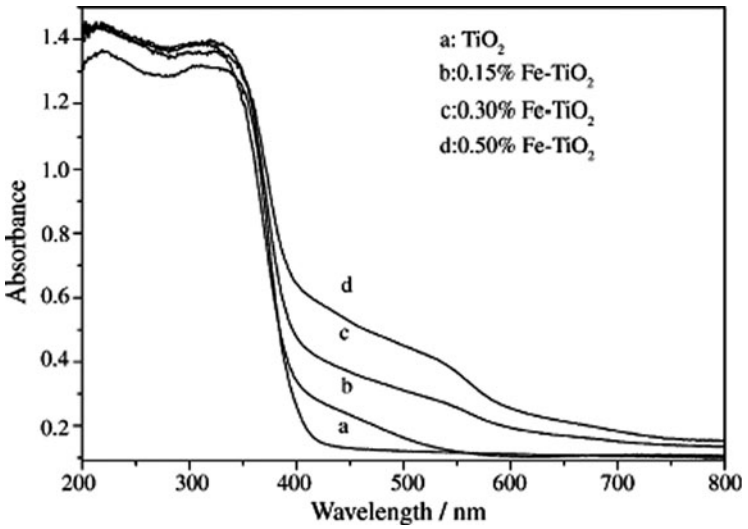

Fig. 12 UV–visible absorption spectra of: (a) TiO_2; (b) 0.15% Fe–TiO_2; (c) 0.3% Fe–TiO_2; and (d) 0.5% Fe–TiO_2. Reproduced with permission from Zhu et al. (2006b). Copyright 2006 by Elsevier B.V.

(3.6–3.8) are reactions involving the scavenging of photogenerated electrons at the surface by O_2 yielding superoxide radical anions, $O_2^{-\bullet}$, and ultimately $^{\bullet}OOH$ radicals on protonation. EPR spectral evidence showed that Fe^{3+} ions also act as traps of photogenerated electrons (Soria et al. 1991).

$$TiO_2 + h\nu \rightarrow e_{cb}^- + h_{vb}^+ \tag{3.6}$$

$$Fe^{3+} + h_{vb}^+ \rightarrow Fe^{4+} \tag{3.7}$$

$$Fe^{4+} + OH^-_{(ads)} \rightarrow Fe^{3+} + {}^{\bullet}OH_{(ads)} \tag{3.8}$$

VLA zinc-ferrite doped titania, $TiO_2/ZnFe_2O_4$, prepared by a sol-gel method followed by calcination at different temperatures (400–600°C) displays DRS spectra that show the absorption edge to be red-shifted to longer wavelengths (Fig. 13) (Cheng et al. 2004). XRD results indicated a stable TiO_2 anatase phase under these conditions.

Thin films of Au-doped TiO_2 on various supports (glass slides, glass helix, silica rashig rings), prepared by sol-gel dip coating from a sol of colloidal gold and titanium peroxide (Sonawane and Dongare 2006), showed a red-shift of the absorption edge (band at 550 nm). This resulted from incorporation of Au particles into the TiO_2 nano-architecture subsequent to calcination at 200–800°C. XRD analyses indicated an anatase structure and no rutile until 600°C. However, at 800°C the XRD pattern showed little change in the anatase/rutile ratio. Apparently, the

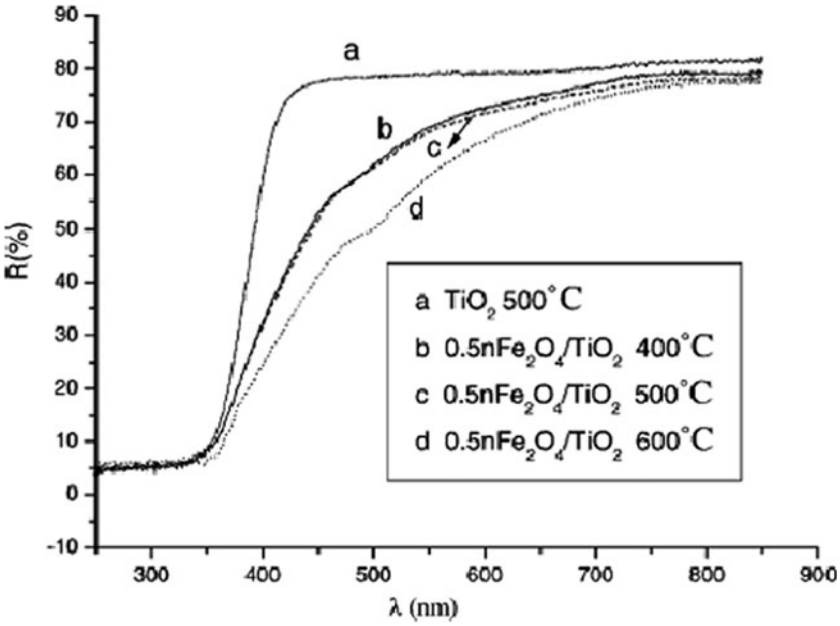

Fig. 13 Diffuse reflectance spectra of $TiO_2/ZnFe_2O_4$ calcined at the various indicated temperatures. Reproduced with permission from Cheng et al. (2004). Copyright 2004 by Elsevier B.V.

anatase-to-rutile phase change was inhibited, or at best slowed down, due to the presence of gold.

VLA platinum-loaded TiO_2 thin films decomposed H_2O in the presence of CH_3OH (H_2 evolved) and in the presence of $AgNO_3$ (O_2 evolved) under visible-light irradiation at $\lambda \geq 420$ nm. The latter process also occurred at $\lambda > 550$ nm on thin films fabricated at 600°C using the RF-MS method (Matsuoka et al. 2005; Kitano et al. 2006a, 2007). A calcined TiO_2 plate was the source material and Ar gas was the sputtering gas at pressures $p_{Ar} = 1.0–3.0$ Pa during deposition. The films, denoted Vis-TiO_2/X (X = 1.0, 2.0 or 3.0 for P_{Ar}), displayed absorption bands extending to the near-IR region with a broad band at ~600–800 nm, particularly for Vis-TiO_2/1.0 due to Ti^{3+} centers. The latter centers were later confirmed by EPR spectroscopy. XRD spectra showed a Pt-loaded TiO_2 and the presence of a small quantity of PtO. This particular specimen displayed only low visible-light-activity toward O_2 evolution, probably because the Ti^{3+} sites acted as charge carrier recombination centers. More successful was the Vis-TiO_2/2.0 specimen for the decomposition of water. A SIMS examination revealed that the latter sample exhibited an O/Ti ratio at the surface of 2.00 ± 0.01; the O/Ti ratio was 1.93 ± 0.01 deep in the bulk. Band gap energies of Vis-TiO_2/X were smaller than for the UV-TiO_2. This particular point will be discussed later in the chapter when we take up the question of whether or not there is band gap narrowing in doped TiO_2s.

Deposition and adsorption of Au on TiO_2 lead to the appearance of occupied metal-induced states above the TiO_2 valence band (~1.6 eV; oxygen vacancies), which enhance the reactivity by altering the rate of exchange of V_Os and thereby facilitating the migration of the V_Os from the bulk to the surface of the oxide, a highly exothermic process; $\Delta E = -41.6$ kcal mol^{-1} (Rodriguez et al. 2002). Gold adatoms also enhance the relative stability of surface V_Os through a complex situation in which the Au adatoms modify the rate of exchange of V_Os. The concomitant presence of V_Os on the TiO_2 surface electronically perturbs the Au adatoms and renders them chemically more active.

Cerium(III)-doped TiO_2 is preparable by a sol-gel process in which Ti(*n*-BuO)$_4$ is hydrolyzed in the presence of $Ce(NO_3)_3$, absolute ethanol and acetic acid (Li et al. 2005d). Aging and drying the gel at –20°C under vacuum followed by calcination at 500°C yields the Ce-doped TiO_2 containing Ti^{3+}, Ce^{3+} and Ce^{4+} ions in the TiO_2 lattice (XPS analysis). Diffuse reflectance spectra showed significant absorption between 400 and 500 nm due to excitation of valence band electrons to the cerium 4*f* levels.

3.3 Anion-Doped Titanium Dioxide Specimens

So far we have seen that VLA TiO_2s, in which the absorption onset is red-shifted to longer visible wavelengths, can be produced by reductive methods (e.g., H_2 plasma, high-temperature treatments, UV-light irradiation) and by doping TiO_2 with suitable first-row transition metal ions by a metal-ion implantation technique. Since the latter requires sophisticated instrumentation, otherwise not available in many laboratories, the combined sol-gel/hydrothermal treatment methods has achieved equivalent aims in preparing VLA-active TiO_2s responsive to sunlight wavelengths with increased photoactivity and photoefficiency. TiO_2s doped with non-metal dopants such C, S, N, and F (and others) have received exceptional attention since they require less sophisticated methods. Accordingly, non-metal doped TiO_2s have attracted the imagination of many aficionados of heterogeneous photocatalysis for both environmental remediation and solar energy harvesting and storage. It is therefore relevant to describe various preparative procedures and the pertinent UV–visible spectral properties that have made non-metal doped TiO_2s such a fascinating topic of current research with recent reports describing TiO_2 materials codoped with two non-metals.

The facile preparation of TiO_2 specimens that respond to visible-light activation, in particular N-doped TiO_2, has attracted considerable interest ever since the study (although not the first) by Asahi and coworkers (2001). It is, therefore, instructive to examine some of the reasons that led this group to propose non-metals as being more suitable dopants to achieve photocatalysis in the visible spectral region.

Asahi et al. (2001) initally set three requirements to achieve visible-light-activity: (i) doping should produce states in the band gap of TiO_2 that absorb visible light; (ii) the CB minimum, including subsequent impurity states, should be as high as that of

TiO_2 or higher than the H_2/H_2O level to ensure photoreductive activity; and (iii) the states in the (band) gap should overlap sufficiently with the band states of TiO_2 to transfer photoexcited carriers to reactive sites at the TiO_2 surface within their lifetime. Metal dopants were not deemed desirable because they did not meet conditions (ii) and (iii) as they often produce localized d states deep in the band gap of TiO_2 and tend to act as recombination centers of e^- and h^+. Calculations of density of states (DOS) of substitutional doping with several non-metals (C, N, F, P, or S) into O sites in anatase TiO_2 by the full-potential linearized augmented plane-wave (FLAPW) formalism in the framework of the local density approximation (LDA), led these workers to chose N as most effective because the N 2*p* states apparently contribute to band gap narrowing (more on this topic later) through mixing with O 2*p* states in the valence band. Though S doping also led to band gap narrowing, it was dismissed because of apparent difficulties in substituting an S^{2-} ion into O^{2-} sites (the size of S^{2-} is greater than O^{2-}), Carbon and phosphorous doping were also dismissed as they may introduce states too deeply buried in the band gap and so would not satisfy condition (iii). However, both C- and S-doped TiO_2s have since been reported, and DFT calculations have since been also refined.

3.3.1 Carbon-Doped Titanium Dioxide

Soon after the study by Asahi et al. (2001), Khan and coworkers (Khan et al. 2002) reported efficient (apparently ~8.35%) photochemical water splitting by C-doped rutile TiO_2 produced by controlled combustion of a Ti metal sheet in the presence of CO_2 and water vapor in a natural gas flame (850°C) that led C atoms to substitute the lattice O atoms. The two rutile TiO_2 films (XRD) absorbed visible light to $\lambda < 535$ nm with two absorption thresholds: 535 nm and 440 nm that were attributed to two compositions of the $TiO_{2-x}C_x$ system. The band gap of TiO_2 was said to be lowered from 3.0 eV of rutile to 2.32 eV.

Hoping to synthesize N-doped TiO_2 through hydrolysis of $TiCl_4$ in the presence of $(Butyl)_4NOH$, Sakthivel and Kisch (2003a) discovered that after calcination of the TiO_2 powder at 400°C, followed by a further heat treatment at 550°C produced C-doped rather than N-doped anatase TiO_2 (XRD; traces of rutile). XPS spectra displayed C 1*s* peaks at 285.6, 287.5, and 288.5 eV with the first peak attributed to adventitious elemental carbon and the latter two peaks to the presence of carbonate species later confirmed by IR spectroscopy. Diffuse reflectance spectra showed new absorption features in the range 400–700 nm with an absorption onset at 735 nm (1.70 eV) attributed to various surface states above the valence band of TiO_2. Benzoic acid was converted to salicylic acid on excitation of the C-doped $TiO_{2-x}C_x$ specimen in the presence of oxygen at $\lambda \geq 320$ nm (3.88 eV), 455 nm (2.73 eV) and 495 nm (2.51 eV); 4-chlorophenol was photomineralized at $\lambda = 455$ nm.

Thermal treatment of TiO_2 photoelectrodes in a hexane-rich environment led (a) to incorporation of C into TiO_2 after annealing in an *n*-hexane/argon atmosphere at 500°C (Enache et al. 2006) and (b) to creation of oxygen vacancies in the blackish-colored TiO_2. The coloring originated with C deposits on the TiO_2 surface, which

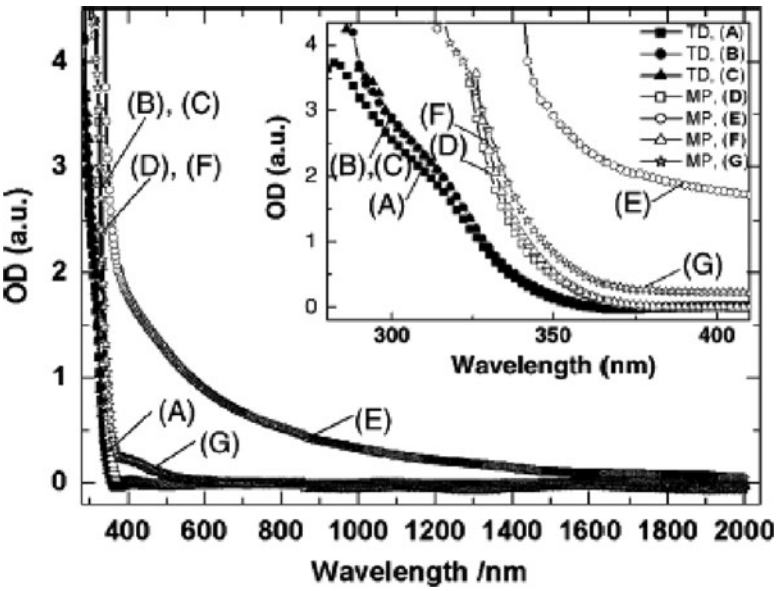

Fig. 14 Optical absorption spectra for thin dense and mesoporous TiO_2 films. (*A*, *D*) undoped TiO_2; (*B*, *E*) annealed in hexane/argon at 500°C; (*C*, *F*) re-oxidized in air at 450°C; (*G*) mesoporous TiO_2 film reduced in an argon/hydrogen atmosphere at 500°C. Reproduced with permission from Enache et al. (2006). Copyright 2006 by Elsevier B.V.

failed to enhance photoactivity in the visible spectral range. Some C (<0.1 at.%) did diffuse into the bulk of TiO_2 causing a very small shift (~0.05–0.1 eV) of the absorption edge to longer wavelengths (Fig. 14). The presence of C atoms prolonged the anatase-to-rutile phase conversion to temperatures greater than 800°C, and the films retained the anatase structure after the hexane treatment even after subsequent reoxidation (XRD measurements).

Using a different approach, Xu et al. (2006) prepared C-doped TiO_2 by hydrolyzing $TiCl_4$ in the presence of $(C_4H_9)_4NOH$ as the C source and in the presence of glucose/NaOH. Extended aging at ambient temperatures and calcination at 400–500°C gave $TiO_{2-x}C_x$ (anatase; XRD) that absorbed visible light to ca. 800 nm (Fig. 15). The $TiO_{2-x}C_x$ sample prepared from $(C_4H_9)_4NOH$ as the C source showed a single band gap energy (2.76 eV), whereas $TiO_{2-x}C_x$ made from glucose exhibited two band gap energies (2.78 and 1.45 eV), in apparent accord with the calculations of Nie and Sohlberg (2004). Although the carbonaceous $TiO_{2-x}C_x$ prepared from $(C_4H_9)_4NOH$ (16 C atoms) vs. glucose (6 carbons) showed enhanced visible light absorption, it nevertheless hindered visible-light activity. With glucose as the C source, more C atoms entered the TiO_2 lattice by replacing O atoms, lowering the band gap energy and contributing to the visible-light activity of $TiO_{2-x}C_x$. Soaking P-25 TiO_2 into a solution of $(C_4H_9)_4NOH$ for ~150 h followed by calcination also produced a TiO_2 material with significant absorption in the visible spectral range (Xu et al. 2006). An alternative to the latter procedure involved

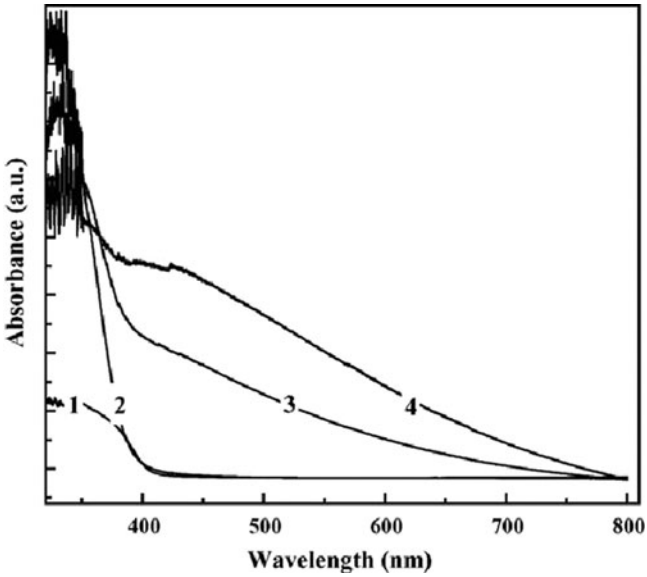

Fig. 15 Effect of aging time on UV–vis spectra of the samples: (1) reference or regular TiO_2 (hydrolysis of $TiCl_4$ with NaOH); (2), (3), and (4) C-doped TiO_2 samples aged for 12, 100,and 150 h, respectively, in the presence of tetrabutylammonium species; all samples were rinsed thoroughly before calcinations at 400–500°C. Reproduced with permission from Xu et al. (2006). Copyright 2006 by Elsevier B.V.

subjecting TiO_2 to ethanol vapors at 150–400°C, yielding a VLA C-doped TiO_2 that could photodegrade phenol (Janus et al. 2006).

The use of a hydrothermal method at temperatures as low as 160°C also produced VLA $TiO_{2-x}C_x$ in two stages (Ren et al. 2007). The first stage prepared amorphous TiO_2 by controlled hydrolysis of $Ti(i\text{-}PrO)_4$. In the second stage, the aqueous TiO_2/glucose (the C source) suspension was autoclaved at 160°C yielding anatase $TiO_{2-x}C_x$ (XRD). The XPS spectrum showed C 1*s* signals at 284.8 and 288.6 eV; the first signal due to elemental carbon and the 288.6 eV peak consistent with C–O bonds in the lattice in which C substituted Ti atoms to form a Ti–O–C structure. This is in fact different from the case (Khan et al. 2002) where C-doped TiO_2 was fabricated by flame oxidation in which the C dopant substituted lattice O atoms. Optical absorption of the as-prepared VLA $TiO_{2-x}C_x$ extended to 450 nm. Three reasons might explain the VLA photoactivity: (i) the C-doped TiO_2 had a high surface area and thus provided more active sites and adsorbed more reactive species, (ii) C substituted lattice Ti atoms close to or on the surface, and (iii) with the apparent narrowing of the band gap more light was absorbed than was otherwise the case for undoped TiO_2.

Photoactivities of photogenerated h^+ during UV or visible laser flash photolyses of pure anatase TiO_2 and S- and C-doped TiO_2 powders have been examined by time-resolved diffuse reflectance (TDR) spectroscopy (Tachikawa et al. 2004).

Although one-electron oxidation of methanol and 4-(methylthio)phenyl methanol occurred under 355-nm laser irradiation, no oxidation of these substrates occurred during the 430-nm laser photolysis of S- and C-doped TiO_2 powders, even though sufficient charge carriers were generated. The C-doped anatase TiO_2 was prepared by mixing thiourea, urea and (ST-01) TiO_2 powder, followed by calcination at 400°C. The content of C atoms on the C-doped TiO_2 surface was ~0.4 at.%; carbonate (CO_3^{2-}) species were incorporated into the bulk phase of the TiO_2. XPS spectra showed no peaks attributable to either N or S atoms in the C-doped specimen. Absorption of visible light by $TiO_{2-x}C_x$ was stronger than for the S-doped TiO_2, even though the content of S atoms (1.6 at.%) on the surface of TiO_2 was greater than that of C (0.4 at.%).

3.3.2 Sulfur-Doped Titanium Dioxides

Despite the earlier reservations by Asahi et al. (2001), Umebayashi and coworkers (2002) synthesized S-doped anatase TiO_2 (XRD) by oxidative annealing of TiS_2 at 600°C, causing S atoms to occupy O-atom sites and to shift the absorption edge to longer wavelengths. *Ab initio* calculations inferred that mixing of the S 3*p* states with the valence band O 2*p* states presumably contributed to the narrowing of the TiO_2 band gap through an increase of the valence band width. In an alternate method, mixing Ti(i-PrO)$_4$ and thiourea in ethanol followed by evaporation of the solvent and calcination of the white residue at 400°C in air gave S-doped anatase TiO_2; S content was 1.6 at.% (Ohno et al. 2003, 2004). XPS analyses revealed no peak attributable to either C or N atoms or to S^{2-} ions after the calcination treatment. The absorption edge shift to lower energy in the spectrum of S-doped TiO_2, relative to pure anatase TiO_2, was again attributed to an increase of the valence band width and to a narrowing of the band gap (Tachikawa et al. 2004). Adsorption of Fe^{3+} ions (0.90 wt.%) on S-doped TiO_2 increased the photoactivity of $TiO_{2-x}S_x$ further, but decreased it at loadings of 1.0 wt.% or greater (Ohno et al. 2006). In their XPS study of S 2*p* spectra, Ohno et al. (2004) detected no signals for S^{2-} ions but clearly detected signals for S^{4+}. They speculated that the latter species substituted Ti^{4+} in cation sites. This led to some controversy about the nature of the S dopants in $TiO_{2-x}S_x$ specimens, because of the likelihood that the quantity of S^{2-} anions in O^{2-} sites may have been too low to be detected and that a large quantity of SO_3^{2-} ions may have been produced by the partial oxidation of thiourea when mixed with TiO_2 particles (Matsushima et al. 2007).

Calcination of a mixture of $TiCl_3$ and NH_4SCN at 400°C yielded (yellowish) S-doped anatase TiO_2 whose XPS spectra showed a S 2*p* signal at 170 eV, consistent with an S^{6+} species doped on the TiO_2 surface. The 170-eV peak vanished following Ar^+-ion etching of the specimen (Katoh et al. 2006). The XPS results inferred the presence of SO_4^{2-} species on the TiO_2 surface. UV–visible absorption spectra (Fig. 16) show the absorption edge of S-doped TiO_2 to be shifted to longer wavelengths (lower band gap energy) relative to undoped TiO_2 prepared under otherwise identical conditions but in the absence of thiocyanate, and relative to ST-01 TiO_2.

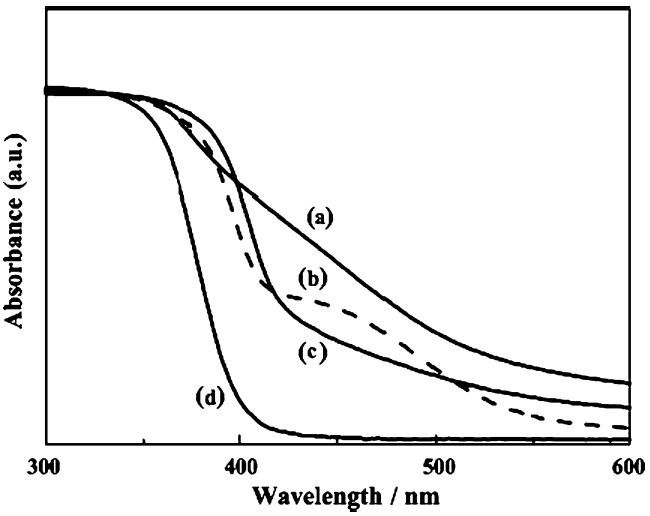

Fig. 16 Diffuse reflectance spectra of (*a*) S-doped TiO_2 (NH_4SCN = 13 M), (*b*) S-doped TiO_2 (NH_4SCN = 1 M), (*c*) TiO_2 prepared without ammonium thiocyanate, and (*d*) ST-01 TiO_2. Reproduced with permission from Katoh et al. (2006). Copyright 2006 by Elsevier Inc.

The degradation of methylene blue was significantly greater for the VLA S-doped specimen (1 M) than for ST-01 TiO_2 alone under otherwise identical irradiation conditions at $\lambda > 400$ nm.

Subjecting a mixture of TiO_2 and TiS_2 powdered samples of different ratios to mechanical grinding, using a planetary ball mill for different times, produced S-doped anatase TiO_2 whose S doping limit was around 1% (Wang et al. 2007b). For short milling times (e.g., 20 min) Raman spectra and XRD analyses indicated the S-doped TiO_2 to consist mostly of anatase. Milling for 60 min produced a specimen with a rutile TiO_2 structure.

3.3.3 Fluorine-Doped Titanium Dioxide

Spray pyrolysis (SP) of an aqueous solution of H_2TiF_6 at temperatures 800, 900, and 1,000°C produced F-doped TiO_2 powders with a single anatase architecture at T <900°C (XRD analysis). The samples showed significant visible-light activity even though F-doping had no effect on the fundamental absorption edge (Fig. 17a) (Li et al. 2005a) in accord with the calculated results of F- doped TiO_2 reported by Yamaki et al. (2003). It appears that localized levels of the F 2*p* state lie below the valence band of TiO_2 and consequently cannot mix with states in the valence and conduction bands. Thus, they cannot contribute to the optical absorption by F-doped TiO_2. PL spectra revealed two kinds of (surface) oxygen vacancies (*F* and F^+ centers) formed by F-doping (Fig. 17b) and responsible for the high visible-light activity in the decomposition of acetaldehyde (CH_3CHO) and trichloroethylene

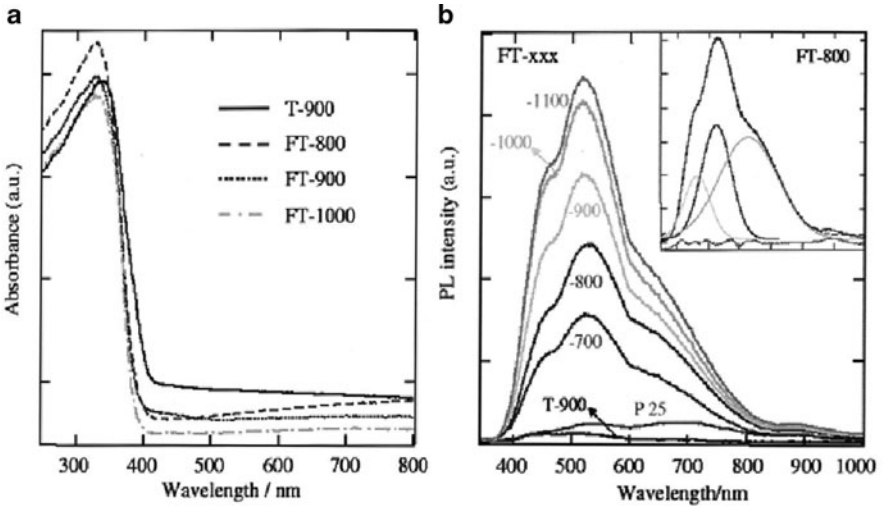

Fig. 17 **(a)** UV–Visible absorption spectra of the F-doped TiO_2 powders. The spectrum of TiO_2 prepared at 900 C under otherwise identical conditions but using a $TiCl_4$ precursor is also reported for comparison. **(b)** Photoluminescence spectra of the F-doped TiO_2 powders prepared by spray pyrolysis at various temperatures. The inset shows the spectral deconvolution of the spectra of the F-doped sample prepared at 800 C. Reproduced with permission from Li et al. (2005a). Copyright 2005 by Elsevier B.V.

($CCl_3CH{=}CH_2$). Evidently, the visible-light-driven photoactivity was achieved by excitation into the absorption bands of the V_Os, i.e., by excitation of the F and F^+ centers. XRD analyses demonstrated a significant inhibition of the anatase-to-rutile phase change by the addition of "complexing" F^- ions. The broad band at 465 nm (peak 1) was attributed to the oxygen vacancy with two trapped electrons (i.e., the F center), whereas peak 2 at 525 nm was due to the oxygen vacancy with one trapped electron, i.e. F^+ center (Li et al. 2005a). However, that one or all three bands originated from the existence of Ti^{3+} centers is not precluded.

3.3.4 Nitrogen-Doped Titanium Dioxides

This section will illustrate several methods used to synthesize N-doped TiO_2 specimens, which Yates and coworkers (2006) have divided into three classes: (i) modify existing TiO_2 by ion bombardment, (ii) modify existing TiO_2 in powdered form, film, and single crystal, or else modify TiN by gas phase chemical impregnation, and (iii) grow $TiO_{2-x}N_x$ (crystals) from liquid or gaseous precursors.

In one of the earliest (1986) studies of N-doping TiO_2, Sato (1986) noted that calcination of $Ti(OH)_4$ in the presence of NH_4Cl, or aqueous NH_3 leads to photosensitization of TiO_2 if exposed to visible-light radiation. The powdered samples were NO_x-doped TiO_2 and NO_x impurity was the sensitizer. The same year, Noda et al. (1986) prepared yellow-colored anatase TiO_2 powders from aqueous

hydrazine and $TiCl_4$ solutions, and inferred that the visible-light absorption was due to the presence of oxygen vacancies.

In their 2001 seminal report in *Science*, Asahi et al. (2001) prepared crystalline $TiO_{2-x}N_x$ films by sputtering a TiO_2 target in a N_2/Ar gas mixture followed by annealing at 550°C in a N_2 atmosphere. XRD features indicated mixed anatase and rutile phases; a clean anatase TiO_2 film formed under an O_2/Ar atmosphere under otherwise identical conditions. The yellowish $TiO_{2-x}N_x$ films absorbed light below 500 nm. XPS N 1*s* spectra of $TiO_{2-x}N_x$ showed signals at 402, 400 and 396 eV, in contrast to the undoped TiO_2 film, which showed no 396 eV peak. In line with the work of Saha and Tompkins (1992), the 396-eV signal was assigned to atomic β-N, whereas the other two peaks were attributed to molecularly chemisorbed dinitrogen γ-N_2. Powdered samples of $TiO_{2-x}N_x$ were prepared using NH_3/Ar as the source of N followed again by calcination at 550–600°C. Only $TiO_{2-x}N_x$ systems with XPS peaks at 396 eV were photoactive toward the decomposition of methylene blue; optimal loading of N was ~0.25 at.%. Combined with theoretical results, Asahi et al. (2001) deduced that the sites for photoactivity under visible-light irradiation were those that substitutionally replaced O, i.e., sites associated with atomic β-N at 396 eV. In an earlier study, Lee et al. (1995) fabricated N-doped TiO_2 anatase films by MOCVD using Ti(i-PrO)$_4$ and N_2O at 420°C. Raman spectra showed no signs of rutile nor of a TiN phase. The XPS Ti 2*p* spectrum indicated that N was incorporated into the TiO_2 lattice forming Ti–N bonds.

A VLA anatase TiO_2 ($\lambda < 550$ nm) has also been prepared (Ihara et al. 2003) by calcining the hydrolysis product from $Ti(SO_4)_2$ with NH_3 in dry air at 400°C. XPS spectra showed only trace amounts of N. Most of the visible-light response was due to the oxygen-deficient stoichiometry.

Pale yellow, yellow, and dark green $TiO_{2-x}N_x$ ($x = 0$, 0.0050, 0.011, 0.019) powdered samples can be prepared by annealing anatase TiO_2 powder (ST-01) in a flow of NH_3 at 550, 575, and 600°C, respectively. XRD patterns indicated the samples retained the anatase structure and no TiN phase was present. XPS patterns revealed a 396 eV signal that confirmed N doping substitutionally into O sites to form O–Ti–N bonds. Noticeable shifts of the absorption edge into the visible spectral region were evident for $TiO_{2-x}N_x$ with the feature at $\lambda > 550$ nm attributed to Ti^{3+} since NH_3 decomposes into N_2 and H_2 at ca. 550°C, and H_2 reduces Ti^{4+} under these conditions. However, according to Irie et al. (2003) the band gap energy remained at 3.2 eV. Degradation of isopropanol with UV-light and visible-light radiations resulted in different quantum yields for the evolution of CO_2. This suggested that N-doping formed a narrow N 2*p* band above the valence band of TiO_2 as the existence of band gap narrowing in $TiO_{2-x}N_x$, espoused by Asahi et al. (2001), would have required identical spectral dependencies of quantum yields. Moreover, when irradiating with visible light the quantum yields decreased with increase in the quantity (x) of the dopant N because of the increase in V_Os with increase of x in $TiO_{2-x}N_x$. In this case, V_Os acted as recombination centers for the photogenerated charge carriers. Under UV irradiation, the quantum yields also decreased with increase in x, suggesting that the doping sites also acted as recombination centers.

Nanocrystalline porous N-doped TiO_2 thin films have been prepared by introducing N into TiO_2 by means of DC magnetron sputtering in N_2-containing plasma (Lindgren et al. 2003). At low N concentrations, the anatase product displayed new spectral features in the range $410 < \lambda < 535$ nm due to excitation of electrons to unoccupied states from local states located close to the valence band edge within the band gap. Nitrogen-doping had no effect on the CB edge. Band gap narrowing was deemed somewhat questionable by these authors. Despite the intense recombination of charge carriers caused by N-doping, the new band gap states created by N-doping improved the visible-light photoresponse at the expense of some losses of the UV response.

An alternative method used by Sakthivel and Kisch (2003b) to prepare slightly yellow N-doped anatase TiO_2 with various N loadings involved hydrolysis of $TiCl_4$ with a N-containing base such as aqueous NH_3, $(NH_4)_2CO_3$, or NH_4HCO_3, followed by calcination at 400°C. XPS spectra showed only a broad signal at ~404 eV, but no 396-eV peak attributable to nitridic N atoms. The broad signal was attributed to hyponitrite (NO^-) whose presence was confirmed by its IR spectrum. Contrary to assertions by Asahi et al. (2001), the valence band edge did not change on N-doping, despite the red shift of the TiO_2 absorption edge to ~520 nm. However, contrary to the inference by Lindgren et al. (2003), results from a photoelectrochemical study (Sakthivel and Kisch 2003b) noted a slight change in the electrochemical potentials of the CB of TiO_2 (Fig. 18) for three of the specimens. N-doping led only to a "modest band gap narrowing." In a subsequent study, Sakthivel et al. (2004) attempted to prepare a S-doped TiO_2 specimen following the procedure of Ohno et al. (2003), only to find that the specimen contained no S but did contain 0.09 wt.% N and 0.03 wt.% C (specimen TiO_2-N/A). XPS analysis of the N 1*s* spectra of this sample before and after sputtering revealed signals at 400.1 eV, 405.3 eV, and 412.2 eV in the "before" case. The lower energy peak was attributed to hyponitrite,

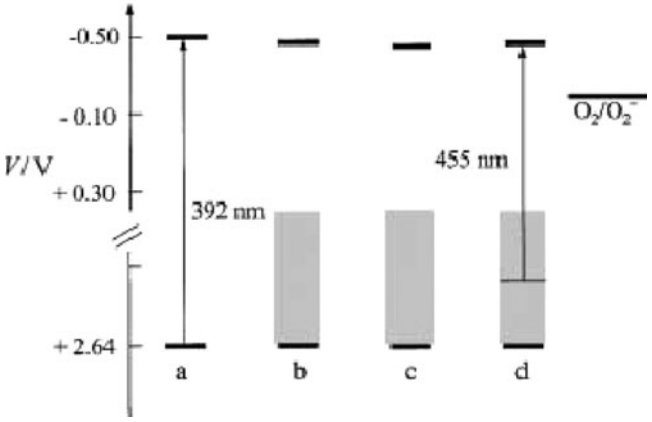

Fig. 18 Electrochemical potentials (vs. NHE) of band edges; shaded areas denote surface states; the oxygen redox potential at pH 7 is also shown. (a) TiO_2, (b) TiO_2–N/1, (c) TiO_2–N/2, (d) TiO_2–N/3. Reproduced from Sakthivel and Kisch (2003b). Copyright 2003 by Wiley-VCH

whereas the latter signals likely originated from NO_2^- ions. On removal of a 5-nm surface layer after sputtering, the 400.1-eV peak disappeared leaving the nitrite peaks that slightly shifted to 405.0 and 411.8 eV and two new peaks appeared at 406.8 and 409.2 eV that were assigned to NO_3^- and NO_2^-, respectively. They deduced that the hyponitrite species was located in the surface region, whereas NO_3^- and NO_2^- were present in the doped TiO_2 bulk lattice. Infrared evidence confirmed the presence of hyponitrite and nitrite ions in the TiO_2-N/A sample and also revealed the presence of CO_3^{2-} species. However, any visible-light photoresponse was due to the N dopants and not to the presence of C. Two additional anatase specimens, TiO_2-N/B and TiO_2-N/C, were prepared from the hydrolysis of Ti(i-PrO)$_4$ and $TiCl_4$ in the presence of thiourea in (absolute) ethanolic media, followed by calcining the resulting powders at 600 and 400°C, respectively. Diffuse reflectance spectra showed only a minor red shift of the TiO_2 absorption edge affording band gap energies 2.99, 2.95, 2.95, and 2.91 eV for non-doped TiO_2 and for the TiO_2-N/A, TiO_2-N/B, and TiO_2-N/C samples, respectively.

Yellowish N-doped rutile TiO_2 samples can also be prepared mechanochemically by high-energy ball milling of P-25 TiO_2 with various quantities of hexamethylenetetramine (HMT) under different milling conditions at near-ambient temperature (Yin et al. 2003). This method converted all the anatase phase (ca. 80%) in P-25 TiO_2 to rutile. Post-milling calcination in air at 400°C gave an N-doped product which displayed two absorption edges at ca. 400 and 550 nm and good visible-light photoresponse toward the oxidation of NO.

Yang and Gao (2004) obtained N-doped TiO_2 by hydrolysis of tetrabutyl titanate in the presence of thiourea in ethanolic media. On treating the white powder in an NH_3 flow at 450 and 500°C for 6 h and at 450°C for 3 h produced, respectively, brown (A), blackish brown (B), and wine-colored (C) specimens. The XPS N 1*s* spectrum of (A) displayed a relatively strong peak at 396 eV assigned to substitutional β-N states (O substituted by N in the TiO_2 lattice) considered the photoactive sites under visible-light irradiation. The peak at ~400 eV was attributed to molecularly chemisorbed nitrogen, γ-N_2. No peak attributable to S was observed for the three samples (XPS analyses).

Crystallized anatase $TiO_{2-x}N_x$ films with considerable amount of substitutional N atoms (1.8 at.%) and chemisorbed molecular N_2 are produced by ion-assisted electron-beam evaporation using rutile titania powder as the TiO_2 source material and molecular nitrogen as the N source (Yang et al. 2004). XPS spectra showed two peaks with binding energies at 402 and 396 eV, also assigned to molecularly chemisorbed γ-N_2 and atomic β-N, respectively; Ti 2*p* XPS spectra revealed Ti^{4+} $2p_{3/2}$ and Ti^{4+} $2p_{1/2}$ in the anatase TiO_2 film indicating the majority of titanium in the $TiO_{2-x}N_x$ film to consist of Ti^{4+} confirming results from XRD patterns. Raman spectra revealed N-doping caused no changes to the anatase TiO_2 structure.

Using a simple nanoscale synthetic route, Gole et al. (2004) produced in a matter of seconds at *room temperature* $TiO_{2-x}N_x$ samples employing direct nitridation of anatase TiO_2 nanostructures with alkylammonium salts. The resulting doped specimens could be tuned to absorb light across the visible spectral region (to λ ~550 nm). The method required first formation of the metal-oxide colloids by controlled

hydrolysis of Ti(i-PrO)$_4$ in an aqueous/isopropanol medium at pH 2 (HNO_3). Subsequent treatment of the initial nanoparticle colloidal sol or the partially agglomerated gel (solution) to excess triethylamine led to nitridation of the TiO_2 nanocolloids to $TiO_{2-x}N_x$. XRD and HRTEM results demonstrated the treated $TiO_{2-x}N_x$ nanoparticle structures to correspond predominantly to the anatase architecture. Diffuse reflectance spectra of the $TiO_{2-x}N_x$ crystallites, generated from the nanoparticle solutions, rose sharply at ~450 nm, whereas the corresponding spectrum for the nitrided $TiO_{2-x}N_x$ from the partially agglomerated nanoparticles rose at ~550 nm. XPS analysis with Ar^+-ion sputtering revealed the presence of N dopants not only at the surface but also incorporated into the sublayers of the $TiO_{2-x}N_x$ agglomerates (N content, 3.6–5.1 at.%). Although interstitially dissolved nitrogen and perturbation of the TiO_2 lattice structure might be associated, at least in part, with γ-N_2 features that contribute to the XPS spectra, no evidence was found for conversion of the anatase structure into the rutile architecture on N-doping for the initial TiO_2 nanocolloids and for the agglomerated gel solutions. More surprisingly, little if any XPS evidence of atomic β-N binding at 396 eV was found that might have been associated with any of the $TiO_{2-x}N_x$ or Pd-treated oxynitride samples. Rather, the XPS observations were consistent with nonstoichiometric surface-based Ti–O–N bonding.

That the visible-light responses of N-doped TiO_2 originates from an N-induced mid-gap level that forms slightly above the top of the O 2*p* valence band was inferred by Nakamura and coworkers (2004) from their mechanistic study into the photooxidation of water (evolution of O_2) through measurements of anodic photocurrents at N-doped TiO_2 film electrodes. These materials were prepared by two methods. In one (the dry method), anatase ST-01 TiO_2 was heated to 550°C in a reactor under a dry NH_3 flow. In the second (the wet method), the Ti(i-PrO)$_4$ precursor was hydrolyzed in aqueous NH_3 at 0°C followed by calcining the resulting white precipitate at 400°C. Both methods produced $TiO_{2-x}N_x$ anatase. The study concluded that photooxidation of organic compounds under visible-light illumination proceeds mainly by reactions with surface intermediates of water oxidation ($^\bullet$OH radicals) or oxygen reduction (superoxide radical anion, $O_2^{-\bullet}$), and not by direct reactions with holes that may have been trapped at the N-induced mid-gap level.

In a single-crystal study, Yates group at the University of Pittsburgh reported (Diwald et al. 2004a) that ion implantation of atomically clean TiO_2(110) surfaces with mixtures of N_2^+ and Ar^+ ions, followed by subsequent annealing under ultra-high-vacuum conditions, leads to incorporation of N into the TiO_2 lattice. XPS spectra revealed only the N 1*s* feature at 396.6 eV that they attributed to substitutionally bound nitride nitrogen (O^{2-} ions substituted by N^{2-} anions). However, contrary to expectations, the N-doped crystals containing only nitride ions exhibited a shift in the photothreshold energy of 0.2 eV to *higher* rather than *lower* energy compared to undoped TiO_2 (110). By contrast, N-doped TiO_2(110) rutile single crystals that had been treated in the presence of an NH_3/Ar gas mixture at ca 600°C exhibited photoactivity at the *lower* photon energy of 2.4 eV, i.e., 0.6 eV below the band gap energy of rutile TiO_2 (3.0 eV) (Diwald et al. 2004b). The active dopant state of the interstitial N responsible for this effect showed a N 1*s* binding energy at 399.6 eV attributed to a form of nitrogen likely bound to H. This is different from the

substitutional nitride state which displays an N 1*s* binding energy at 396.7 eV. Thus, a codoping effect between N and H may have been responsible for the enhanced visible-light photoactivity. Doped and undoped TiO_2(110) samples also showed an impurity XPS feature centered at 399.6 eV, which upon UV treatment in air and/or removal of the first 5 Å of the surface by Ar^+-ion sputtering led to extensive depletion of this signal. Evidently, traces of nitrogen had contaminated the metal-oxide surface. The inferences made by the Yates group *disagree totally* with the conclusions of Asahi et al. (2001) and those of others who claimed that nitridic nitrogens that substitute O^{2-} ions in the TiO_2 lattice are the necessary dopant species for TiO_2 photoactivity in the visible-light region.

In a subsequent report, Thompson and Yates (2005) again emphasized that the exclusive XPS N 1*s* signal at 396.7 eV, typically attributed to substitutional β-nitrogen seen in ion-implanted N-doped TiO_2, in and by itself alone cannot account for the *decrease* in the photothreshold of TiO_2(110) as observed for interstitially located N–H bound species. They proposed that the 0.2-eV *increase* in the photothreshold energy of N-doped TiO_2 systems was due to the deposition of charge in the low levels of the CB (the band-filling mechanism), thus the need for higher energy photons to excite valence band electrons into higher levels of the CB.

Although there is clear XPS evidence for the incorporation of β-substitutional N in N-doped TiO_2, there is no firm evidence of any appreciable photoactivity when these doped systems are irradiated with visible light (Yates et al. 2006), a point also raised by Frach et al. (2004) who noted no improvement in visible-light activity on N-doping TiO_2, and by Li and coworkers (2004b) who reported that the nature and level of visible-light activity depend on the nitriding compound employed. To confirm that N is indeed incorporated into TiO_2, Yates and coworkers (2006) used an atmospheric pressure thermal CVD coater to grow thin films of N-doped TiO_2 on glass substrates. The precursors were $TiCl_4$, ethylacetate and NH_3 with N_2 as the carrier gas. Of all the samples grown, only three displayed the XPS N 1*s* peak at 396 eV of atomic β-substituted N. These were films denoted N(1), N(2), and N(6) grown at 650°C under N_2 with flow rates of NH_3 in excess of 100 sccm. However, XPS N 1*s* spectra showed no evidence of the 397-eV signal typically due to the N^{3-} ion (TiN), but did reveal the presence of other fairly weak signals at 400 and 402 eV that may have arisen from molecularly chemisorbed N_2, from NH_x species located at interstitial sites (399.6 eV), from NO_x or NH_x (400 eV), or from an oxynitride (399.3 eV) of stoichiometry equivalent to $TiN_{0.5}O_{0.5}$. Some of the films displayed absorption features in the visible spectral region, but so did nominally undoped TiO_2 films indicating that N incorporation cannot be assumed on the basis of red-shifts of the absorption edge, a point that cannot be overemphasized enough. XPS evidence is required. And even though the presence of β-N incorporation and absorption spectral features in the visible region were seen in N-doped TiO_2 specimens, no visible light-induced photoactivity was observed, while the more conventional UV photoactivity was considerably reduced compared to films grown in the absence of NH_3. This led to the suggestion that the presence of β-nitrogen alone cannot be claimed to induce visible-light activity in N-doped TiO_2 films. This point has also been raised by Mrowetz and coworkers (2004) who prepared

two different yellow-colored N-doped TiO_2 samples: sample *A* obtained by the room temperature procedure described by Gole et al. (2004) using triethylamine as the N source, and sample *H* prepared by high-temperature nitridation of commercial anatase TiO_2 at 550°C under a NH_3/Ar gas flow. XPS spectra of sample *A* surface revealed intense peaks at 399.6 and 404.5 eV in the N 1*s* region. By contrast, the peak at 396 eV in the XPS spectra of *H* powders was weak and diffuse, even after Ar^+-ion sputtering. Despite these observations, however, the N-doped TiO_2 materials *failed to catalyze* the oxidation of $HCOO^-$ into $CO_2^{-}\bullet$, or NH_3-OH^+ into NO_3^- under visible-light illumination. The reaction between colloidal TiO_2 and triethylamine at 25°C most likely led to the formation of surficial organotitanium complexes that are readily degraded by UV light, rather than to substitutional N-doped TiO_2.

Nitrogen-doped TiO_2 nanoparticles consisting (XRD patterns) of pure anatase (pH 9, methanol), rutile (pH 9, ethanol), and brookite (pH 1, methanol) phases have been prepared successfully by a solvothermal process using a $TiCl_3$/HMT/alcohol (methanol or ethanol) mixed solution in an autoclave at 90°C, and then at 190°C yielding yellow and beige powders. These showed excellent visible-light absorption and visible-light activity at wavelengths greater than 510 nm (Fig. 19) (Aita et al. 2004). The two-step absorption seen in the DRS spectra of these samples became apparent only after calcination at 400°C. The first absorption edge related to the band structure of nondoped TiO_2, whereas the second absorption edge around 520–535 nm was due to the formation of an N 2*p* band located above the O 2*p* valence band in $TiO_{2-x}N_y$. No XPS data was reported.

Nitrogen-doped nanocrystalline TiO_2 (yellow) powders have also been synthesized by a procedure developed by Ma and coworkers (2005). It involved commercial anatase ST-01 TiO_2 heated at 500°C under a dry N_2 gas flow in the presence of

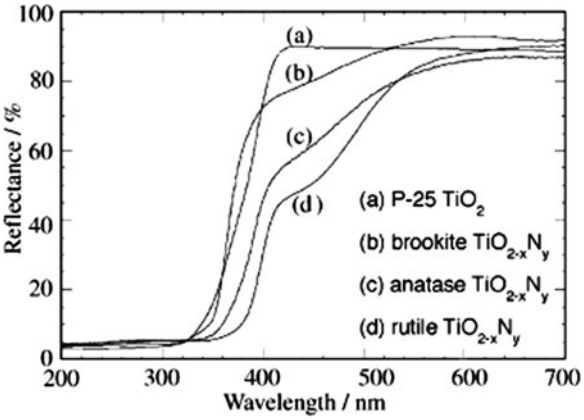

Fig. 19 Diffuse reflectance spectra of (a) P-25 titania powder, and N-doped TiO_2 powders prepared at 190°C and calcined at 400°C in (b) $TiCl_3$–HMT–methanol solution at final pH 1, (c) $TiCl_3$–HMT–methanol solution at final pH 9, and (d) $TiCl_3$–HMT–ethanol solution at final pH 9. Reproduced with permission from Aita et al. (2004). Copyright 2004 by Elsevier Inc.

a small quantity of carbon. X-ray diffraction patterns were consistent only with the anatase crystal phase, even after annealing at 500°C. XPS spectra displayed three binding energy peaks at 396.2, 398.3, and 400.4 eV in the N 1*s* region. The first two signals were attributed to a chemically bound N-species and to O–Ti–N linkages within the crystalline TiO_2 lattice, respectively, whereas the signal at 400.4 eV was assigned to molecularly chemisorbed N_2 species.

The RF-MS deposition method using various N_2/Ar mixtures as the sputtering gas ($X = 2, 4, 10, 40$) and a calcined TiO_2 plate as the source material has been used to prepare N-substituted TiO_2 (denoted N-TiO_2(X)) photoactive thin films (Kitano et al. 2006b). The absorption edge of the samples shifted smoothly to the visible spectral region to 550 nm, with the extent of the shift depending on the concentration of N (X) substituted within the TiO_2 lattice (range 2.0–16.5%). The specimen with 6.0% N exhibited the highest visible-light activity in the photooxidation of isopropanol in aqueous media at $\lambda \geq 450$ nm, and the photo-oxidation of H_2O at wavelengths up to 550 nm. Specimens were thermodynamically stable even up to 400°C. XPS and XRD measurements showed significant substitution of lattice O atoms of TiO_2 by N atoms, which, according to these authors, played a crucial role in the *band gap narrowing* of the TiO_2 thin films (from 2.58 to 2.25 eV relative to 3.2 eV for anatase depending on X) enabling the visible-light photo-response. In samples with $X > 4$, Ti^{3+} species formed in the N-TiO_2(X) samples, which acted as recombination centers for electrons and holes causing a decrease of photoactivity.

Factors that govern the relationship between photoactivity and preparative conditions of VLA N-doped TiO_2 materials were reported in a study by Joung et al. (2006). The materials were prepared by hydrolysis of Ti(i-PrO)$_4$ in anhydrous ethanol containing HCl, followed by treatment of the resulting colloids in a stream of NH_3 at different temperatures (400, 500 and 600°C) and at various times (5–60 min). The highest photo-activities were seen for samples prepared at 400 and 600°C and calcination times of 5 and 10 min, whereas for samples prepared at 500°C the highest photoactivity was observed for a calcination time of 60 min. XRD patterns of the TiO_2 powders taken before and after N-doping as a function of calcination time showed only the anatase phase. The N 1*s* XPS spectra of the $TiO_{2-x}N_x$ samples displayed a peak at 399.95 eV that was tentatively assigned to adsorbed NO or to N in Ti–O–N. No peak attributable to Ti–N bonding at 396 eV was observed. Band gap energies of N-doped TiO_2 inferred from absorption spectra ranged from 2.92 to 3.04 eV, for samples prepared at 400°C (5 min) and at 500°C (60 min), respectively. Active species for each calcination temperature were tentatively identified: for samples prepared at 400°C (5 and 10 min) the active species were NO, NO_2, NO_2^-, NH_2, whereas for samples prepared at 500°C (60 min) the active species was doped atomic N and active species for samples prepared at 600°C (5 and 10 min) may be doped atomic N and the above nitrogeneous species. EPR spectra indicated the presence of both Ti^{3+} and $O^{-\bullet}$ ions in the doped specimens.

At this time it is important to realize that visible-light photoactivity of N-doped TiO_2 materials are sensitive to the preparative routes, because even though such systems may absorb visible light, they are nonetheless frequently inactive in photo-oxidations. With the realization that photogenerated charge carriers in and by

themselves do not impart photoactvity and that charge carrier recombination must be muted to allow the carriers to reach the metal-oxide surface, In and coworkers (In et al. 2006) prepared a series of $TiO_{2-x}N_x$ systems with nominal N loadings from 0.2 to 1.0 wt.% involving the sequential reaction of H_2O with a small known excess of $TiCl_4$ in toluene (step 1) under dry O_2-free argon. This was followed by the stoichiometric reaction of the remaining $TiCl_4$ with a standard solution of NH_3 in dioxane (step 2). The resulting species were heat-treated in air at 400, 500, and 600°C. Testing the $TiO_{2-x}N_x$ specimens for visible-light photoactivity they discovered (i) that calcination at 400°C yielded a solid with pronounced absorption in the visible spectral region but no visible-light photo-activity, (ii) that 500°C calcination produced an effective (yellow) VLA sample, and (iii) that the heat treatment at 600°C resulted in an inactive white material.

In addition to films and powdered specimens, self-organized N-doped TiO_2 nano-tubes can be fabricated (Vitiello et al. 2006) by electrochemical anodization of titanium in HF/H_2SO_4 electrolyte, followed by calcination at different temperatures (range 300–600°C) in pure NH_3. This converted the initial amorphous nanotubes into anatase with some rutile present depending on the heat-treatment temperature. Absorption spectra of the $TiO_{2-x}N_x$ nanotubes showed a sub-bandgap energy of ~2.2 eV and the regular band gap energy of anatase of ~3.2 eV. The N 1*s* XPS spectrum revealed two clear peaks: one at 400 ± 0.2 eV ascribed to molecularly chemisorbed dinitrogen (γ-N_2 state), and the second at 396 ± 0.2 eV atributed to the atomic β-N state.

In two extensive reports, Belver and coworkers (2006a, b) prepared and characterized a series of nanosized N-doped TiO_2-based materials by a reverse micelle microemulsion method using a $Ti(i\text{-}PrO)_4$ precursor and three N sources that were used as ligands (2-methoxyethylamine, N,N,N′,N′-tetramethylethylenediamine and 1,2-phenylenediamine) to produce titanium(IV) complexes in dry isopropanol under a N_2 atmosphere (in Schlench-type flasks). Dropwise addition of the solution to the inverse microemulsion, containing H_2O dispersed in n-heptane and Triton X-100 as the surfactant with hexanol as the co-surfactant, produced materials that were subsequently calcined at 200°C and then at 450°C. A XANES examination confirmed the anatase nature of $TiO_{2-x}N_x$, and also revealed a lack of correlation between the number of oxygen vacancies (V_Os) and the N content in the samples. Above a certain limit, the association of point defects, such as V_Os, and/or the presence of non-point extended defects, was detrimental to photoactivity. The distribution of defects and the nature of defects present in the N-doped samples were examined in a joint XANES/EXAFS investigation. It revealed that defect distribution was not simply related to V_Os since strong differences existed in the first cation–cation coordination shell, thus inferring the possible presence of non-point defects. The joint study confirmed the point defects to be the V_Os; no interstitial defects were seen and the O/Ti atom ratio was less than 2. Evidently, there exists an optimal O/Ti ratio for maximum photoactivity achieved when oxygen vacancies are located in the bulk lattice that act as electron traps subsequent to visible-light photoactivation of the doped specimens. No apparent effect due to N-doping on the valence band edge was detected; some localized states were,

however, detected at the bottom of the CB with broad absorption around 500 nm. Results from diffuse reflectance Fourier transform spectra (DRIFTS) indicated the presence of several anion-related impurities of a substitutional (N^{n-}) and interstitial (NO^{+}) nature. Although they contributed to the absorption features, no clear correlation existed between any of these species and photoactivity. In fact, photoactivity best correlated with an optimal number of oxygen vacancies, above and below which a decrease of steady-state reaction rates occurred.

Nitrogen-doped or nitrogen-/sulfur-codoped titania $TiO_{2-x}A_y$ (A = N, S) systems that can be excited by visible light (400–550 nm) have been prepared (Yin et al. 2006) by mixing aqueous $TiCl_3$ solutions with various nitrogen sources, e.g., hydroxylamine (NH_2OH), HMT, urea $\{(NH_2)_2CO\}$ and thiourea $\{(NH_2)_2CS\}$ followed by hydrothermal treatment at 190°C in an autoclave. The TiO_2 powders prepared with NH_2OH consisted of rutile crystals with non-homogeneous size distribution. The N-doped titania powders prepared using HMT consisted mainly of mono-size spherical brookite crystals, whereas those using urea and thiourea consisted of belt-like rutile particles (see Fig. 20). The $TiO_{2-x}A_y$ (A = N, S) powders showed excellent visible-light absorption with two absorption edges, one at 410 nm and the other at 530 nm, and displayed good visible-light photoactivity in the oxidative destruction of NO, except for the powder prepared in $TiCl_3/NH_2OH$ solution. Nearly 25 and 86% of NO was continuously destroyed under visible light ($\lambda > 500$) and UV–visible light irradiation ($\lambda > 290$) as shown in Fig. 21. In the XPS spectra, the N 1*s* peak around 400 eV was observed but not the peak at 396 eV for all the as-prepared $TiO_{2-x}A_y$ samples before Ar^{+}-ion sputtering treatment. Apparently, the large amount of NH_3 and other nitrogen compounds adsorbed on the metal-oxide surface (400 eV) may have masked the existence of Ti–N binding (396 eV).

Yet an N-doped titania photocatalyst with high visible-light activity has been synthesized using a layered titania/isostearate nanocomposite prepared by a sol-gel technique (Matsumoto et al. 2007). Nitrogen-doping was achieved by treating the composite with aqueous NH_3 followed by calcination either in an O_2/N_2 mixture or in pure N_2 at various temperatures (300, 350, 400, 450, and 500°C). The vivid yellow samples absorbed visible light in the region 380–500 nm, and correlated with doped-N content in the samples. Not so for the visible-light photoactivity, which *failed to correlate* with the N content. Highest visible-light photoactivity was observed for the 400-°C calcined sample whose absorption spectrum is illustrated in Fig. 22. The quantity of N content in the sample decreased on increasing the calcination temperature, particularly significant between 300 and 350°C, with the decrease being more important for the sample calcined in O_2/N_2 than for the sample calcined in pure N_2. The former was probably due to oxidation of doped N species by the O_2 during the heat treatment.

Thus far we have witnessed that VLA TiO_2 systems doped with either C, S, or N possess, in most cases, good attributes toward the photo-oxidation of organic and inorganic (e.g., NO_x) substrates. Of particular interest have been the materials doped with N whose preparative methods have been varied, but otherwise simple in a large number of cases. Most important, however, although all the C-, S-, and N-doped TiO_2 materials displayed absorption features and absorption edges

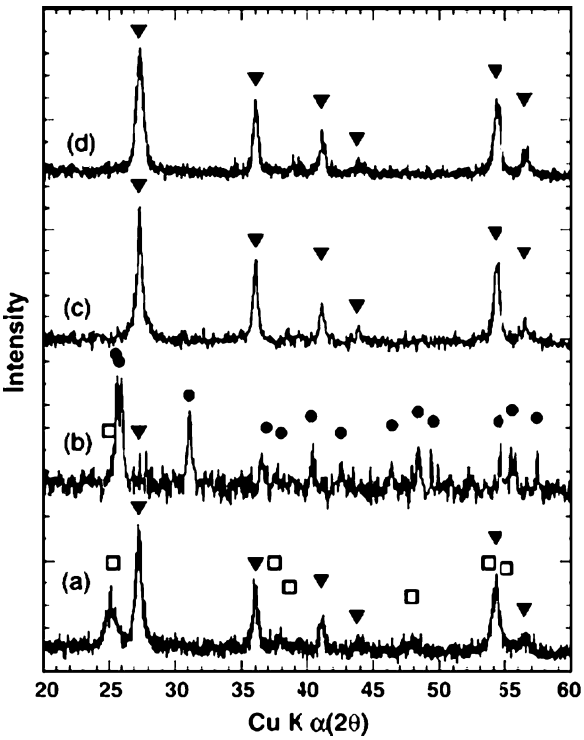

Fig. 20 XRD patterns of the titania powders prepared at 190°C for 2 h using (a) NH_2OH, (b) $C_6H_{12}N_4$, (c) $(NH_2)_2CO$, and (d) $(NH_2)_2CS$ as precipitation reagents. (*square*) Anatase; (*inverted triangle*) rutile; (*filled circle*) brookite. Reproduced with permission from Yin et al. (2006). Copyright 2006 by Elsevier B.V.

red-shifted to the visible spectral region (at least to 550 nm), photoactivity of these systems under visible-light irradiation has not always correlated with these absorption features. In a recent study, Tachikawa and coworkers (2007) addressed some of these issues and described mechanisms of the photoactivity of VLA TiO_2 specimens. Using solid-state NMR measurements combined with transient diffuse reflectance (TDR) spectroscopy, they provided direct evidence of the degradation of ethylene glycol with VLA-active $TiO_{2-x}N_x$ under visible-light irradiation. It appears that photoassisted oxidations of organic compounds on the surface of $TiO_{2-x}N_x$ proceed by surface intermediates generated from oxygen reduction (the superoxide radical anion, $O_2^{-\bullet}$) or otherwise water oxidation (the $^\bullet$OH radical) *and not* by direct reaction with h^+ that may be trapped at the N-induced midgap level (see Fig. 23). Based on their experimental results, it is rather evident that both an appropriate lower-energy photothershold for visible-light absorption and high carrier mobilities are needed for advanced VLA TiO_2-based photocatalysts.

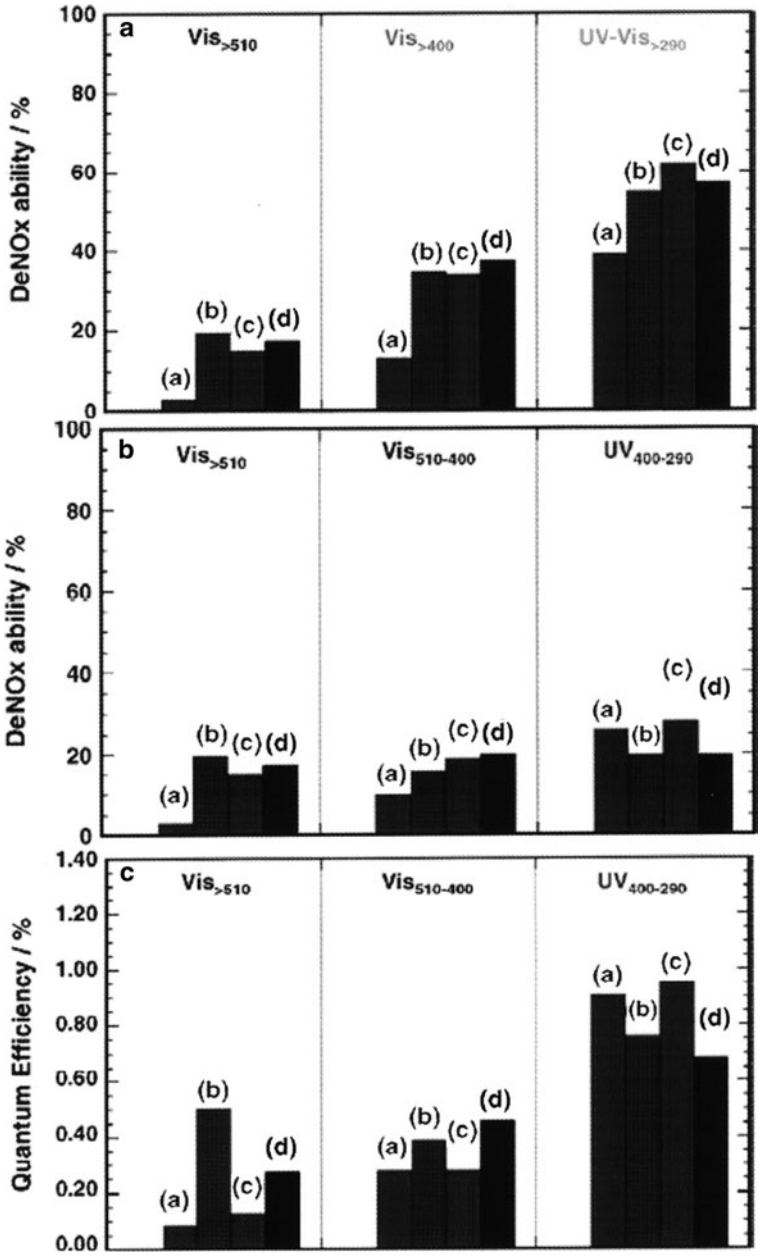

Fig. 21 Photocatalytic activity and quantum efficiencies in the degradation of NO_x by samples prepared at 190°C for 2 h using (a) NH_2OH, (b) HMT, (c) urea, and (d) thiourea as precipitation reagents. Data were treated against various wavelength ranges. Reproduced with permission from Yin et al. (2006). Copyright 2006 by Elsevier B.V.

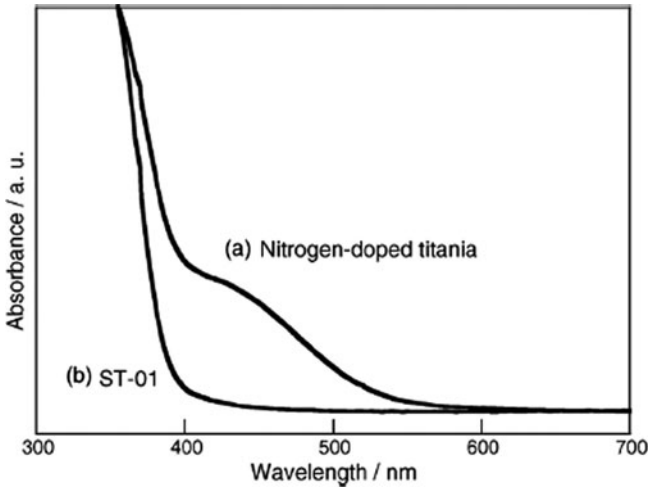

Fig. 22 UV–visible absorption spectra of (a) nitrogen-doped titania powder obtained by 400°C calcination and (b) commercial ST-01 anatase powder. Reproduced with permission from Matsumoto et al. (2007). Copyright 2007 by Elsevier B.V.

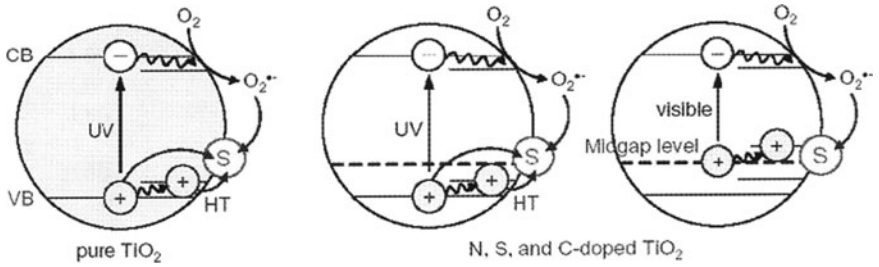

Fig. 23 Cartoons illustrating possible photoassisted processes of a substrate adsorbed on the surfaces of pure, N-, S-, and C-doped TiO_2 nanoparticles. Reproduced with permission from Tachikawa et al. (2007). Copyright 2007 by the American Chemical Society

3.3.5 N,F- and N,S-Codoped Titanium Dioxides

Vivid yellow N,F-codoped TiO_2 (NFT) powders have been prepared by SP at various temperatrures from a mixed aqueous solution containing $TiCl_4$ and NH_4F with the aim of introducing new active sites by F-doping, while the visible-light absorption might be improved by N-doping (Li et al. 2005b, c). The powders showed new absorption features to $\lambda < 550$ nm (Fig. 24) and PL bands spanning the range 350–1,000 nm (Fig. 25) for a series of NFT systems (denoted NFT-xxx, where xxx is the temperature of the SP method) The new absorption features in the visible spectral region originated from the doped N atoms rather than F atoms, because doping only with F atoms caused no changes in the optical absorption of TiO_2.

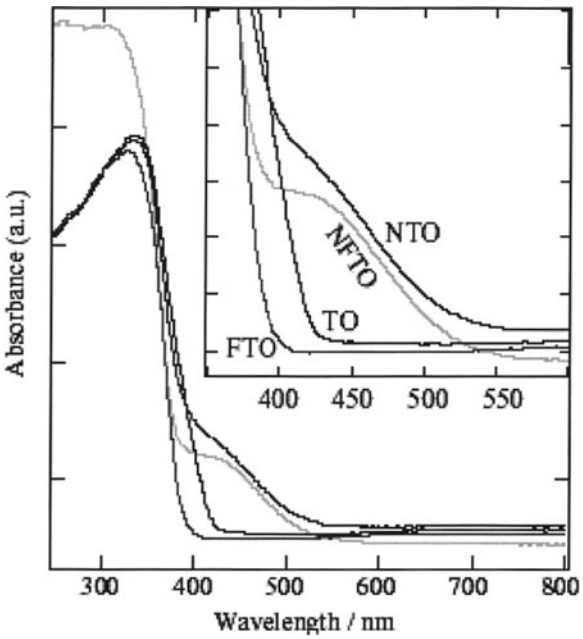

Fig. 24 UV–visible absorption spectra of pristine TiO_2 (TO), N-doped TiO_2 (NTO), F-doped TiO_2 (FTO) and N,F-codoped TiO_2 (NFTO) powders. The inset shows an expanded view of part of the adsorption spectra from 350 to 600 nm. Reproduced with permission from Li et al. (2005c). Copyright 2005 by Elsevier Inc.

The PL spectrum for the NFT-900 sample (Fig. 25a) was deconvoluted into no less than five bands. Band 1 at 465 nm arose from an oxygen vacancy with two trapped electrons, i.e., an *F* center, whereas band 2 at 525 nm was due to an oxygen vacancy with one trapped electron, i.e., an F^+ center. This assignment was based on the recognition that shallow traps exist at 0.51 and 0.82 eV below the CB of TiO_2. A deep trap also exists at 2.0 eV below the CB, identified as an origin unidentified energy state (OUES). The band at 627 nm (3) was likely a consequence of the Franck–Condon principle and the polarizability of the lattice ions surrounding the vacancy, with the emitting center likely involving Ti^{3+} color centers. However, because the energy state induced by Ti^{3+} ions may be located just below the CB of TiO_2, the authors attributed this band to OUES. Band 4 at 700 nm was said to originate from doped N atoms because no such band appeared for the T-800 and P25 TiO_2 samples: it was therefore assigned to the transfer of excited electrons between the F^+ center and the impurity energy state (IES), whereas band 5 at 905 nm was assigned to the transfer of excited electrons between the *F* center and the OUES. The presence of oxygen vacancies was significant because formation of the superoxide radical anion ($O_2^{-\bullet}$) and hydroxyl ($^\bullet OH$) radicals, two important active species in initiating photoreaction, requires oxygen vacancy sites. These assignments are summarized in the scheme shown in Fig. 26.

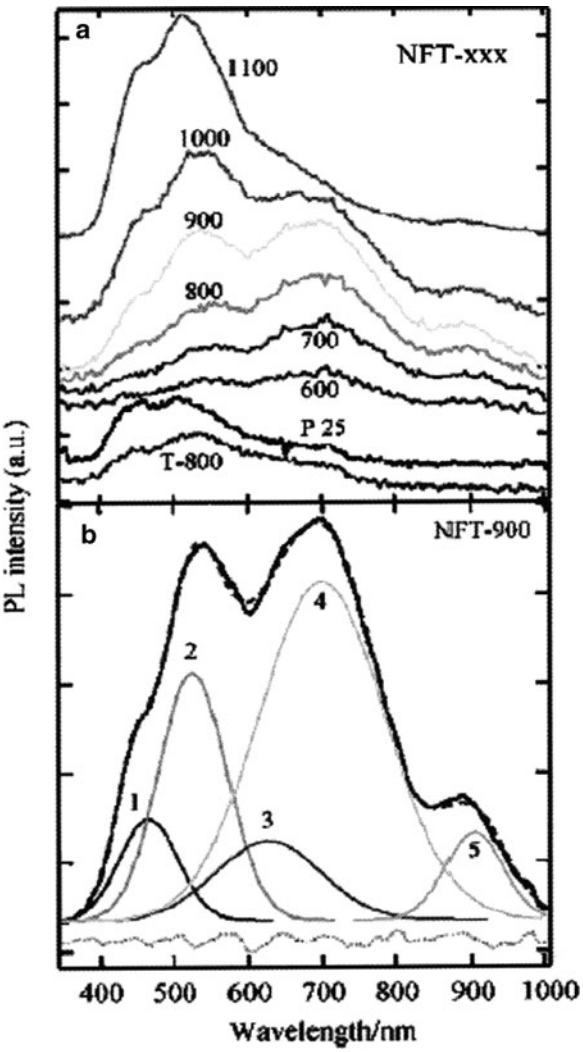

Fig. 25 (**a**) PL spectra of N-F co-doped TiO_2 (NFT-xxx) powders and reference samples; (**b**) deconvolution of the broad envelope for NFT-900. *Solid line* represents the original profile and deconvoluted peaks; *broken line* is the fitting curve, and the *dotted line* is the error of the fitting. Reproduced with permission from Li et al. (2005b). Copyright 2005 by the American Chemical Society

The photoactivity of the NFT powder prepared at 900°C proved superior to that of P25 TiO_2 under both UV- and visible-light irradiation in the decomposition of CH_3CHO. The reasons for such improved photoactivity may be closely related to the unique characteristics of the surface (porous, strongly acidic, and enhanced adsorptivity), to the doped N atoms, and to the doped F atoms. In this regard, the UV–visible spectra unequivocally indicated that N-doping caused no narrowing

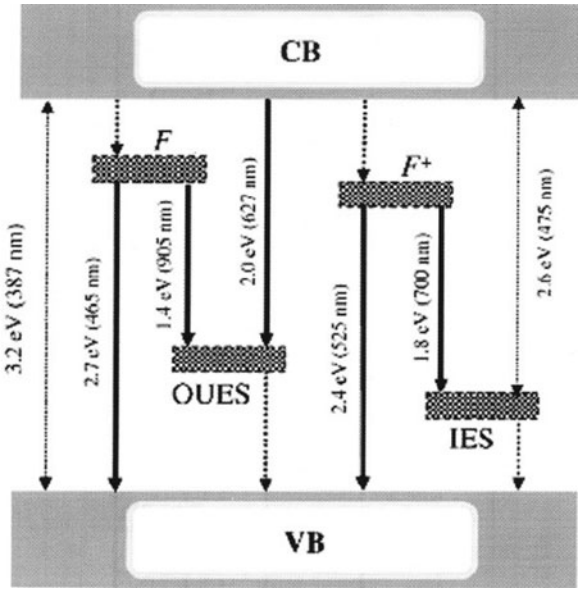

Fig. 26 Scheme of proposed energy states existing between the valence band and the conduction band of TiO_2. *Dotted arrows* represent additional possible existing PL emissions beyond 1,000 nm. Reproduced with permission from Li et al. (2005c). Copyright 2005 by Elsevier Inc.

of the band gap of the TiO_2 because no shift in the fundamental absorption edge of TiO_2 was observed. Rather, an isolated IES located near the VB of the TiO_2 improved light absorption in the visible region and increased the number of photons that can take part in surface photoreactions. Undoubtedly, this enhanced the photoactivity. However, in these N,F-codoped systems, the contribution of N-doping to the visible light photoactivity through oxygen vacancies may not be the sole factor, since the NFT powders displayed greater photoactivity than did N-doped TiO_2 alone. Thus, it appears that the contribution of N-doping to the visible-light photoactivity in the NFT systems is achieved mainly by improving the visible-light absorption. By contrast, F-doping produced several beneficial effects on photoactivity, namely (1) F-doping led to formation of new active sites such as oxygen vacancies (F and F^+ centers), (2) F-doping resulted in the formation of surface acid sites that led to increased adsorptive ability of the NFT powders for a substrate as well as acting as electron acceptors, and (3) F-doping increased the mobility of photogenerated electrons in TiO_2 so that they could easily diffuse from the inner lattice to the surface of the particles where reactions occurred. Consequently, the high visible-light photoactivity of NFT powders was likely the result of a synergetic effect of their unique surface characteristics, doped N atoms, and doped F atoms.

An overall comparative study carried out on N-doped, F-doped, and N, F-codoped TiO_2 powders (also denoted as NTO, FTO, NFTO) synthesized by SP confirmed the origins of the visible-light-driven photoactivity (Li et al. 2005c).

N-doping of TiO_2 resulted not only in improving visible-light absorption but also in creating surface oxygen vacancies, whereas F-doping produced several beneficial effects not least of which was the creation of surface oxygen vacancies, the enhancement of surface acidity and the increase in the number of Ti^{3+} color centers (EPR). Doped N atoms formed a localized energy state above the valence band of TiO_2, whereas doped F atoms had no influence on the band structure. To complete this analysis of N,F-codoped titania, the N 1*s* XPS spectra of N-doped, F-doped and NFT powders after 60 min of Ar^+-ion sputtering are illustrated in Fig. 27a, The figure clearly shows a peak (1) at 400 eV and a second peak (2) at 396.5 eV for the NTO and NFTO systems. By contrast, only one broad peak centered at ca. 400 eV is seen for FTO, likely the result of contamination from N_2 in air, since no N-source was used during the FTO preparation. In line with earlier assignments, peak 1 was attributed to the N atoms from molecularly adsorbed N-containing compounds (e.g., NH_3 and NO_x), which may have formed during the decomposition and oxidation of the N-precursors. Peak 2 was assigned to the presence of Ti–N bonds formed when N atoms replaced oxygen in the TiO_2 crystal lattice. The corresponding F 1*s* XPS spectra after 60 min of Ar^+-ion sputtering are depicted in Fig. 27b. Peak 3 located at 687.8 eV originated from substitutional F atoms in the TiO_2 lattice; peak 4 located at 685.3 eV originated from the F atoms of $TiOF_2$.

Anatase NFT powders can also be prepared by a sol-gel/solvothermal method using tetrabutyl titanate as a precursor, triethylamine as the N source and

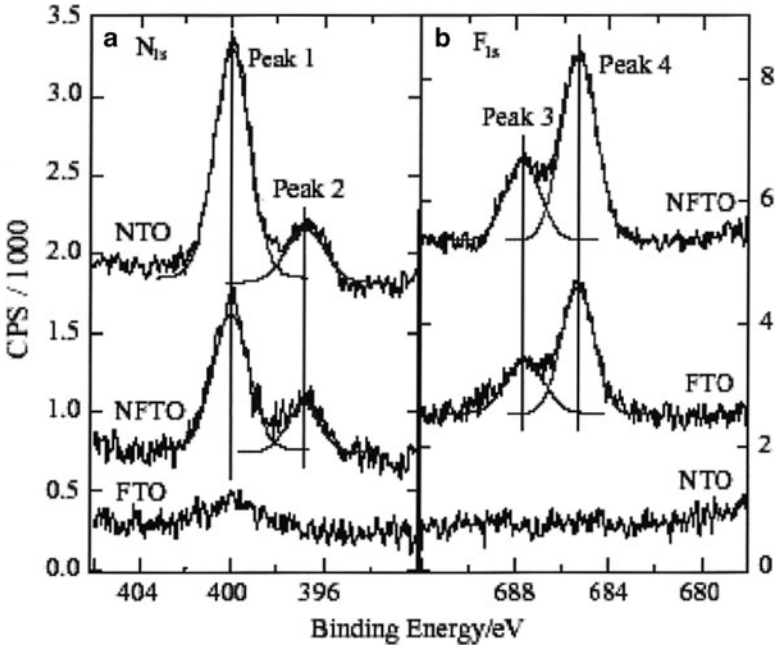

Fig. 27 XPS spectra of (a) N 1s and (b) F 1s for anion-doped TiO_2 powders after 60 min of Ar^+ ion sputtering. Reproduced with permission from Li et al. (2005c). Copyright 2005 by Elsevier Inc.

ammonium fluoride as the F source (Huang et al. 2006). Centrifugation of the powders followed by drying at 60°C in vacuum and calcining at 320°C for 6 h in air resulted in well-crystallized anatase NFT (XRD) specimens formed without contamination by any other phase, such as rutile or brookite, and by TiN, TiF_4, $TiOF_2$ for all samples prepared in different solvents. The UV–visible absorption spectra of TiO_2, N-doped TiO_2, F-doped TiO_2 and NFT samples showed that, apart from the fundamental absorption edge of TiO_2 at ca. 385 nm, a new absorption band appeared in the range 400–600 nm for the N-doped TiO_2 and NFT samples. The band caused by N- and F-codoping appeared slightly stronger than that caused by N-doping alone, contrary to the earlier observations reported in Fig. 23. However, it is again clear that F atoms caused no significant shift in the fundamental absorption edge of TiO_2. The NFT powder displayed good visible-light activity in the photoassisted degradation of *p*-chlorophenol and rhodamine-B under visible-light irradiation (400–500 nm). This high activity originated from a synergetic effect between the doped N and F atoms. The doped N atoms improved visible-light absorption, whereas doped F atoms enhanced surface acidity, increased the adsorption of the reactant, and further enhanced the photoactivity. XPS spectra revealed that the NFT powder contained only Ti, O, F, N elements and a trace amount of C whose presence was due to residual carbon from the precursor solution and from adventitious hydrocarbons from the XPS instrument. The N 1*s* XPS spectra of the NFT and N-doped TiO_2 taken after calcination at 320°C displayed a peak at 400.0 eV ascribed to N atoms from adventitious N–N, N–H, O–N, or N-containing organic compounds adsorbed on the surface (Huang et al. 2006). The small peak 396.0 eV was taken as evidence for Ti–N bonds formed when N atoms replaced the oxygen in the TiO_2 lattice. The F 1*s* XPS spectra of NFT were composed of two contributions: a symmetrical peak at 685.5 eV originating from the F-containing compounds adsorbed on the surface, and a small peak at ca. 688.5 eV due to F atoms that occupy oxygen sites in the TiO_2 lattice. No evidence of TiF_4 and $TiOF_2$ bonds were evident in the XRD pattern.

A simple method for preparing highly photoactive nanocrystalline mesoporous N,S-codoped TiO_2 powders involved hydrolysis of $Ti(SO_4)_2$ in aqueous ammonia at room temperature yielding xerogels that were then calcined at 400, 500, 600, 700, and 800°C in air for 3 h, respectively (Yu et al. 2006). The as-prepared powders were amorphous, but at ca 400°C the XRD patterns (Fig. 28) indicated the appearance of the anatase phase which remained stable up to 700°C, after which the rutile phase began to appear.

An XPS survey spectrum of the N,S-codoped TiO_2 powders calcined at 500°C indicated that the powders contained Ti and O elements as well as a small amount of N, S, and C elements at binding energies: Ti 2*p*, 458 eV; O 1*s*, 531 eV; N 1*s*, 400 eV; S 2*p*, 169 eV; and C 1*s*, 285 eV (Yu et al. 2006). The latter peak for carbon was due to adventitious hydrocarbons from the XPS instrument. XPS spectra of other samples gave similar results. The high-resolution XPS spectra in Fig. 29a of the N 1*s* region taken on the surface of the TiO_2 powders show an asymmetric band that is resolved into two peaks: one at 400.4 eV attributed to Ti–N bonding formed by the nucleophilic substitution reaction between NH_3 and $Ti(SO_4)_2$ during the

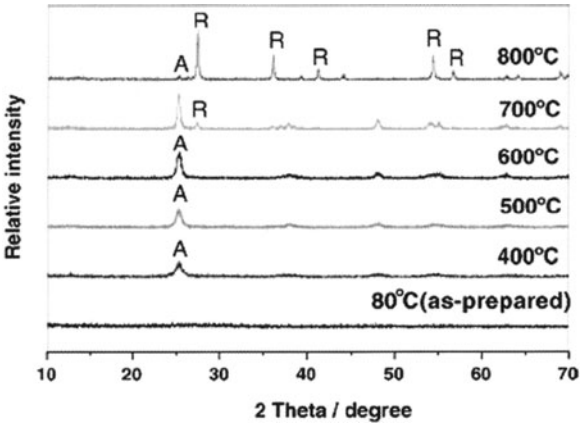

Fig. 28 XRD patterns of as-prepared TiO_2 powders calcined at different temperatures. Reproduced with permission from Yu et al. (2006). Copyright 2006 by Elsevier B.V.

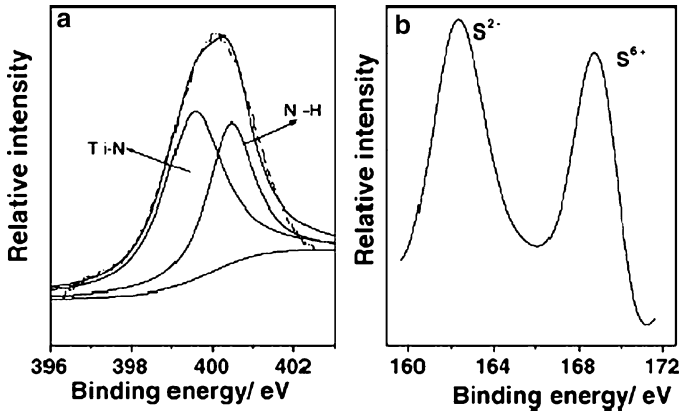

Fig. 29 High-resolution XPS spectra of (a) N 1s and (b) S 2p regions of the as-prepared N,S-codoped TiO_2 powders calcined at 500°C. Reproduced with permission from Yu et al. (2006). Copyright 2006 by Elsevier B.V.

hydrolysis, whereas the other was assigned to some NH_3 adsorbed on the surface of TiO_2. In the case of the S $2p_{3/2}$ XPS spectra (Fig. 29b), two isolated peaks are seen at binding energies 168.7 and 162.3 eV that have been attributed to S^{6+} and S^{2-} species, respectively. The former was associated with some SO_4^{2-} ions on the surface of TiO_2, whereas the peak at 162.3 eV corresponds to the Ti–S bond from substituting the O^{2-} in TiO_2 by S^{2-} species. Substitution of S^{2-} into O^{2-} sites should lead to some distortion of the TiO_2 lattice owing to the larger size of S^{2-} (1.7 A) relative to O^{2-} (1.11 A). XRD results confirmed this supposition. Absorption spectra of N,S-co-doped TiO_2 samples showed stronger absorption in the UV–visible spectral region than undoped TiO_2, and a red shift in the band gap

transition, taken by Yu and coworkers (2006) as giving rise to band gap narrowing by the presence of dopants. The largest red shift was seen for the N,S-codoped TiO_2 powders calcined at 800°C because of the formation of rutile and growth of the TiO_2 crystallite.

The high visible-light photoactivities of as-prepared N,S-codoped TiO_2 powders heat-treated at 400–700°C toward the photooxidation of acetone and formaldehyde may be the result of synergetic effects of the strong absorption in the UV–visible light region, the red-shift of the absorption edge, good crystallization, large surface area, and the two-phase structures of undoped TiO_2 and N,S-codoped TiO_2 (Yu et al. 2006).

4 Theoretical Calculations of Band Gap Energies in Doped TiO_2

In Sect. Nitrogen-Doped Titanium Dioxides, we described some of the principal preparative methods and strategies of doping TiO_2 (anatase or rutile) with nitrogen dopants. These have included (i) sol-gel syntheses, (ii) chemical treatment of the TiO_2, (iii) oxidation of TiN, (iv) ion implantation, and (v) RF-MS. There can be no doubt that these different methods lead to anion-doped metal-oxide materials with entirely different properties. The key question that keeps coming up in the literature is: what is the chemical nature and the location of the species that lead(s) to the red-shift of the absorption edge of TiO_2 and consequently to the visible-light activity of TiO_2? Species such as NO_x, NH_x, and N^{2-} have been proposed, not to mention the hyponitrite, nitrite and nitrate species that have in some cases been confirmed experimentally. Another key question regards the electronic structure(s) of the (anion)-doped materials and their fate when subjected to UV- and/or visible-light irradiation. Although these questions have been addressed in several interesting computational studies (see below), a consensual acceptance of the results has yet to be reached. As we shall witness below, significant advances can be made toward a clarification of these key questions by a combination of experimental and computational studies within the same laboratory or among collaborating laboratories.

Densities of states in anatase TiO_2 for subsitutional doping of oxygen in the lattice by C, N, F, P, and S were first reported by Asahi and coworkers (2000, 2001) using the FLAPW formalism in the framework of the LDA. The calculations were carried out without geometry optimization for the five anion-dopings because the resulting atomic forces were apparently too large to obtain reasonable positions in the unit cell (eight TiO_2 units per cell). Sulfur has much larger formation energy for substitution (4.1 eV) than is required for N (1.6 eV). Thus, it was inferred that because of its large ionic radius it would be difficult to incorporate S^{2-} into the TiO_2 lattice. Carbon- and phosphorous-doping seemingly introduce states too deep in the band gap of TiO_2 to satisfy the condition that states within the band gap should overlap sufficiently with band states of TiO_2 to transfer photoexcited carriers to reactive sites at the catalyst surface within their lifetime. Three types of doping for N

were considered in the computations: (a) substitutional N doping (N_S), (b) interstitial N doping (N_I), and (c) both types of doping (N_{S+I}) in the anatase TiO_2 architecture. Optimization of the N positions in the cell inferred molecularly bonding states – NO and N_2 – for cases (b) and (c) with bond lengths (improved by the *generalized gradient approximation*, GGA) in fair agreement with accepted values: 1.20 vs. 1.15 A (N–O) and 1.16 vs. 1.10 A (N_2). Substitutional doping of N was the most effective because its 2*p* states (apparently) contributed to band gap narrowing by mixing with O 2*p* states of the valence band (Asahi et al. 2001). Calculated imaginary parts of the dielectric functions of $TiO_{2-x}N_x$ showed a shift of the absorption edge to lower energy by N doping, with dominant transitions from N $2p_\pi \rightarrow$ Ti d_{xy} rather than from O $2p_\pi$ as in TiO_2. However, the calculated band gap energies were considerably underestimated relative to the experimental value ($E_{bg} = 2.0$ eV vs. $E_{bg} = 3.2$ eV for anatase). This was attributed, in part, to the well-known shortcomings of the LDA approach. Accordingly, to correct this underestimated band gap a scissors operator (a sort of *fudge factor*) was used that apparently displaces the empty and occupied bands relative to each other by a rigid shift of 1.14 eV, so that the minimum band gap would now be in line with experiment (corrected $E_{bg} = 3.14$ eV) for the band gap of anatase TiO_2. The band gaps of the N-doped $TiO_{2-x}N_x$ systems were also adjusted by 1.14 eV on the assumption that the underestimated energy of the band gap in the LDA approach was not affected by N-doping, because long-range screening properties in $TiO_{2-x}N_x$ were likely similar to those in TiO_2.

Contrary to the expectations of Asahi et al. (2000, 2001), Umebayashi and coworkers (2002) did incorporate S into anatase TiO_2 by oxidative annealing of TiS_2 at 600°C in which the S dopant caused a significant shift of the absorption edge (of TiO_2) to lower energy. However, in accord with Asahi et al. (2000, 2001), their ab initio band calculations also involved mixing S 3*p* states with O 2*p* states of the valence band, and thus taken to mean that the mixing contributes to the band gap narrowing of TiO_2 through an increase in the valence band width. A fuller study involving first-principles band calculations (WIEN97 code) by the FPLAPW method, again based on density functional theory (DFT) within the GGA approximation, led Umebayashi et al. (2003a) to conclude again that mixing of S 3*p* states with O 2*p* valence band states increases the width of the valence band and narrows the band gap.

In the work reported by Ohno and coworkers (2004), S-doped TiO_2 displayed significant visible-light activity attributed to the presence of S^{4+} species that substituted Ti^{4+} in the lattice. No S^{2-} species were seen from XPS spectral measurements. One possibility for the XPS presence of S^{4+} might have been due to SO_3^{2-} species formed by the partial oxidation of thiourea during the preparation of the S-doped TiO_2 sample. This peculiarity led Matsushima and coworkers (2007) to re-examine the electronic structure through first-principles DFT band calculations and to explore the plausible locations of the S atoms in the anatase TiO_2 structure. Four types of supercells were examined: type A (12 atoms) and B (48 atoms) in which a Ti atom was substituted by an S atom, and type C (12 atoms) and D (48 atoms) in which an O atom was substituted by an S atom. A tetragonal-to-orthorhombic phase transition occurred in type C and D supercells. In the small

supercell A, band-like S-related states appeared at energies in the range ~1.6 to 0 eV, whereas in the larger B supercell atomic-like S 3*p* states appeared at ca. 0.9 eV above the valence band. By contrast, in the large D supercell the S 3*p* states merged with the O 2*p* states of the valence band leading to a band gap shrinkage (narrowing) of ca. 0.7 eV. It would seem that, according to these calculations, the S atom could be located at either Ti or O sites in the anatase structure. The choice might depend on the preparative conditions. DFT calculations also predicted that S atoms located at Ti sites in S-doped TiO_2 lead to lower visible-light activity.

Contrary to this prediction, as-prepared sulfur-doped TiO_2 (Umebayashi et al. 2003b) was twofold more VLA than as-prepared N-doped specimens under visible-light irradiation (Sathish et al. 2005). Mixing of S 3*p* states with the O 2*p* states in the upper edge of the valence band of TiO_2 accounted for the visible-light activity from DFT considerations that used a two-unit-cell supercell as the basis of the calculations (Umebayashi et al. 2002). The effects of S-doping have been examined further theoretically by Tian and Liu (2006) using plane-wave-based pseudopotential DFT to characterize the electronic structure when O atoms are subsituted by S in anatase TiO_2 to determine how its absorption behavior might be affected, and to probe how different doping levels through S concentration changes might impact the electronic structure and the optical absorption characteristics of S-doped TiO_2. Larger supercells were used: 72, 48, and 24 atom supercells to simulate S-doping levels of 0.0139, 0.0208, and 0.0417, respectively. The first observation was that the S-doped anatase TiO_2 is converted into a direct band gap semiconductor at the Γ position (in the Brillouin zone), in line with results for S-doped rutile TiO_2 (Yamamoto et al. 2004) caused by the presence of S 3*p* states localized above the upper edge of the valence band. However, band-to-band excitation was retained for anatase at different S-doping levels; that is, the *intrinsic band gap* of TiO_2 is retained on S doping. Another aspect resulting from the DFT analysis was the concentration-dependent behavior of band gap energies 3.20, 2.75, 2.67, and 2.55 eV (absorption edge at 387, 451, 465 and 488 nm) with doping levels of 0.0000, 0.0139, 0.0208 and 0.0417 (Table 1), respectively. Also, the width of the valence band increased as the doping level increased. In the data of Table 1, a scissors operator of +1.40 eV (note that others used a value of +1.14 eV; see above) was used to shift the CB states so that the estimated band gap energies corresponded to the expeirmental values. Effective mixing of S 3*p* with O 2*p* states occurred at about 4.2% doping level for S-doped anatase TiO_2, thus widening the valence band width, narrowing the band gap, and inducing visible-light activity for TiO_2. The table also shows that band gap lowering and red-shifts of the absorption edge increase as the S concentration increases.

The picture as to the exact cause of the red-shift of the absorption edge of TiO_2 seen experimentally for various N-doped TiO_2 (anatase) powders became somewhat confused with the report from Yates group (Diwald et al. 2004a) that the absorption edge of a N-doped TiO_2 rutile single crystal shifted to higher energy (see Sect. Nitrogen-Doped Titanium Dioxides). Using spin-polarized DFT calculations within the GGA approximation, Di Valentin and coworkers (2004) determined that whereas in anatase the localized N 2*p* states located just above the O 2*p* states of the

Table 1 DFT calculated properties of S-doped TiO_2 specimens.From Tian and Liu (2006)

Concentration (%)	Band gap energy (eV)	Corrected band gap energy (+1.4 eV)	Δ^a (eV)	Absorption edge (nm)	D^b (eV)
0.00	1.80	3.20	–	387	–
1.39	1.35	2.75	0.45	451	0.21
2.08	1.27	2.67	0.53	465	0.066
4.17	1.15	2.55	0.66	488	0.002

[a]Lowering of band gap relative to undoped TiO_2

[b]Energy difference between the lower energy levels of the S states and the upper edge states of the valence band

valence band red-shift the absorption edge to lower energy, in rutile the tendency to red-shift the absorption edge is offset by the concomitant contraction of the O 2*p* band resulting in an overall increase in the optical transition energy by ca. 0.08 eV (experimentally this blue-shift was 0.20 eV). Compared to anatase, rutile has a wider O 2*p* band due to both its higher density and its different structure (see Fig. 30).

Nitrogen-doping was modeled by replacing 1, 2, or 3 oxygen atoms in the 96-atom anatase supercell and 1 or 2 oxygen atoms in the 72-atom rutile supercell (Di Valentin et al. 2004), giving a stoichiometry comparable to that used in experiments for $TiO_{2-x}N_x$: $0.031 < x < 0.094$ for anatase and $0.042 < x < 0.084$ for rutile (note that a higher level of N-doping was used by Asahi et al. (2000, 2001) giving a stoichiometry of $TiO_{1.875}N_{0.125}$). Apparently, inclusion of more N atoms in the same supercell yields more accurate results than using smaller supercells. The calculated band gaps were 2.19 eV and 1.81 eV (at the Γ position) vs. the experimental 3.2 and 3.0 eV, respectively, for pure undoped anatase and rutile TiO_2, again because of the shortcomings of the DFT method. Nonetheless, analysis of the electronic energy levels showed that N-doping causes no shift of the position of both top and bottom of the O 2*p* valence band and of the CB relative to pure undoped TiO_2. This is in significant contrast with the conclusions of Asahi et al. (2000, 2001) with respect to the undoped material. Structural variations in the rutile TiO_2 structure subsequent to substitution of one O atom with N in the 72-atom supercell appear to be significant in rutile relative to anatase in which the variations were inconsequential. In any case, the N impurity states can act as deep electron traps in $TiO_{2-x}N_x$ systems (Fig. 30). Di Valentin et al. (2004) also considered the contribution of oxygen vacancies (V_Os), experimentally estimated to be located 0.75–1.18 eV below the CB (their DFT calculations placed them at 0.3 eV below the CB E_C), to the overall visible-light photoactivity of N-doped systems when V_Os trap electrons to produce *F*-type color centers. The simultaneous presence of N dopants and V_Os may also lead to charge transfer states (reaction 3.9) that can also contribute to the photoactivity.

$$V_O(F) + N \rightarrow V_O^{\bullet}(F^+) + N^{--} \tag{3.9}$$

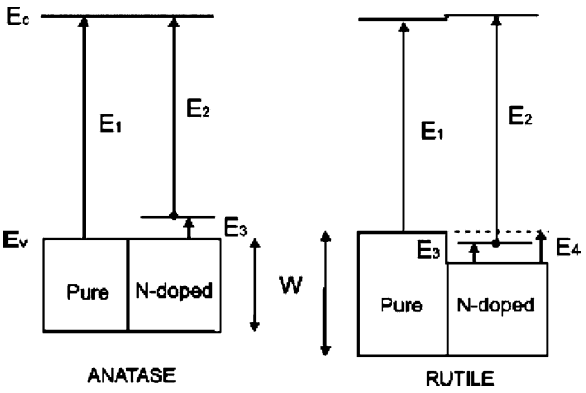

Fig. 30 Schematic representation of the energy band structure of pure and N-doped anatase and rutile (energies not to scale). Note the modest shift of 0.03 eV in E_C of the conduction band to higher energies and the contraction energy E_4 in the N-doped rutile TiO_2. E_3 represents the energy of the N dopant levels above the valence band. Higher levels of doping, e.g., three N atoms per supercell, cause a small shift of ~0.05 eV to higher energies for E_C which is overcompensated by the presence of N-derived states just above VB, so that the excitation energy E_2 from these states to the conduction band is reduced by <0.1 eV compared to pure anatase. Reproduced from Di Valentin et al. (2004).Copyright 2004 by the American Physical Society

In a subsequent study, Di Valentin and coworkers (2005a) combined experiments (EPR, XPS) and DFT calculations, performed using the plane-wave-pseudopotential approach together with the Perdew–Burke–Ernzerhof (PBE) exchange correlation functional and ultrasoft pseudopotentials, to characterize the paramagnetic species present in N-doped anatase TiO_2 powders obtained by sol-gel synthesis, and to unravel some of the mechanistic details of the visible-light activity of N-doped TiO_2s as to whether photoactivity is due to the presence of NO_x or NH_x species or simply to substitutional N-doping. The $TiO_{2-x}N_x$ sample was obtained by hydrolysis of Ti(i-PrO)$_4$ in isopropanol media in the presence of an aqueous NH_4Cl solution as the N source, followed by calcination of the N-doped specimen at ca. 500°C for 2 h. XPS N 1*s* spectra indicated only a peak at ca. 400 eV, typically assigned to interstitial N (without precluding others), but no 396 eV peak usually originating from substitutional N-doping. EPR results indicated the presence of two different paramagnetic N-related species, whose hyperfine coupling constants were consistent with substitutional and interstitial N species. Accordingly, two structurally different locations were considered for the N dopant in the DFT calculations: substitutional N (N_S) and interstitial N (N_I) atoms in the TiO_2 anatase matrix. In the substitutional model, N that replaces O in the TiO_2 lattice was taken to be bonded to three Ti atoms in the 96-atom supercell so that the paramagnetic species is formally N^{2-}, whereas in the interstitial model N is added to the 96-atom supercell bonded to one or more O, and thus is in a positive oxidation state as in NO^-, NO_2^- and/or NO_3^-. Figure 31 illustrates the DFT band structure of the N-doped TiO_2 and reports the calculated albeit underestimated band gap energy of titania.

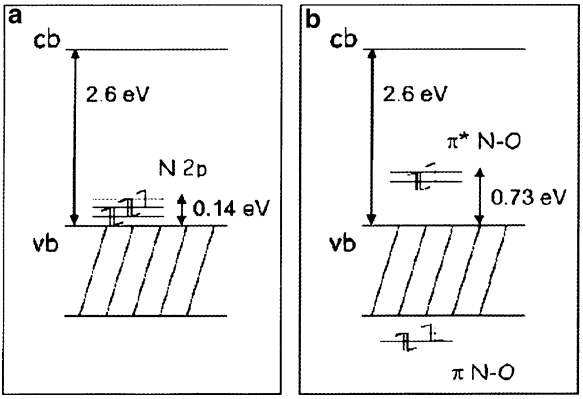

Fig. 31 Electronic band structure for (**a**) substitutional and (**b**) interstitial N-doped anatase TiO_2 as given by PBE calculations at a low-symmetry *k*-point. In the former, the site contains the paramagnetic N^{2-} species making the site electrically neutral (replaced O^{2-}), whereas in the latter the site is occupied by the radical NO. The estimated band gap energy is also indicated. Reproduced with permission from Di Valentin et al. (2005a). Copyright 2005 by the American Chemical Society

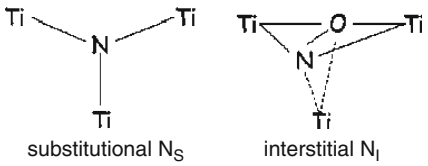

The two bonding π states in Fig. 31b for NO lie deep below the O 2*p* band but the two π* still occupied states lie above (0.73 eV) the O 2*p* band and lie at higher energy than the 2*p* states of substitutional N (0.14 eV). A more interesting consequ ence of the portrait shown in Fig. 31 is that the two electrons left in the formation of an oxygen vacancy, that typically would form two Ti^{3+} color centers, might also be trapped by these two different N dopants yielding the azide species (N^{3-} denoted as N_S^-) and the hyponitrite species (NO^-). Another significant result deriving from the DFT calculations of Di Valentin and coworkers (2005a) is that N-doping led to a substantively reduced energy of formation of V_Os (4.3–0.6 eV for anatase) with important consequences in the generation of *F*-type and Ti^{3+} color centers. Experimentally, which of the two types of N dopants predominates in the N-doped TiO_2 will depend on the experimental conditions, e.g., nitrogen and oxygen concentrations, and calcination temperatures. What Fig. 31 also implies is that moving from substitutional N to interstitial N is in fact an oxidative step, which according to DFT estimates is ca. 0.8 eV exothermic. Thus, there is a cost for the reverse, i.e., interstitial N-doping is preferred when $TiO_{2-x}N_x$ systems are prepared in excess nitrogen and oxygen, whereas high-temperature calcination of N-doped systems, commonly done in most

experiments, both substitutional N and formation of oxygen vacancies are likely the preferred occurrences.

The question on the blue-shift of the absorption edge of N-doped TiO_2 rutile single crystals contrasting the red-shifts in N-doped TiO_2 powders was also taken up in a DFT study by Yang and coworkers (Yang et al. 2007) using the plane-wave method. Results confirmed those of Di Valentin et al. (2004) that some N 2*p* states lie above the O 2*p* valence band when N substitutes O in the TiO_2 lattice and when N is located at interstitial positions. However, no band gap narrowing was predicted by these calculations. But when N substitutes Ti atoms in the rutile lattice, a bandgap narrowing in the rutile crystal is apparently possible because the N dopant introduces some energy states (the N 2*p* states) into the bottom of the CB. The authors rationalized this inference by the fact that removal of electrons from the supercell on replacing one Ti with a N atom leads to a reduction of the Coulomb repulsion and thus to a shift of the energy band edges, i.e., the band gap energy is reduced by ca. 0.25 eV relative to the undoped rutile supercell whose estimated band gap energy was calculated to be 1.88 eV. This is reminescent of the assertion by Asahi et al. (2000, 2001) that N-doping TiO_2 causes band gap narrowing because the N 2*p* states mix with the O 2*p* states in the valence band, thereby widening the valence band and shrinking the band gap.

We have seen above that substitutional N-doping is stabilized by the presence of oxygen vacancies ($N_{S\text{-}O} + V_O$) under oxygen-poor experimental conditions, whereas under oxygen-rich conditions interstitial N species (N_I) become favored. According to DFT calculations of C-doping TiO_2 (Di Valentin et al. 2005b), otherwise performed in a manner identical to those for N-doping (96-atom supercell for anatase and 72-atom supercell for rutile; see above), at low C concentrations and under oxygen-poor conditions, substitutional (to oxygen) carbon and oxygen vacancies seem to be favored. By contrast, under oxygen-rich conditions, both interstitial and substitutional (to Ti) C dopings are preferred. However, in the latter case, no C states were found in the band gap except for a small band gap shrinking. Thus, C-doping of TiO_2 causes a modest variation of the band gap energy but induces several localized occupied states within the band gap. These features accounted for the experimentally observed red-shifts of the absorption edge toward the visible region (up to nearly 1.7 eV). The nature and density of localized mid-gap C-related states depended on the concentration of the doping C atoms, on the oxygen pressure, and on the calcination temperature during the preparation of C-doped TiO_2. DFT results also seem to indicate that C-doping favors formation of oxygen vacancies in bulk TiO_2. Once again, DFT calculations underestimated the band gaps: 2.19 eV (2.61 eV) and 1.81 eV (2.14 eV) at Γ (and at the low-symmetry κ-point) for anatase and rutile, respectively. In the case of carbon-doped anatase (as might also occur for N- and S-doped TiO_2s; see Sect. Nitrogen-Doped Titanium Dioxides), holes formed upon visible-light excitation are less reactive than those formed upon UV-light excitation in pure TiO_2, because holes are trapped at the midgap levels induced by carbon doping (Tachikawa et al. 2004). This means that holes are less mobile than the electrons excited to the CB, so that visible-light irradiated C-doped TiO_2 are less likely to be involved in direct oxidation of substrates by photogenerated holes. The

concomitant presence of C species and O vacancies in $TiO_{2-x}C_x$ (XPS and EPR) are responsible for the improved photoactivity in the visible region, as also predicted for N-doped TiO_2. Evidently, the origin of increased photoactivity of C- and N-doped TiO_2 may be associated with more complex phenomena than the simple presence of dopant atoms, e.g., by concomitant changes in the stoichiometry of the sample (Di Valentin et al. 2005b).

The N-doped sample prepared by the sol-gel process of stoichiometry near $TiO_{1.907}N_{0.062}$ examined earlier by Di Valentin and coworkers (2005a) was re-examined more closely in a series of experiments and DFT calculations aimed at determining the fate of the doped specimen when irradiated at different wavelengths in the presence of adsorbates (Livraghi et al. 2006). The experiments asserted that N species were responsible for the absorption of visible-light radiation, and consequently for the visible-light activity, as well as for the photoinduced electron transfer from the solid to surface electron scavengers (adsorbates) such as molecular O_2. The UV–visible diffuse reflectance spectrum of the sample (Fig. 32) is nearly identical to the many reported DRS spectra of N-doped TiO_2 specimens prepared in a variety of ways. However, as we shall see later, this spectral behavior is identical to the spectral behavior of so many other doped TiO_2 samples that have been doped with different types of dopants (e.g., transition metal ions, C, S, and others) and synthesized by different methods.

Previous EPR work (Di Valentin et al. 2005a) had identified two distinct nitrogeneous paramagnetic species in N-doped TiO_2, one of which was the molecular NO radical (Livraghi et al. 2005) located in closed pores within the crystals and thus had no influence on the electronic structure of the solid. No evidence of hydrogen EPR hyperfine lines were found, thus ruling out NH_x-type paramagnetic species as had been inferred by Yates' group (Diwald et al. 2004a, b). Whatever the nature of the paramagnetic species, it was stable to washing and to calcination in air up to ca. 500°C. This was taken to mean that the nitrogen radical species identified as $N_b^{\bullet}$ interacted strongly with the TiO_2 lattice. DFT calculations carried out on a

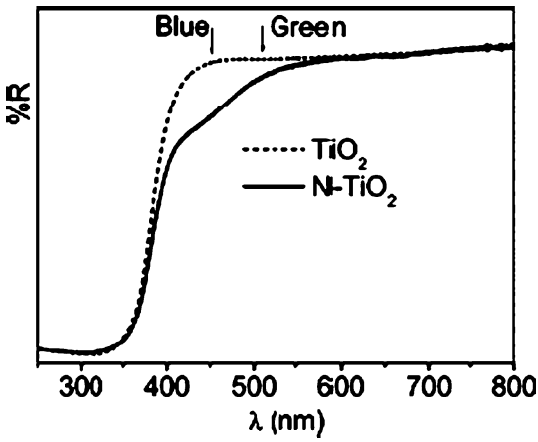

Fig. 32 UV–visible diffuse reflectance spectra of undoped and N-doped TiO_2. Reproduced with permission from Livraghi et al. (2006). Copyright 2006 by the American Chemical Society

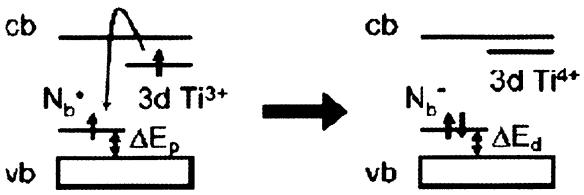

Fig. 33 Electronic band structure changes from interactions between $N_b^{\bullet}$ ($N_S^{\bullet}$ or $N_I^{\bullet}$) and Ti^{3+} color centers. Reproduced with permission from Livraghi et al. (2006). Copyright 2006 by the American Chemical Society

96-atom supercell involved two interstitial nitrogen ($N_I^{\bullet}$) or two substitutional nitrogen ($N_S^{\bullet}$) paramagnetic species plus an oxygen vacancy (V_O) located far away from these N-centers to avoid direct defect/impurity interactions. We need to recall that removal of an O atom from the TiO_2 lattice leaves behind two electrons to form the *neutral F* center (V_O in the Kroger–Vink notation), or they may be trapped by neighboring Ti^{4+} species to give two Ti^{3+} color centers, which Henderson et al. (2003) positioned 0.8 eV below the bottom of the CB. However, other studies have indicated otherwise, although there are electron traps around this energy; Ti^{3+} color centers certainly do exist as demonstrated by EPR measurements (Berger et al. 2005; Hurum et al. 2003). One of the consequences of the high number of V_Os under oxygen-poor conditions in N-doped TiO_2 is the partial quenching of $N_b^{\bullet}$ paramagnetic species, which according to Di Valentin et al. (2005a) are transformed into N_b^- through reduction by Ti^{3+} color centers (Fig. 33). The energetically favored reduction of $N_b^{\bullet}$ species may be the cause for the small energy cost in the formation of V_Os in N-doped TiO_2 (see above). The EPR peaks attributed to $N_b^{\bullet}$centers disappeared on reduction of the sample (reaction 3.10) whether by annealing in vacuo or by other means to then reappear on re-oxidation. Thus, the N-doped TiO_2 specimen (at least the one prepared by the sol-gel method) contained paramagnetic N-related species in the bulk lattice ($N_b^{\bullet}$) and a number of diamagnetic species (N_b^-) in the presence of

$$N_b^{\bullet} + Ti^{3+} \rightarrow N_b^- + Ti^{4+} \tag{3.10}$$

which depended on the oxygen content in the metal-oxide sample. The EPR signal due to $N_b^{\bullet}$ increased on irradiation of the doped sample at 437 nm in O_2($p_{O2} = 5$ kPa) and a new EPR line appeared, attributed to $O_2^{-\bullet}$ radical anions (reactions 11 and 12). These anions are apparently stabilized on two different surface

$$N_b^- + h\nu \rightarrow N_b^{\bullet} + e_{surf}^- \tag{3.11}$$

$$e_{surf}^- + O_2 \rightarrow O_2^{-\bullet} \tag{3.12}$$

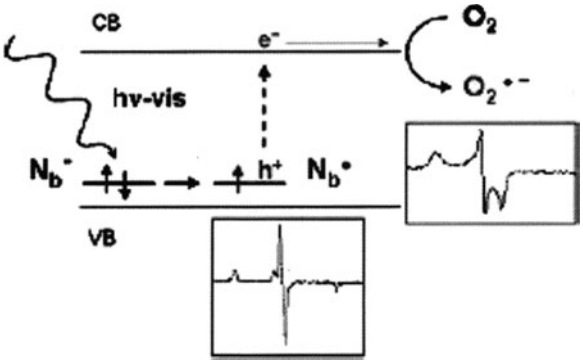

Fig. 34 Sketch of the proposed mechanism for the processes induced by vis-light irradiation of the N-doped sample in O_2 atmosphere. Reproduced with permission from Livraghi et al. (2006). Copyright by the American Chemical Society

Ti^{4+} species, which Livraghi et al. (2006) claimed could be typical of N-doped TiO_2s. Figure 34 illustrates the process embodied in the formation of the superoxide radical anions.

So far all the DFT-based calculations *have failed* to calculate experimentally commensurate band gap energies for undoped anatase and rutile TiO_2, and consequently for all anion-doped TiO_2 systems unless, as some have done, one resorts to the scissor operator.

In a comprehensive theoretical investigation of substitutional anion doping in TiO_2, Wang and Lewis (2006) explored the electronic properties of C-, N-, and S-doped TiO_2 materials using an ab initio tight-binding method (FIREBALL) based on DFT and a nonlocal pseudopotential scheme. FIREBALL is a first-principles tight-binding molecular dynamics (TBMD) simulation technique based on a self-consistent version of the Harris–Foulkes functional. The method uses confined atomic-like orbitals as the basis set. To test the methodology, the electronic structures of bulk TiO_2 in the rutile and anatase architectures were examined first for comparison. The calculated direct band gap from Γ to Γ of 3.05 eV for rutile accords with the reported experimental gap of 3.06 eV (Pascual et al. 1978). We have seen that the LDA approach generally underestimates the experimental band gap for insulators and semiconductors, whereas the band gap obtained from *ab initio* plane-wave calculations for TiO_2 is around 2.0 eV (Glassford and Chelikowsky 1992). This underestimation by the LDA approach was compensated in the theoretical treatment of Wang and Lewis (2006) using a local-orbital basis set. For anatase, the direct band gap from Γ to Γ of 3.26 eV is in agreement with the experimentally observed gaps of 3.20 eV (Sanjines et al. 1994). The upper valence bands are composed mainly of O 2*p* states with band widths of 5.75 and 4.86 eV for rutile and anatase structures, respectively, in accord with experimental values of 5.50 and 4.75 eV. The lower CBs consist primarily of unoccupied Ti 3*d* states and have a full width of 5.8 eV (rutile) and 5.6 eV (anatase). The results are summarized in Table 2.

Table 2 Comparison of calculated values (Wang and Lewis 2006) for the electronic properties of undoped rutile and anatase TiO_2 with experimental and calculated values reported by others (E_{BG} is the direct band gap, and E_{VB} is the valence band width)

	E_{BG} (rutile), eV	E_{BG} (anatase), eV
Wang and Lewis	3.05	3.26
Experiments	3.06 (1)	3.20 (2), 3.42 (3)
Other calculations	2.00 (4); 1.78 (5)	2.22 (5), 2.00 (6)
	E_{VB} (rutile), eV	E_{VB} (anatase), eV
Wang and Lewis	5.75	4.86
Experiments	5.50 (7)	4.75 (2)
Other calculations	5.70 (4), 6.22 (5)	5.17 (5), 5.05 (6)

Pascual et al. (1978); Sanjines et al. (1994); Tang et al. (1995); Glassford and Chelikowsky (1992); Mo and Ching (1995); Asahi et al. (2000); Kowalczyk et al. (1977)

The congruence of the above results provides some confidence on calculations pertaining to anion-doped TiO_2 systems.

For C-doped anatase and rutile TiO_2, a 384-atom (64 primitive unit cells) supercell was employed (Wang and Lewis 2006) at two doping levels in carbon: one O atom was randomly substituted by C (doping level 0.26%), and 20 oxygen sites were randomly substituted by C (doping level 5.20%). Carbon-doping had no effect on the CB of TiO_2 but did introduce new states above the valence band edge of bulk TiO_2 in C-doped structures. Substituting C atoms for O atoms shifted the valence band edge to higher energy compared to bulk TiO_2 so that the band gap narrowed. For the 5.2% C-doping level, the new valence band states were fairly continuous leading to a significant red shift of the valence band edge such that the corresponding band gap was narrowed to 2.0 eV for *anatase* and 2.35 eV for *rutile*, in apparent reasonable accord with the experimental absorption edges reported by Khan and coworkers (2002) of 2.32 and 2.82 eV in ca. 5% C-doping. By contrast, at low C- doping (0.26%) the C states were isolated (localized) and only slightly affected the anatase TiO_2 O 2*p* valence band states. Accordingly, the mobility of the hole created under these conditions must be rather poor (hole is trapped in these localized states), which explains why the photoactivity was low at low C-dopings. However, at the high C concentration of 5.2% the states near the valence band edge of anatase TiO_2 were less localized; there was significant overlap with the O 2*p* states, and there were a greater number of occupied states near the valence band edge. These observations explained why the high C-doping level led to greater visible-light absorption and thus to higher visible-light photoactivity (Wang and Lewis 2006). In C-doped *rutile* TiO_2, both high and low doping concentrations shifted the valence band edge upward by 0.7 eV.

Because of the odd number of electrons in the N atom, two O atoms were replaced by one N yielding an effective N-doping level of 0.52% for the low concentration case (Wang and Lewis 2006). Here also, the CB minimum remained unchanged. New states were introduced by N-doping just above the valence band edge of bulk TiO_2, as well as states that penetrated into the upper valence band of the bulk states. Unlike C-doped *rutile* TiO_2, however, no significant energy shift (<0.05 eV) in the

valence band edge was seen in N-doped *rutile* TiO_2 at the high N concentration of 5.2%. A significant shift was observed only at the low N-doping level of 0.52% resulting in a narrowed band gap of 2.55 eV. DOS calculations inferred that low doping concentrations greatly improved the visible-light photoactivity. There was no significant overlap between the N 2*p* states and the O 2*p* states for the 0.52% N-doping level. Moreover, at the low N concentration the valence band edge was more localized compared to the high N-doping level in N-doped *rutile* TiO_2. Unlike N-doped *rutile* TiO_2, however, identical shifts of ca. 0.44 eV were obtained in N-doped *anatase* TiO_2 at both high and low doping levels resulting in a band gap of ca. 2.82 eV(440 nm). DOS calculations indicated a significant overlap between the N 2*p* states and O 2*p* states for the 5.2% N-doping. By contrast, at the low N-doping level, the states introduced by N were distinct and highly localized on the single dopant state, and there was no significant overlap for structures containing 0.52% N. Thus, the high N-doping level in N-doped *anatase* TiO_2 should lead to greater visible-light photoactivity.

Comparison of results of C-doped *rutile* with N-doped *rutile* TiO_2 shows that incorporation of C dopants produces a narrower band gap than does N-doping, regardless of the doping concentration (Wang and Lewis 2006). Hence, C-doped TiO_2 materials should absorb more energy in the visible-light region than N-doped materials, and should provide greater visible-light activity owing to less localized states at the high concentrations. Similar to the C-doped case, the greater number of occupied states near the valence band edge at the high N-doping concentration should lead to a greater participation of N-doped TiO_2 in photoreactions taking place under visible light.

For S-doped TiO_2s, DOS results showed that at low doping levels (0.26%) there was no significant shift of the valence band edge, which implies that at low S-doping levels the S-doped TiO_2 materials should show poor visible-light photoactivity because of the large band gap in such systems (>3 eV) (Wang and Lewis 2006). In contrast, a significant red-shift of the valence band edge was seen at the high S-doping levels in both *rutile* and *anatase* structures; the corresponding band gaps were narrowed down to 2.3 and 2.2 eV, respectively. In contrast to the C- and N-doped TiO_2, the valence band edge was much delocalized for the low S-doping level in S-doped TiO_2. And since the valence band edge remained virtually unchanged, there should be no great photoactivity when S-doped systems are subjected to visible-light irradiation. At the high S-doping concentration, photoactivity in the visible region should be more pronounced than at the low S concentration due to band gap narrowing and to delocalization of the valence band edge (Wang and Lewis 2006). According to this theoretical treatment, S-doped TiO_2 materials should afford the smallest visible-light photoresponse among the C, N, and S anion dopants. Indeed, among the anion dopants examined, C-doping should be the most promising candidate for second-generation photocatalytic TiO_2-based materials, because C dopants produce the largest red-shift of the valence band edge amongst the three anion-doped TiO_2 examined.

It is clear from the extensive discussion above that there is no consensus about whether or not there is *band gap narrowing* in doped TiO_2 materials based on DFT

calculations. Some of the theoretical studies have deduced from these calculations that there is a *rigid shift of the valence band edge* to higher energies, thus narrowing the *intrinsic* band gap of TiO_2 as a consequence of doping. The discrepancies cannot be a semantic problem. One thing is certain. Anion-doping (or for that matter any type of doping) of TiO_2 does shift the *absorption edge* of the doped metal oxide to longer wavelengths, thus affording visible-light potentially photoactive materials useful in several important applications of surface processes occurring on the TiO_2 surface. In the past, we have referred to the longest visible-light wavelength at which photoactivity was seen as the *red limit of photocatalysis*. What does change, however, is the lowest photothreshold (i.e., *extrinsic* absorption edge) of the actinic light that can activate TiO_2 by introducing dopants into the metal-oxide lattice. When C-, S- and N-doped TiO_2 systems are photoactivated by visible light absorption, they also generate electrons and holes, although the latter carrier will have a decreased oxidative power (lower redox potential) *vis-a-vis* holes photogenerated from pristine TiO_2. The *intrinsic* absorption edge of the metal oxide itself is not changed by the doping. In other words, the valence and conduction bands are not affected by the doping, *at least* at low doping levels and weak interactions. But if they were to be affected through strong coupling interactions between the dopant states and the O 2*p* states of the valence band of TiO_2, then we must face the inescapable conclusion that the material may no longer be TiO_2, but more appropriately may be described as titanium oxynitride, titanium oxycarbide, or titanium oxysulfide materials possessing entirely different properties, not least of which are new electronic structures of their respective valence and conduction bands.

Next, we examine the optical properties of doped TiO_2 and TiO_2/polymer compositions, and provide some evidence based on the photobleaching phenomenon that the absorption bands observed in the visible spectral region of the TiO_2/polymer compositions can be bleached. That is, the species that give rise to or that are responsible for the absorption bands in the visible spectral region can be destroyed by irradiating the compositions with visible-light wavelengths corresponding to the absorption bands in the visible spectral region. In the TiO_2/polymer compositions, the above-referred to species are located on the *particle surface*, or at best in the *near subsurface region*, and thus can be annihilated by oxygen-assisted photoreactions. Under these conditons, neither the *intrinsic* valence band nor the *intrinsic* CB can be destroyed.

5 Optical Features of Doped TiO_2

Optical properties of doped TiO_2 specimens are best analyzed by difference DRS methods. Calculation of difference spectra to obtain the more typical absorption spectra requires DRS spectra of various doped TiO_2 samples absorbing in the visible region [$\rho_{ab}(h\nu)$] and of undoped TiO_2 samples non-absorbing in the visible spectral region [$\rho_{non\text{-}ab}(h\nu)$]. The latter is typically the DRS spectrum of a nominally clean

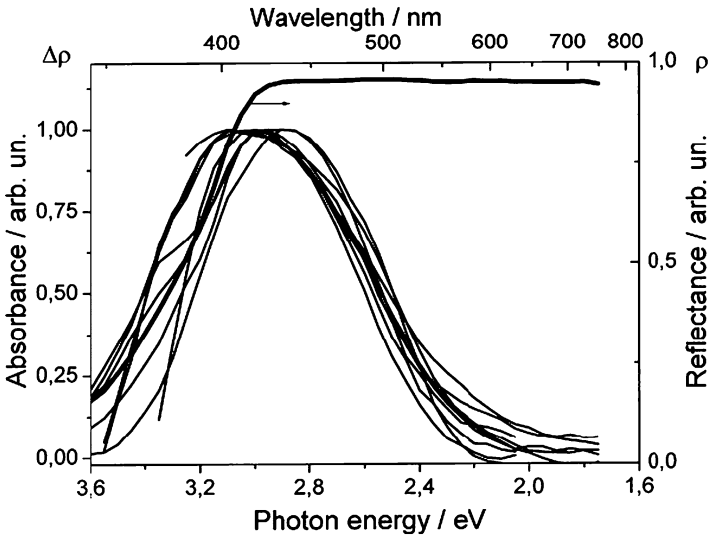

Fig. 35 Absorption spectra of various anion-doped TiO_2 specimens before averaging (see text) and the diffuse reflectance spectrum (DRS) of Degussa P25 TiO_2

TiO_2 sample or the DRS spectrum of the doped sample *prior* to any heat treatment that might induce visible-light absorption. For compositions consisting of TiO_2 and a number of polymeric substrates examined by Kuznetsov and Serpone (2006), the notation $[\rho_{non\text{-}abs}(h\nu)]$ and $[\rho_{abs}(h\nu)]$ referred, respectively, to the DRS spectra before and after the sample's treatment (heat or irradiation). If the DRS transmittance spectrum of a thick enough sample is 0, then the change in reflectance $\Delta\rho(h\nu)$, i.e., $[\rho_{non\text{-}abs}(h\nu) - \rho_{abs}(h\nu)]$, is identical to the change in absorbance $\Delta A(h\nu)$. Where optical properties of doped specimens have been characterized by absorption spectra $A(h\nu)$, the difference absorption spectra $\Delta A(h\nu)$ were calculated in a manner similar to difference DRS spectra, $\Delta\rho(h\nu)$. It should be emphasized that usage of difference diffuse reflectance and/or difference absorption spectra provide a means for numerical analysis of the optical characteristics of the samples. The numerical analysis typically involves (i) the characterization of each absorption spectrum by the position of the spectral maximum ($h\nu_{max}$), the intensity of this maximum ($\Delta\rho_{max}$, ΔA_{max}), and the spectral bandwidth at half-maximum amplitude; (ii) the comparison of the spectra of different samples after normalization by the $\Delta\rho_{max}/\Delta A_{max}$ factor; and (iii) the analysis of the shape of the absorption spectra, i.e., the ability of presenting the spectra as a sum of individual absorption bands.

The analysis illustrated below for anion-doped TiO_2 specimens involved (a) digitization (numbering) of the DRS spectra or the absorption spectra of the sample in non-VLA and VLA states, (b) calculation of the difference spectra, and (c) normalization of the spectra by the $\Delta\rho_{max}/\Delta A_{max}$ factor. The resulting absorption spectra display maximal absorption around 3.0 eV (Fig. 35); however, the shape of the spectra may differ (significantly for some). In some cases, the long-wavelength tail of the absorption may extend well into the near-infrared region ($h\nu < 1.5$ eV). Such

broad absorption spectra would be very complex for a numerical analysis. Only a few relatively narrow absorption spectra were selected for the numerical analysis to evaluate the inherent similarities among the spectral characteristics of anion-doped titania samples. Selected results are illustrated in Fig. 35, which reports the absorption spectra of several N-doped titania specimens: (i) mechanochemically activated N-doped TiO_2 (Yin et al. 2003), (ii) N-doped oxygen-deficient TiO_2 (Ihara et al. 2003), (iii) NFT sample prepared by a spray pyrolytic method (Li et al. 2005c), (iv) N-doped *anatase* TiO_2 specimen prepared by a solvothermal process (Aita et al. 2004), (v) N-doped *rutile* TiO_2 sample also prepared by a solvothermal process (Aita et al. 2004), (vi) *yellow* N-doped TiO_2 specimen synthesized in short time at ambient temperatures using a nanoscale exclusive direct nitridation of TiO_2 nanocolloids with alkyl ammonium compounds (Gole et al. 2004), (vii, viii) N-doped TiO_2 samples prepared by evaporation of the sol-gel with N-doping carried out under a stream of ammonia gas at different temperatures (Joung et al. 2006), and (ix) N-doped TiO_2 prepared via sol-gel by mixing a solution of titanium(IV) isopropoxide in isopropyl alcohol in the presence of an NH_4Cl solution (Livraghi et al. 2006).

Broad absorption spectra are often obtained for samples prepared by a procedure otherwise identical to that of samples exhibiting the narrow spectra. Temperature and time of calcination are frequently reported as factors that affect the shape of the spectra. For instance, an increase of temperature from 247 to 347°C for 2 h (Wang et al. 2007a) or prolonging the time of calcination from 5 min to 30 min at 400°C

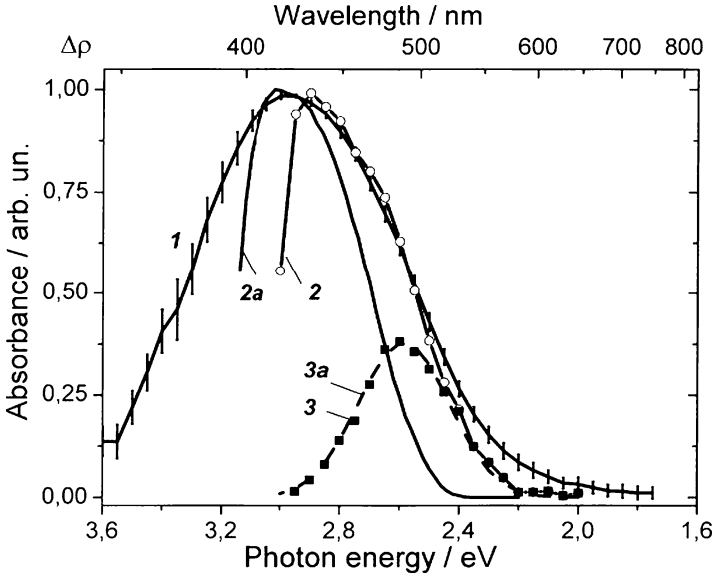

Fig. 36 Average absorption spectrum of visible-light-active N-doped TiO_2 specimens (curve *1*); difference absorption spectra of N-doped rutile crystal (curve *2*) and of the color centers in the yellow anatase TiO_2 crystal (curve *2a*). Curve *3* (*solid squares*) depicts the difference between curves *2* and *2a*; curve *3a* (*line*) is the Gaussian fit of curve *3* (see text for more details)

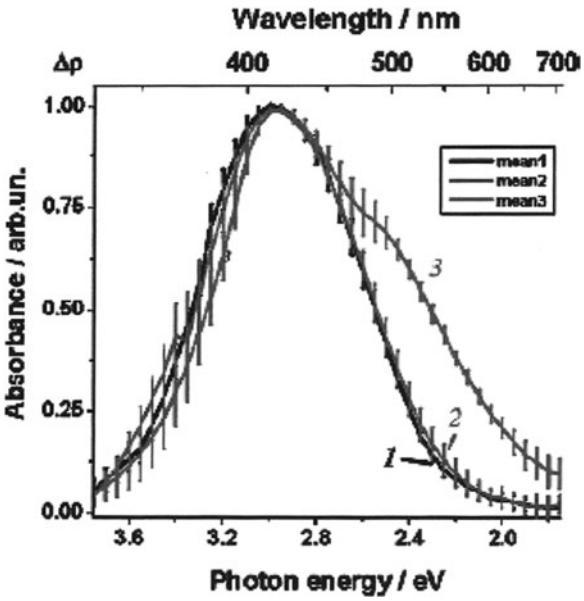

Fig. 37 Average absorption spectra (Δρ) of various titania systems. See text for details of the origins of these spectra. Reproduced with permission from Kuznetsov and Serpone (2006). Copyright 2006 by the American Chemical Society

(Joung et al. 2006) decreased the absorption in the range hν <2.0 eV, such that the absorption spectra then adopt a narrower shape. As an example, the broad absorption spectrum of the *orange* N-doped TiO_2 specimen, prepared in nearly the same manner as the *yellow* N-doped TiO_2 sample by Gole et al. (2004), shows a shoulder on the low-energy side at ca. 2.5 eV (see Fig. 37).

Figure 35 clearly demonstrates the strong similarity of selected spectra in the visible region at energies hν <3.0 eV, and the noticeable differences in the range of *intrinsic* absorption at hν >3.0 eV. The latter differences are not surprising because the samples differed in phase composition (see e.g., Aita et al. 2004) and sample thickness. Moreover, some workers often choose any available sample, e.g., Degussa P25 TiO_2, as the non-absorbing specimen in the visible spectral region, rather than a specimen prepared in an otherwise identical fashion as the doped samples.

The spectral similarities in Fig. 35 allowed Kuznetsov and Serpone (2006) to calculate the average (mean) spectrum of the VLA N-doped TiO_2 samples that is illustrated in Fig. 36 (curve *1*). Note that the standard error for the mean spectrum does not exceed 2.3% in the energy range hν <3.0 eV.

Figure 36 also displays the absorption spectrum of the nitrogen-doped rutile crystal prepared by an NH_3 treatment at 597°C (curve *2*) (Diwald et al. 2004b) and the absorption spectrum (curve *2a*) of the anatase crystal reported by Sekiya and co-workers (2000, 2004). The difference in spectra *2* and *2a* in the region hν >3.0 eV originates from the difference in the phase composition of the TiO_2,

whereas the difference between curves *2a* and *2* at hν <3.0 eV exhibits a single absorption band with $h\nu_{max} = 2.6$ eV, half-width of 0.35 eV and a near-Gaussian shape, i.e., the band is very similar to the 2.55-eV AB2 band reported earlier by Kuznetsov and Serpone (2006).

Sekiya and coworkers (2000, 2004) attributed the absorption band at 3.0 eV in the spectrum of anatase to oxygen vacancies that can trap electrons to yield *F*-type centers (Sekiya et al. 2004). It is important to emphasize that the absorption band AB1 can be obtained in a variety of ways: for instance, (i) by annealing the *as-grown* crystals under an oxygen atmosphere at T >374°C (Sekiya et al. 2000, 2004) and (ii) by annealing *colorless* crystals by subjecting them first to a reductive H_2 atmosphere at 647°C and then to an O_2 atmosphere at 497°C (Sekiya et al. 2004). In both cases, only prolonged (ca. 60 h) annealing of the crystals at 797°C in an O_2 atmosphere, not in inert (a nitrogen) atmosphere, transformed the yellow crystals that display the absorption band at 3.0 eV to a colorless state (Sekiya et al. 2004). In the first case, the origin of the oxygen vacancies is associated with the uncontrolled reduction of TiO_2 assisted by impurities introduced into the crystal during its growth (Sekiya et al. 2000). The absorption of N-doped rutile crystals in the visible spectral region has only been partially associated with reduction of the TiO_2 bulk lattice (Diwald et al. 2004b). However, the main reason for the shift in the photochemical threshold from 3.0 eV to 2.4 eV was suggested by Yates and coworkers (Diwald et al. 2004a, b; Thompson and Yates 2005) to originate from the nitrogen dopant located in an interstitial site and probably bonded to hydrogen. This inference contrasts the interpretation given by Sekiya and coworkers (2000, 2004) for the spectral features in the visible region, by Di Valentin et al. (2005a) from their EPR study, and with our assignments of the absorption bands in the visible spectral region of titania/polymer compositions (Kuznetsov and Serpone 2006).

As a further attestation of the remarkable similarities in the absorption spectra of doped TiO_2 systems, Fig. 37 summarizes additional averaged spectra. Curve *1* depicts the average spectrum obtained from the absorption spectra reported in the literature (see Kuznetsov and Serpone 2006 for details) of (i) Cr-implanted TiO_2, (ii) Ce-doped TiO_2, (iii) mechanochemically activated N-doped TiO_2, (iv) N-doped oxygen-deficient TiO_2, and (v) from $Sr_{0.95}La_{0.05}TiO_{3+\delta}$ treated with HNO_3 acid. Curve *2* represents the average spectrum obtained from the difference DRS's (absorption spectra) of various anion-doped titania specimens: (i) NFT, (ii) N-doped anatase TiO_2, (iii) N-doped rutile TiO_2, and (iv) yellow nitrided $TiO_{2-x}N_x$ nanocolloids. Curve *3* illustrates the averaged spectra of cation-doped TiO_2s, namely (i) Fe-doped TiO_2 nano-powders prepared by oxidative pyrolysis of organo-metallic precursors in an induction thermal plasma reactor, (ii) zinc-ferrite- doped titania ($TiO_2/ZnFe_2O_4$) synthesized by sol-gel methods followed by calcinations at various temperatures, and (iii) the orange N-doped TiO_2 sample prepared by a procedure otherwise identical to that of yellow N-doped TiO_2 but with the former consisting of partially agglomerated nanocolloids (i.e., larger $TiO_{2-x}N_x$ clusters). Hence, note the remarkable overlap of the relatively narrow average spectra *1* and *2* in Fig. 37, which illustrates convincingly the independence of the spectra on the method of photocatalyst preparation. This appears to be a general feature of the

electronic and spectral features of the color centers/defects in TiO_2. Comparison of the broader mean spectrum *3* in Fig. 37 with the narrower spectra *1* and *2* indicates that broadening of the absorption spectrum of TiO_2 photocatalysts originated from the long-wavelength absorption band, in this case the 2.55-eV AB2 band in the study of Kuznetsov and Serpone (2006).

The coincidence of the absorption bands in the visible spectral region for reduced TiO_2 with those of VLA TiO_2 samples indicates that the processes involved in the preparation of VLA TiO_2 specimens (irrespective of the method) implicate a stage of TiO_2 reduction. As we saw earlier, many of the preparative methods included a heating stage at various temperatures. For instance, the absorption band appearing at 3.0 eV in anatase crystals and attributed to oxygen vacancies results from the removal of impurities at ca. 300°C introduced during the crystal growth (Sekiya et al. 2000). Related to this, the visible-light absorption of metal-ion-implanted TiO_2 systems reported by Anpo and Takeuchi (2003) was observed only after the samples had been calcined in the temperature range 450–550°C.

The absorption features displayed by TiO_2 specimens in the visible spectral region most likely originate from the formation of color centers through the reduction of TiO_2 after some form of heat treatment or after some photostimulated process.

Kuznetsov and Serpone (2006) concluded that the absorption spectra of anion-doped (or otherwise) TiO_2 in the visible spectral region originated from the existence of color centers, rather than from a narrowing of the original band gap of TiO_2 ($E_{bg} = 3.2$ eV; anatase), as originally espoused by Asahi et al. (2000, 2001), through mixing of oxygen and dopant states. True narrowing of the original band gap of the metal-oxide TiO_2 semiconductor would necessitate heavy anion or cation doping, which would require somewhat high concentrations of the dopants. In the latter case, however, one must ask whether the metal oxide retains its original integrity.

What is the nature of these color centers? Although we have seen these in various contexts earlier, it is nonetheless instructive to reiterate what they are and how they may be formed. On loss of an O atom in a metal oxide (reaction 3.13), the electron pair remaining behind is trapped in the V_O cavity (reaction 3.14) left behind giving rise to an *F* center, whereas a positively charged F^+ center is equivalent to a single electron associated with the oxygen vacancy, $V_O^{\bullet}$ (reaction 3.15; again in the Kroger–Vink notation). The electron-pair deficient oxygen vacancy, $V_O^{\bullet\bullet}$, also known as an anion vacancy, V_A, can be viewed as a doubly charged F^{++} center (reaction 3.13). Thus, the color centers associated with oxygen vacancies imply the existence of *F*-type centers in TiO_2 and other metal oxides. The electrons left behind can also interact with Ti^{4+} ions in regular lattice sites (Ti_{reg}^{4+}) adjacent to the oxygen vacancy or located at interstitial lattice sites (Ti_{int}^{4+}) to give Ti_{reg}^{3+} and Ti_{int}^{3+} color centers, respectively (reactions 3.16); *F*-type centers can also generate the latter color centers through charge transfer (reaction 3.17).

$$Ti^{4+} - O^{2-} - Ti^{4+} \rightarrow Ti^{4+} - O^{2-} - Ti^{4+} + V_O^{\bullet\bullet}(F^{++}) + 2e^- \qquad (3.13)$$

$$V_O^{\bullet\bullet} + 2e^- \rightarrow V_O(F) \tag{3.14}$$

$$V_O^{\bullet\bullet} + e^- \rightarrow V_O^{\bullet}(F^+) \tag{3.15}$$

$$e^- + Ti^{4+}{}_{reg}\left\{Ti^{4+}{}_{int}\right\} \rightarrow Ti^{3+}{}_{reg}\left\{Ti^{3+}{}_{int}\right\} \tag{3.16}$$

$$F(\text{or } F^+) + Ti^{4+}{}_{reg}\left\{Ti^{4+}{}_{int}\right\} \rightarrow Ti^{3+}{}_{reg}\left\{Ti^{3+}{}_{int}\right\} + F^+(\text{or } F^{++}) \tag{3.17}$$

Spectrum *3* of Fig. 37 can be deconvoluted into 3 overlapping absorption bands depicted in Fig. 38 (Serpone 2006). Of these three bands, one is centered at 2.1 eV (590 nm; band *1*), another at ca. 2.40 eV (517 nm; band *2*), and band *3* occurs around 2.93 eV (413 nm) in good accord with the band positions reported by Kuznetsov and Serpone (2006) for the reduction of TiO_2 in polymeric media. The congruence of the bands in the absorption spectra of such disparate TiO_2 systems is remarkable when considering the large variations in the experimental conditions, which re-affirms the notion that the absorption bands all share the same origins. Bands 1–3 in Fig. 38 originate either from electron transitions involving *F*-type centers and/or from d–d transitions in Ti^{3+} color centers. Evidence for both has appeared in the literature (see references in Serpone 2006).

Using the embedded-cluster numerical discrete variational method, Chen et al. (2001) estimated the band gap energy of rutile TiO_2 as 3.05 eV in very good agreement with the experimental 3.0 eV for this polymorph. Calculations of the energy levels of the *F*-type centers gave energies for the *F*, F^+ and F^{2+} centers, respectively, of 0.87, 1.78, and 0.20 eV below the bottom level of the CB.

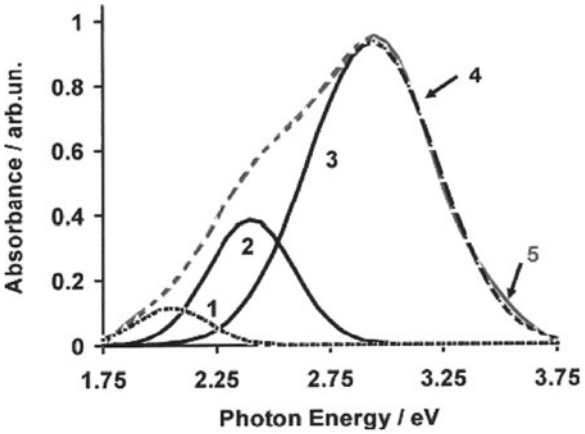

Fig. 38 Deconvolution of spectrum 3 of Fig. 37 (curve *5* herein). Band 4 represents the deconvolution sum of curves 1, 2, and 3. Reproduced with permission from Serpone (2006).Copyright 2006 by the American Chemical Society

The scheme below summarizes the positions of these *F* centers in rutile. A band seen at 760 nm (1.61 eV) was ascribed to the electron transition from the F^+ center to the CB of TiO_2. The 0.87-eV level consisted of an admixture of the *F* center's 1*s* orbital and a Ti 3*d* orbital; the respective charge population densities were −1.325 and −0.3014, indicating that *F* color center electrons may be influenced by neighboring Ti^{4+} cations, and that (partial) charge transfer from the *F* center to adjacent Ti^{4+} ions may occur yielding formally Ti^{3+} color centers. Photoinduced detrapping of electrons from the *F* center to the CB followed by retrapping by the shallow F^{2+} centers can increase the number of F^+ centers

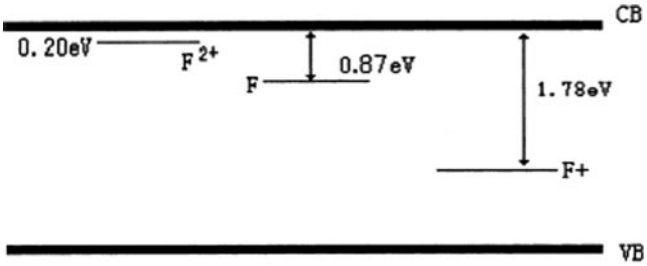

From past extensive experimental and theoretical studies, Serpone (2006) tentatively attributed the deconvoluted bands 3 and 2 in the three average spectra of Fig. 37 at 2.9–3.0 eV (428–413 nm) and 2.4–2.6 eV (ca. 517–477 nm), respectively, to Jahn–Teller split $^2T_2 \rightarrow {}^2E$ transitions of Ti^{3+} centers. The existence of these centers has been confirmed by EPR examination of N-doped TiO_2 specimens calcined at various temperatures (Joung et al. 2006; Suriye et al. 2006). Band 1 at 1.7–2.1 eV (729–590 nm) was tentatively assigned to a transition from the ground state of the F^+ center to its corresponding excited F^{+}* state, though transition to the CB of TiO_2 was not precluded. The transition from the singlet ground state S_o of the *F* center to the first *F** excited singlet state ($S_o \rightarrow S_1$) or to the CB likely occurs at much lower energies (in the infrared) as predicted from the energies in the above scheme. Nonetheless, ascertaining such assignments will require some rigorous systematic studies that will examine anion- and cation-doped TiO_2 specimens by diffuse reflectance spectroscopy, by EPR techniques and by photoconductivity methods. In this regard, in a recent feature article Kuznetsov and Serpone (2009) carried out a systematic analysis of the absorption spectral features of various titanium dioxide specimens, whether doped or undoped, in the visible spectral domain reported extensively in the literature. In addition they briefly examined the origins of such bands in visible-light-active TiO_2 photocatalysts, i.e. second-generation photocatalysts. They deduced that at energies of h less than 2.0 eV (i.e. > ~600 nm) the three spectral features occurring in the near-infrared and infrared regions originate from Ti^{n+}-related (n = 3, 2) color centers, whereas the three absorption bands seen in the visible spectral region AB1 (2.75–2.95 eV), AB2 (2.50–2.55 eV),and AB3 (2.00–2.30 eV) are associated with oxygen vacancies (i.e. with *F*-type color centers) on the basis of demonstrated experimental observations. Also discussed was the question as to why reduction of TiO_2 that accompanies the

process of TiO_2 doping results only in the formation of the absorption bands AB1, AB2, and in some cases AB3; that is, the absorption features of Ti-related centers are totally suppressed. Recent studies that have demonstrated the reduction of TiO_2 during the doping process were also examined to argue on the dominant role of *F*-type color centers in the visible-light-activity of TiO_2 photocatalysts.

6 The Question of Band Gap Narrowing in Doped TiO_2

Taken literally, band gap narrowing in doped TiO_2 materials means that the band gap energy of TiO_2 has been decreased by the presence of dopants. To re-emphasize the point, however, what does change is the energy photothreshold for activating doped titania specimens to carry out surface photoinduced redox processes. Perhaps a better term in referring to the long-wavelength absorption edge might be (i) the *red-limit of TiO_2 photocatalysis* as used in the past to refer to photooxidations and photoreductions occurring in the visible spectral region or we might refer to the lowest-energy photothreshold or long-wavelength absorption edge as (ii) the *extrinsic band gap(s)* of doped TiO_2 vs. the term *intrinsic band gap* (for anatase, 3.2 eV; for rutile, 3.0 eV) that refers to pristine undoped titania. Nonetheless, band gap narrowing as used by some workers (e.g., by Asahi et al. 2000, 2001; and others) meant a rigid upward shift of the valence band edge toward the CB of TiO_2. If the absorption features seen in the visible spectral region were truly due to this rigid shift, then irradiation into these bands should cause no bleaching of the absorption bands. However, if the absorption features are due, as we have claimed, to the existence of color centers (*F*-type and/or Ti^{3+}), then bleaching of the spectral features can be observed if photostimulated destruction of color centers occurs. Recent work has addressed this issue for both TiO_2/polymer compositions (Kuznetsov and Serpone 2007) and for an N-doped TiO_2 system (Emeline et al. 2007).

In the first instance, we examined the photocoloration of TiO_2 compositions with various polymers and the photobleaching of the color centers (Fig. 39) at various selected irradiation wavelengths (UV to the near infrared region) to probe the photoactivation of the color centers by irradiating into the absorption bands with maxima at 2.90 eV (427 nm; AB1), 2.55 eV (486 nm; AB2), and 2.05 eV (604 nm; AB3). This procedure aided in clarifying the mechanism of the photobleaching phenomenon as an oxygen-assisted photochemical reaction. A great advantage of degraded TiO_2/polymer compositions over VLA TiO_2s is that the color centers in the former are located at or near the surface. The color centers in the volume bulk lattice can be destroyed by a high-temperature treatment in the presence of oxygen, as for example in single crystals (Sekiya et al. 2000, 2004). Two principal types of photostimulated absorbance changes can occur: (i) increase in absorbance or (ii) decrease in absorbance. The decrease in absorbance would be a direct experimental manifestation of the photobleaching phenomenon of colored TiO_2/polymer compositions, which would clearly demonstrate the presence and the photoinduced

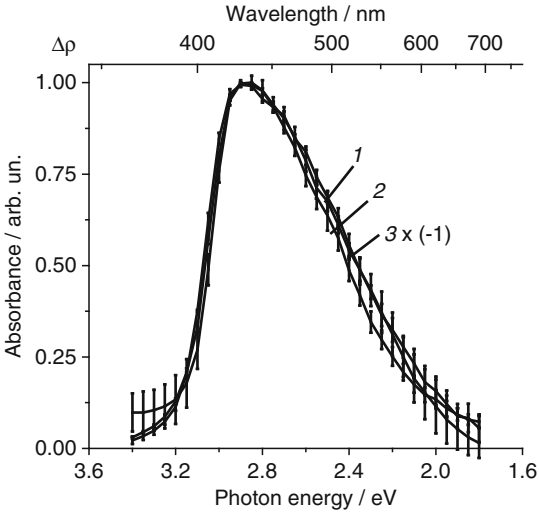

Fig. 39 Averaged absorption spectra (*1, 2*) of various TiO_2/polymer compositions normalized by $\Delta\rho_{max}$ and averaged bleaching spectrum (*3*) of the TiO_2/[P(VDF-HFP)] composition irradiated at different wavelengths. From Kuznetsov and Serpone (2007)

disappearance/destruction of color centers in these titanium dioxide systems. In Fig. 39, the average spectrum of the bleaching of one colored TiO_2/ [P(VDF-HFP)] composition, where P(VDF-HFP) refers to the poly(vinylidene fluoride/co-hexafluoropropylene polymer, irradiated at different wavelengths is depicted as curve *3* and is compared to the average heat-induced absorption spectrum (curve *1*) and photoinduced absorption spectrum (curve *2*) of several other TiO_2/polymer compositions (Kuznetsov and Serpone 2007). The unambiguous experimental data obtained confirmed an earlier proposal (Kuznetsov and Serpone 2006) that absorption of light by various TiO_2 systems in the visible region originates *only* from color centers and *not* from a narrowing of the band gap of pristine TiO_2. Also, results indicate that photobleaching of colored TiO_2/polymer compositions originates both from *intrinsic* absorption of light ($h\nu > 3.2$ eV, anatase) by TiO_2 and from (*extrinsic*) absorption of light by the color centers at wavelengths corresponding to their absorption spectral bands in the visible region. Note that these bands are also active in the photodestruction of the color centers. It is also relevant to point out that spectrum *3* in Fig. 39 corresponds to the nearly complete discoloration of the compositions under irradiation mostly in the visible region. The total overlap of the absorption and bleaching spectra illustrated in Fig. 39 *demonstrate unambiguously* that the *same* color centers are formed during the treatment that induced the absorption, and that they are subsequently destroyed on irradiation during the photobleaching process. This result obviously negates any inference of broadening of the valence band of TiO_2 to account for the red-shifts of the absorption edges in various doped VLA TiO_2 systems. The valence and conduction bands *can neither* be photodestroyed *nor* phototransformed, contrary to the color centers.

In another study, we examined the effect of molecular oxygen and hydrogen on the photostimulated formation of defects (color centers) on irradiation of $TiO_{2-x}N_x$ with visible light at 546 nm; results are displayed in Fig. 40 as ΔR vs. λ (Emeline

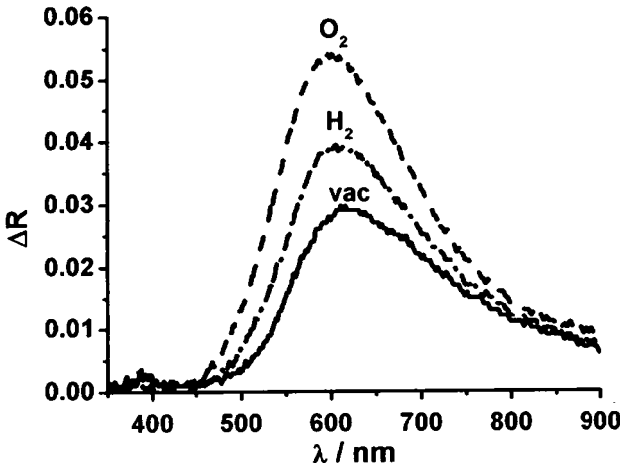

Fig. 40 Absorption spectra of photoinduced color centers in N-doped TiO_2 obtained after pre-irradiation at 546 nm in vacuum, in the presence of O_2 and H_2. From Emeline et al. (2007)

et al. 2007); note that ΔR and Δρ have the same meaning. A similar behavior was observed on irradiating at 436 and 578 nm. The influence of hydrogen on photocoloration on irradiation at 546 nm was nearly the same as under UV irradiation, in that the number of photoinduced defects increased, in contrast to the presence of O_2 for which photostimulated adsorption of oxygen was the exact opposite at the visible wavelength to that seen under UV irradiation. That is, the ultimate level of photocoloration (increase in absorption) in the presence of oxygen was considerably greater under 546-nm irradiation relative to the level in vacuum and relative to what was observed under UV-light irradiation. This could only mean that the mechanism of photoexcitation and surface photoreaction that occur under visible-light excitation of $TiO_{2-x}N_x$ in the presence of O_2 must be different from the mechanism of processes that take place under UV irradiation. The effect of photobleaching of photoinduced color centers by red light at $\lambda > 610$ nm in vacuum and in the presence of oxygen and hydrogen is reported in Fig. 41. No significant changes in absorption of photoinduced color centers occurred during photoexcitation in vacuum and in the presence of hydrogen. However, the presence of oxygen caused significant changes on the absorption as seen by the effect of photobleaching (negative absorbance) of UV-induced defects, a typical behavior of electron-type color centers (i.e., *F*-type centers and Ti^{3+} centers).

7 Concluding Remarks

In this chapter, we have attempted to expose and explore some of the root causes that have had such an impact and so changed the field of heterogeneous

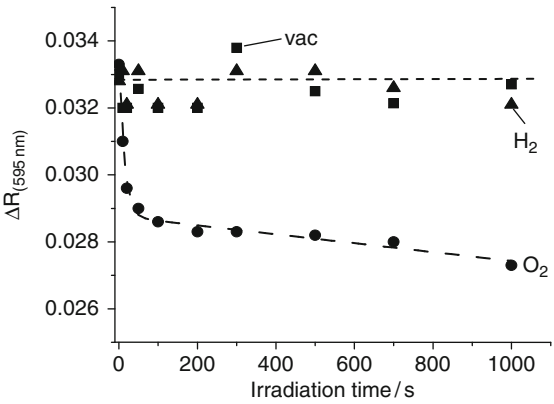

Fig. 41 Kinetics of photobleaching (recorded at $\lambda = 595$ nm) of photoinduced color centers on irradiation of $TiO_{2-x}N_x$ at $\lambda > 610$ nm in vacuum, in the presence of oxygen and in the presence of hydrogen. From Emeline et al. (2007)

photocatalysis involving second-generation materials. Various preparative methods have been described briefly and some characteristics features of the resulting cation- and anion-doped titanium dioxides presented. As in any healthy and novel scientific field of endeavor, controversies and debates are bound to occur. They are the expected norms. In this regard, note the variance in the experimental results and in the interpretations of X-ray photoelectron spectra with regard to assignments, particularly as they pertain to N-doped TiO_2 systems. Relative to pristine nominally clean TiO_2, whose absorption edges are at 3.2 eV for anatase and at 3.0 eV for the rutile polymorph, cation- and anion-doped TiO_2 specimens of both architectures have displayed red-shifted absorption edges well into the visible spectral region. Several workers have taken this to mean that the *intrinsic band gap* of TiO_2 had been narrowed by the interactions of dopant energy states with valence band states. Calculations based mostly on DFT using various supercell sizes have supported such an inference, while other workers, also using DFT methods, have proposed that the red-shifted absorption edges, i.e., decreased photothresholds in activating TiO_2, were due to the presence of dopant states within the band gap located above the upper level of the valence band. Irradiating into these dopant states with visible-light wavelengths would generate conduction band electrons and holes, the latter charge carrier remaining trapped at the dopant energy level(s). Analyses of the optical spectral features in the visible region, however, have inferred a common origin for the doped TiO_2s as deduced from the strong similarities in the absorption envelopes of a large number of specimens, irrespective of the preparative methods and of the nature of the dopants, whether they be transition metal ions or non-metals such as nitrogen, carbon, sulfur, fluorine and others. Workers interested in photo-oxidative and/or photoreductive processes in degrading environmental polluting substances should find greater process engineering photoefficiencies in utilizing the second-generation photocatalytic materials (or perhaps not, as we saw in a few cases) as doped titanias absorb a greater quantity of sunlight. By contrast, workers interested in the fundamental science that underscores heterogeneous photocatalysis in general, and second-generation photocatalysts in particular will find a rich

playing field ripe for further research and exploration limited only by one's imagination.

Acknowledgments One of us (NS) wishes to thank Prof. Angelo Albini for his kind hospitality during the writing of this contribution in the winter semester 2007. It gave NS the opportunity to escape the rigors of the Canadian cold winters.

References

Aita Y, Komatsu M, Yin S, Sato T (2004) Phase-compositional control and visible light photocatalytic activity of nitrogen-doped titania via solvothermal process. J Solid State Chem 177:3235–3238

Anpo M, Takeuchi M (2003) The design and development of highly reactive titanium oxide photocatalysts operating under visible light irradiation. J Catal 216:505–516

Asahi R, Taga Y, Mannstadt W, Freeman AJ (2000) Electronic and optical properties of anatase TiO_2. Phys Rev B 61:7459–7465

Asahi R, Morikawa T, Ohwaki T, Aoki K, Taga Y (2001) Visible-light photo-catalysis in nitrogen-doped titanium oxides. Science 293:269–275

Beck DD, White JM, Ratcliffe CT (1986) Catalytic reduction of carbon monoxide with hydrogen sulfide. 3. Study of adsorption of oxygen, carbon monoxide and carbon monoxide coadsorbed with hydrogen sulfide on anatase and rutile using Auger electron spectroscopy and temperature-programmed desorption. J Phys Chem 90:3132–3136

Belver C, Bellod R, Fuerte A, Fernandez-Garcia M (2006a) Nitrogen-containing TiO_2 photocatalysts part 1. Synthesis and solid characterization. Appl Catal B 65:301–308

Belver C, Bellod R, Stewart SJ, Requejo FG, Fernandez-Garcia M (2006b) Nitrogen-containing TiO_2 photocatalysts part 2. Photocatalytic behavior under sunlight excitation. Appl Catal B Environ 65:309–314

Berger T, Sterrer M, Diwald O, Knozinger E, Panayotov D, Thompson TL, Yates JT Jr (2005) Light-induced charge separation in anatase TiO_2 particles. J Phys Chem B 109:6061–6068

Chen J, Lin L-B, Jing F-Q (2001) Theoretical study of *F*-type color center in rutile TiO_2. J Phys Chem Solids 62:1257–1262

Cheng P, Li W, Zhou T, Jin Y, Gu M (2004) Physical and photocatalytic properties of zinc ferrite doped titania under visible light irradiation. J Photochem Photobiol A Chem 168:97–101

Cherkashin, A.E., Volodin, A.M., Koshcheev, S.V. and Zakharenko, V.S. (1980) Energy structure and photosorption and photocatalytic properties of titanium dioxide in carbon monoxide oxidation. Uspekhi Fotoniki, Issue 7, Leningrad State University (LGU), Leningrad, pp. 86–142

Colon G, Hidalgo MC, Munuera G, Ferino I, Cutrufello MG, Navio JA (2006) Structural and surface approach to the enhanced photocatalytic activity of sulfated TiO_2 photocatalyst. Appl Catal B 63:45–59

Di Valentin C, Pacchioni G-F, Selloni A (2004) Origin of the different photoactivity of N-doped anatase and rutile TiO_2. Phys Rev B 70:085116

Di Valentin C, Pacchioni G-F, Selloni A, Livraghi S, Giamello E (2005a) Characterization of paramagnetic species in N-doped TiO_2 powders by EPR spectroscopy and DFT calculations. J Phys Chem B 109:11414–11419

Di Valentin C, Pacchioni G-F, Selloni A (2005b) Theory of carbon doping of titanium dioxide. Chem Mater 17:6656–6665

Diebold U (2003) The surface science of titanium dioxide. Surf Sci Rep 48:53–229

Diwald O, Thompson TL, Goralski EG, Walck SD, Yates JT Jr (2004a) The effect of nitrogen ion implantation on the photoactivity of TiO_2 rutile single crystals. J Phys Chem B 108:52–57

Diwald O, Thompson TL, Zubkov T, Goralski EG, Walck SD, Yates JT Jr (2004b) Photochemical activity of nitrogen-doped rutile TiO_2(110) in visible light. J Phys Chem B 108:6004–6008

Dong CX, Xian AP, Han EH, Shang JK (2006) Acid-mediated sol-gel synthesis of visible-light active photocatalysts. J Mater Sci 41:6168–6170

Emeline AV, Kuzmin GN, Purevdorj D, Ryabchuk VK, Serpone N (2000) Spectral dependencies of the quantum yield of photochemical processes on the surface of wide band gap solids. 3. Gas/Solid Systems. J Phys Chem B 104:2989–2999

Emeline AV, Smirnova LG, Kuzmin GN, Basov LL, Serpone N (2002) Spectral dependence of quantum yields in gas-solid heterogeneous photosystems. Influence of anatase/rutile content on the photostimulated adsorption of dioxygen and dihydrogen on titania. J Photochem Photobiol A Chem 148:97–102

Emeline AV, Sheremetyeva NV, Khomchenko NV, Ryabchuk VK, Serpone N (2007) Photoinduced formation of defects and nitrogen-stabilization of color centers in N-doped titanium dioxide. J Phys Chem 111(30):11456–11462

Enache CS, Schoonman J, van de Krol R (2006) Addition of carbon to anatase TiO_2 by n-hexane treatment – surface or bulk doping? Appl Surf Sci 252:6342–6347

Formenti M, Juillet F, Meriaudeau P, Teichner SJ (1971) Heterogeneous photo-catalysis for partial oxidation of paraffins. Chem Technol 1:680–686

Frach P, Gloess D, Vergohl M, Neumann F, Hund-Rinke K (2004) EJIPAC, Saarbrucken, Germany. Quoted by Yates et al (2006).

Ghicov A, Schmidt B, Kunze J, Schmuki P (2007) Photoresponse in the visible range from Cr-doped TiO_2 nanotubes. Chem Phys Lett 433:323–326

Glassford KM, Chelikowsky JR (1992) Structural and electronic properties of titanium dioxide. Phys Rev B 46:1284–1298

Gole JL, Stout JD, Burda C, Lou Y, Chen X (2004) Highly efficient formation of visible light tunable $TiO_{2-x}N_x$ photocatalysts and their transformation at the nanoscale. J Phys Chem B 108:1230–1240. See also the web-site: http://www.physics.gatech.edu/people/faculty/jgole.html#links

Henderson MA, Epling WS, Perkins CL, Peden CHF, Diebold U (1999) Interaction of Molecular oxygen with the vacuum-annealed TiO_2(110) surface: molecular and dissociative channels. J Phys Chem B 103:5328–5337

Henderson MA, Epling WS, Peden CHF, Perkins CL (2003) Insights into photo-excited electron scavenging processes on TiO2 obtained from studies of the reaction of O_2 with OH groups adsorbed at electronic defects on TiO_2(110). J Phys Chem B 107:534–545

Huang D-G, Liao S-J, Liu J-M, Danga Z, Petrik L (2006) Preparation of visible-light responsive N–F-codoped TiO_2 photocatalyst by a sol–gel-solvothermal method. J Photochem Photobiol A Chem 184:282–288

Hurum DC, Agrios AG, Gray KA, Rajh T, Thurnauer MC (2003) Explaining the enhanced photocatalytic activity of degussa P25 mixed-phase TiO_2 using EPR. J Phys Chem B 107:4545–4549

Ihara T, Miyoshi M, Ando M, Sugihara S, Iriyama Y (2001) Preparation of a visible-light-active TiO_2 photocatalyst by RF plasma treatment. J Mater Sci 36:4201–4207

Ihara T, Miyoshi M, Iriyama Y, Matsumoto O, Sugihara S (2003) Visible-light-active titanium oxide photocatalyst realized by an oxygen-deficient structure and by nitrogen doping. Appl Catal B Environ 42:403–409

In S, Orlov A, Garcia F, Tikhov M, Wright DS, Lambert RM (2006) Efficient visible light-active N-doped TiO_2 photocatalysts by a reproducible and controllable synthetic route. Chem Commun 40:4236–4238

Irie H, Watanabe Y, Hashimoto K (2003) Nitrogen-concentration dependence on photocatalytic activity of $TiO_{2-x}N_x$ powders. J Phys Chem B 107:5483–5486

Janus M, Inagaki M, Tryba B, Toyoda M, Morawski AW (2006) Carbon-modified TiO_2 photocatalyst by ethanol carbonization. Appl Catal B Environ 63:272–276

Joung S-K, Amemiya T, Murabayashi M, Itoh K (2006) Relation between photo-catalytic activity and preparation conditions for nitrogen-doped visible light-driven TiO_2 photocatalysts. Appl Catal A Gen 312:20–26

Katoh M, Aihara H, Horikawa T, Tomida T (2006) Spectroscopic study for photo-catalytic decomposition of organic compounds on titanium dioxide containing sulfur under visible light irradiation. J Colloid Interf Sci 298:805–809

Khan SUM, Al-Shahry M, Ingler WB Jr (2002) Efficient photochemical water splitting by a chemically modified n-TiO_2. Science 297:2243–2244

Kitano M, Tsujimaru K, Anpo M (2006a) Decomposition of water in the separate evolution of hydrogen and oxygen using visible light-responsive TiO_2 thin film photo-catalysts: effect of the work function of the substrates on the yield of the reaction. Appl Catal A Gen 314:179–183

Kitano M, Funatsu K, Matsuoka M, Ueshima M, Anpo M (2006b) Preparation of nitrogen-substituted TiO_2 thin film photocatalysts by the radio frequency magnetron sputtering deposition method and their photocatalytic reactivity under visible light irradiation. J Phys Chem B 110:25266–25272

Kitano M, Takeuchi M, Matsuoka M, Thomas JM, Anpo M (2007) Photocatalytic water splitting using Pt-loaded visible light-responsive TiO_2 thin film photocatalysts. Catal Today 120:133–138

Kowalczyk SP, McFeely FR, Ley L, Gritsyna VT, Shirley DA (1977) The electronic structure of strontium titanate(IV) and some simple related oxides (magnesium oxide, aluminum oxide, strontium oxide, titanium oxide). Solid State Commun 23:161–169

Kuznetsov VN (2002) Study of oxygen adsorption and reoxidation of reduced titanium dioxide by thermal desorption mass spectrometry. Kinet Catal 43:868–873

Kuznetsov VN, Serpone N (2006) Visible light absorption by various titanium dioxide specimens. J Phys Chem B 110:25203–25209

Kuznetsov VN, Serpone N (2007) Photo-induced coloration and photobleaching of titanium dioxide in TiO_2/polymer compositions on UV- and visible-light excitation into the color centers' absorption bands. Direct experimental evidence negating band gap narrowing in anion-/cation-doped TiO_2. Chem Phys 111(42):15277–15288

Kuznetsov VN, Serpone N (2009) On the Origin of the Spectral Bands in the Visible Absorption Spectra of Visible-Light-Active TiO_2 Specimens. Analysis and Assignments, J Phys Chem C 113:15110–15123

Lawless D (1993) Photophysical studies on materials of interest to heterogeneous photocatalysis and to imaging science: CdS quantum dots, doped and undoped ultrasmall semiconductor TiO_2 particles, and silver halides. Ph.D. Thesis, Concordia University, Montreal, Canada (work carried out between 1988 and 2002)

Lee DH, Cho YS, Yi WI, Kim TS, Lee JK, Jung HJ (1995) Metalorganic chemical vapor deposition of TiO_2:N anatase thin film on Si substrate. Appl Phys Lett 66:815–816

Lei Y, Zhang LD, Meng GW, Li GH, Zhang XY, Liang CH, Chen W, Wang SX (2001) Preparation and photoluminescence of highly ordered TiO_2 nanowire arrays. Appl Phys Lett 78:1125–1127

Lettmann C, Hildenbrand K, Kisch H, Macyk W, Maier WF (2001) Visible light photodegradation of 4-chlorophenol with a coke-containing titanium dioxide photo-catalyst. Appl Catal B Environ 32:215–227

Li X, Yue P-L, Kutal C (2003) Synthesis and photocatalytic oxidation properties of iron doped titanium dioxide nanosemiconductor particles. New J Chem 27:1264–1269

Li D, Haneda H, Ohashi N, Hishita S, Yoshikawa Y (2004a) Synthesis of nanosized nitrogen-containing MO_x-ZnO (M = W, V, Fe) composite powders by spray pyrolysis and their visible-light-driven photocatalysis in gas-phase acetaldehyde decomposition. Catal Today 93–95:895–901

Li D, Haneda H, Hishita S, Ohashi N (2004b) Visible-light-driven nitrogen-doped TiO_2 photocatalysts: effect of nitrogen precursors on their photocatalysis for decomposition of gas-phase organic pollutants. Mater Sci Eng B B117:67–75

Li D, Haneda H, Labhsetwar NK, Hishita S, Ohashi N (2005a) Visible-light-driven photocatalysis on fluorine-doped TiO_2 powders by the creation of surface oxygen vacancies. Chem Phys Lett 401:579–584

Li D, Haneda H, Hishita S, Ohashi N (2005b) Visible-light-driven N-F-codoped TiO_2 photocatalysts. 2. Optical characterization, photocatalysis, and potential application to air purification. Chem Mater 17:2596–2602

Li D, Ohashi N, Hishita S, Kolodiazhnyi T, Haneda H (2005c) Origin of visible-light-driven photocatalysis: A comparative study on N/F-doped and N–F-codoped TiO_2 powders by means of experimental characterizations and theoretical calculations. J Solid State Chem 178:3293–3302

Li FB, Li XZ, Hou MF, Cheah KW, Choy WCH (2005d) Enhanced photocatalytic activity of Ce^{3+}–TiO_2 for 2-mercaptobenzothiazole degradation in aqueous suspension for odour control. Appl Catal A Gen 285:181–189

Lin Y-M, Tseng Y-H, Huang J-H, Chao CC, Chen C-C, Wang A (2006) Photocatalytic activity for degradation of nitrogen oxides over visible light responsive titania-based photocatalysts. Environ Sci Technol 40:1616–1621

Lindgren T, Mwabora JM, Avendan E, Jonsson J, Hoel A, Granqvist C-G, Lindquist S-E (2003) Photoelectrochemical and optical properties of nitrogen doped titanium dioxide films prepared by reactive DC magnetron sputtering. J Phys Chem B 107:5709–5716

Livraghi S, Votta A, Paganini MC, Giamello E (2005) The nature of paramagnetic species in nitrogen doped TiO_2 active in visible light photocatalysis. Chem Commun 28(4):498–500

Livraghi S, Paganini MC, Giamello E, Selloni A, Di Valentin C, Pacchioni G (2006) Origin of photoactivity of nitrogen-doped titanium dioxide under visible light. J Am Chem Soc 128:15666–15671

Ma T, Akiyama M, Abe E, Imai I (2005) High-efficiency dye-sensitized solar cell based on a nitrogen-doped nanostructured titania electrode. Nano Lett 5:2543–2547

Matsumoto T, Iyi N, Kaneko Y, Kitamura K, Ishihara S, Takasu Y, Murakami Y (2007) High visible-light photocatalytic activity of nitrogen-doped titania prepared from layered titania/isostearate nanocomposite. Catal Today 120:226–232

Matsuoka M, Kitano M, Takeuchi M, Anpo M, Thomas JM (2005) Photocatalytic water splitting on visible light-responsive TiO_2 thin films prepared by a RF magnetron sputtering deposition method. Top Catal 35:305–310

Matsushima S, Takehara K, Yamane H, Yamada K, Nakamura H, Arai M, Kobayashi K (2007) First-principles energy band calculation for undoped and S-doped TiO_2 with anatase structure. J Phys Chem Solids 68:206–210

Mo SD, Ching WY (1995) Electronic and optical properties of three phases of titanium dioxide: rutile, anatase, and brookite. Phys Rev B Condens Matter 51:13023–13032

Morikawa T, Asahi R, Ohwaki T, Aoki A, Taga Y (2001) Band-gap narrowing of titanium dioxide by nitrogen doping. Jpn J Appl Phys 2(40):L561–L563

Mori-Sanchez P, Recio JM, Silvi B, Sousa C, Martin Pendas A, Luana V, Illas F (2002) Rigorous characterization of oxygen vacancies in ionic oxides. Phys Rev B Condens Matter 66:075103

Mrowetz M, Balcerski W, Colussi AJ, Hoffmann MR (2004) Oxidative power of nitrogen-doped TiO_2 photocatalysts under visible illumination. J Phys Chem B 108:17269–17273

Nakamura I, Negishi N, Kutsuna S, Ihara T, Sugihara S, Takeuchi K (2000) Role of oxygen vacancy in the plasma-treated TiO_2 photocatalyst with visible light activity for NO removal. J Mol Catal A Chem 161:205–212

Nakamura R, Tanaka T, Nakato Y (2004) Mechanism for visible light responses in anodic photocurrents at N-doped TiO_2 film electrodes. J Phys Chem B 108:10617–10620

Navio JA, Colon G, Litter MI, Bianco GN (1996) Synthesis, characterization and photocatalytic properties of iron-doped titania semiconductors prepared from TiO_2 and iron(III) acetylacetonate. J Mol Catal A Chem 106:267–276

Nie X, Sohlberg K (2004) The influence of surface reconstruction and C-impurities on photocatalytic water dissociation by TiO_2. Mater Res Soc Symp Proc 801:205–210

Noda H, Oikawa K, Ogata T, Matsuki K, Kamata H (1986) Preparation of titanium(IV) oxides and its characterization. Chem Soc Jpn 8:1084–1090

Ohno T, Mitsui T, Matsumura M (2003) Photocatalytic activity of S-doped TiO_2 photocatalyst under visible light. Chem Lett 32:364–365

Ohno T, Akiyoshi M, Umebayashi T, Asai K, Mitsui T, Matsumura M (2004) Preparation of S-doped TiO_2 photocatalysts and their photocatalytic activities under visible light. Appl Catal A Gen 265:115–121

Ohno T, Miyamoto Z, Nishijima K, Kanemitsu H, Xueyuan F (2006) Sensitization of photocatalytic activity of S- or N-doped TiO_2 particles by adsorbing Fe^{3+} cations. Appl Catal A Gen 302:62–68

Pascual J, Camassel J, Mathieu H (1978) Fine structure in the intrinsic absorption edge of titanium dioxide. Phys Rev B Condens Matter 18:5606–5614

Redhead PA (1962) Thermal desorption of gases. Vacuum 12:203–211

Ren W, Ai Z, Jia F, Zhang L, Fan X, Zou Z (2007) Low temperature preparation and visible light photocatalytic activity of mesoporous carbon-doped crystalline TiO_2. Appl Catal B Environ 69:138–144

Rodriguez JA, Liu G, Jirsak T, Hrbek J, Chang Z, Dvorak J, Maiti A (2002) Activation of gold on titania: adsorption and reaction of SO_2 on Au/TiO_2(110). J Am Chem Soc 124:5242–5250

Saha NC, Tompkins HG (1992) Titanium nitride oxidation chemistry: an X-ray photo-electron spectroscopy study. J Appl Phys 72:3072–3079

Sakthivel S, Kisch H (2003a) Daylight photocatalysis by carbon-modified titanium dioxide. Angew Chem Int Ed 42:4908–4911

Sakthivel S, Kisch H (2003b) Photocatalytic and photoelectrochemical properties of nitrogen-doped titanium dioxide. Chemphyschem 4:487–490

Sakthivel S, Janczarek M, Kisch H (2004) Visible light activity and photoelectrochemical properties of nitrogen-doped TiO_2. J Phys Chem B 108:19384–19387

Sanjines R, Tang H, Berger H, Gozzo F, Margaritondo G, Levy F (1994) Electronic structure of anatase TiO_2 oxide. J Appl Phys 75:2945–2951

Saraf LV, Patil SI, Ogale SB, Sainkar SR, Kshirsager ST (1998) Synthesis of nanophase TiO_2 by ion beam sputtering and cold condensation technique. Int J Mod Phys B 12:2635–2647

Sathish M, Viswanathan B, Viswanath RP, Gopinath ChS (2005) Synthesis, characterization, electronic structure, and photocatalytic activity of nitrogen-doped TiO_2 nanocatalyst. Chem Mater 17:6349–6353

Sato S (1986) Photocatalytic activity of nitrogen oxide (NO_x)-doped titanium dioxide in the visible light region. Chem Phys Lett 123:126–128

Sato S, Nakamura R, Abe S (2005) Visible-light sensitization of TiO_2 photocatalysts by wet-method N doping. Appl Catal A Gen 284:131–137

Sekiya T, Ichimura K, Igarashi M, Kurita S (2000) Absorption spectra of anatase TiO_2 single crystals heat-treated under oxygen atmosphere. J Phys Chem Solids 61:1237–1242

Sekiya T, Yagisawa T, Kamura N, Mulmi DD, Kurita S, Murakami Y, Kodaira T (2004) Defects in anatase TiO_2 single crystal controlled by heat treatments. J Phys Soc Jpn 73:703–710

Serpone N (2006) Is the band gap of pristine TiO_2 narrowed by anion- and cation-doping of titanium dioxide in second-generation photocatalysts? J Phys Chem B 110:24287–24293

Sonawane RS, Dongare MK (2006) Sol–gel synthesis of Au/TiO_2 thin films for photo-catalytic degradation of phenol in sunlight. J Mol Catal A Chem 243:68–76

Soria J, Conesa JC, Augugliaro V, Palmisano L, Schiavello M, Sclafani A (1991) Dinitrogen photoreduction to ammonia over titanium dioxide powders doped with ferric ions. J Phys Chem 95:274–282

Sun Y, Egawa T, Shao C, Zhang L, Yao X (2004a) EPR line broadening of F center in high-surface-area anatase titania nanoparticles prepared by MOCVD. J Cryst Growth 268:118–122

Sun Y, Egawa T, Shao C, Zhang L, Yao X (2004b) Quantitative study of *F* center in high-surface-area anatase titania nanoparticles prepared by MOCVD. J Phys Chem Solids 75:1793–1797

Suriye K, Praserthdam P, Jongsomjit B (2006) Control of Ti^{3+} surface defect on TiO_2 nanocrystal using various calcination atmospheres as the first step for surface defect creation and its application in photocatalysis. Appl Surf Sci 253:3849–3855

Tachikawa T, Tojo S, Kawai K, Endo M, Fujitsuka M, Ohno T, Nishijima K, Miyamoto Z, Majima T (2004) Photocatalytic oxidation reactivity of holes in the sulfur- and carbon-doped TiO_2 powders studied by time-resolved diffuse reflectance spectroscopy. J Phys Chem B 108:19299–19306

Tachikawa T, Fujitsuka M, Majima T (2007) Mechanistic insight into the TiO_2 photocatalytic reactions: design of new photocatalysts. J Phys Chem B 111(14):5259–5275

Takeuchi M, Yamashita H, Matsuoka M, Anpo M, Hirao T, Itoh N, Iwamoto N (2000) Photocatalytic decomposition of NO under visible light irradiation on the Cr-ion-implanted TiO_2 thin film photocatalyst. Catal Lett 67:135–137

Tang H, Levy F, Berger H, Schmid PE (1995) Urbach tail of anatase TiO_2. Phys Rev B 52:7771–7774

Teoh WY, Amal R, Madler L, Pratsinis SE (2007) Flame sprayed visible light-active Fe-TiO_2 for photomineralisation of oxalic acid. Catal Today 120:203–213

Thompson TL, Yates JT Jr (2005) TiO_2-based photocatalysis: surface defects, oxygen and charge transfer. Top Catal 35:197–210

Tian F-H, Liu C-B (2006) DFT description on electronic structure and optical absorption properties of anionic S-doped anatase TiO_2. J Phys Chem B 110:17866–17871

Umebayashi T, Yamaki T, Itoh H, Asai K (2002) Band gap narrowing of titanium dioxide by sulfur doping. Appl Phys Lett 81:454–456

Umebayashi T, Yamaki T, Yamamoto S, Miyashita A, Tanaka S, Sumita T, Asai K (2003a) Sulfur-doping of rutile-titanium dioxide by ion implantation: Photocurrent spectroscopy and first-principles band calculation studies. J Appl Phys 93:5156–5160

Umebayashi T, Yamaki T, Tanaka S, Asai K (2003b) Visible light-induced degradation of methylene blue on S-doped TiO_2. Chem Lett 32:330–331

Vitiello RP, Macak JM, Ghicov A, Tsuchiya H, Dick LFP, Schmuki P (2006) N-doping of anodic TiO_2 nanotubes using heat treatment in ammonia. Electrochem Commun 8:544–548

Wang H, Lewis JP (2005) Effects of dopant states on photoactivity in carbon-doped TiO_2. J Phys Condens Matter 17:L209–L213

Wang H, Lewis JP (2006) Second-generation photocatalytic materials: anion-doped TiO_2. J Phys Condens Matter 18:421–434

Wang J, Wen F-Y, Zhang Z-H, Zhang X-D, Pan Z-J, Zhang P, Kang P-L, Tong J, Wang L, Xu L (2006) Investigation on degradation of dyestuff wastewater using visible light in the presence of a novel nano TiO_2 catalyst doped with upconversion luminescence agent. J Photochem Photobiol A:Chem 180:189–195

Wang J, Zhu W, Zhang Y, Liu S (2007a) An efficient two-step technique for nitrogen-doped titanium dioxide synthesizing: visible-light-induced photodecomposition of methyl-ene blue. J Phys Chem C 111:1010–1014

Wang J, Zhang Q, Yin S, Sato T, Saito F (2007b) Raman spectroscopic analysis of sulfur-doped TiO_2 by co-grinding with TiS_2. J Phys Chem Solids 68:189–192

Xu C, Killmeyer R, McMahan L, Gray S, Khan UM (2006) Photocatalytic effect of carbon-modified n-TiO_2 nanoparticles under visible light illumination. Appl Catal B Environ 64:312–317

Yamaki T, Umebayashi T, Sumita T, Yamamoto S, Maekawa M, Kawasuso A, Itoh H (2003) Fluorine-doping in titanium dioxide by ion implantation technique. Nucl Instrum Methods Phys Res B 306:254–258

Yamamoto T, Yamashita F, Tanaka I, Matsubara E, Muramatsu A (2004) Electronic states of sulfur doped TiO_2 by first principles calculations. Mater Trans 45:1987–1990

Yanagisawa Y, Sumimoto T (1994) Oxygen exchange between CO_2 adsorbate and TiO_2 surfaces. Appl Phys Lett 64:343–344

Yang S, Gao L (2004) New method to prepare nitrogen-doped titanium dioxide and its photocatalytic activities irradiated by visible light. J Am Ceram Soc 87:1803–1805

Yang M-C, Yang T-S, Wong M-S (2004) Nitrogen-doped titanium oxide films as visible light photocatalyst by vapor deposition. Thin Solid Films 469(470):1–5

Yang K, Dai Y, Huang B, Han S (2007) Theoretical study of N-doped TiO_2 rutile crystals. J Phys Chem B 110:24011–24014

Yates HM, Nolan MG, Sheel DW, Pemble ME (2006) The role of nitrogen doping on the development of visible light-induced photocatalytic activity in thin TiO_2 films grown on glass by chemical vapour deposition. J Photochem Photobiol A:Chem 179:213–223

Yin S, Yamaki H, Komatsu M, Zhang Q, Wang J, Tang Q, Saito F, Sato T (2003) Preparation of nitrogen-doped titania with high visible light induced photocatalytic activity by mechanochemical reaction of titania and hexamethylenetetramine". J Mater Chem 13:2996–3001

Yin S, Ihara K, Aita Y, Komatsu M, Sato T (2006) Visible-light induced photo-catalytic activity of $TiO_{2-x}A_y$ (A = N, S) prepared by precipitation route. J Photochem Photobiol A Chem 179:105–114

Yu J, Zhou M, Cheng B, Zhao X (2006) Preparation, characterization and photo-catalytic activity of in situ N, S-codoped TiO2 powders. J Mol Catal A Chem 246:176–184

Zhou J, Takeuchi M, Zhao XS, Ray AK, Anpo M (2006) Photocatalytic decomposition of formic acid under visible light irradiation over V-ion-implanted TiO_2 thin film photocatalysts prepared on quartz substrate by ionized cluster beam (ICB) deposition method. Catal Lett 106:67–70

Zhu J, Deng Z, Chen F, Zhang J, Chen H, Anpo M, Huang J, Zhang L (2006a) Hydrothermal doping method for preparation of Cr^{3+}-TiO_2 photocatalysts with concentration gradient distribution of Cr^{3+}. Appl Catal B Environ 62:329–335

Zhu J, Chen F, Zhang J, Chen H, Anpo M (2006b) Fe^{3+}-TiO_2 photocatalysts prepared by combining sol-gel method with hydrothermal treatment and their characterization. J Photochem Photobiol A Chem 180:196–204